بِسْمِ ٱللَّهِ ٱلرَّحْمَٰنِ ٱلرَّحِيمِ

Sudan University of Science and Technology

College of Graduate Studies

A Study of the Behavior of Hybrid Fiber Reinforced Concrete Slabs Exposed to Impact Loading

دراسة لسلوك البلاطات الخرسانية المسلحة بالألياف الهجين المعرضة لأحمال الصدم

Thesis submitted to the School of Civil Engineering in Fulfillment of the Requirements for the Degree of Doctor Philosophy in Civil Engineering

By: Mai Abdel Raheem Sofyan Hamed

(MSc: Structural Engineering. B Eng.:Civil Engineering (Structures))

Supervisor: Prof.Dr Abdelrahman Elzubair Mohamed

June 2022

الآية

بِسْمِ ٱللَّهِ ٱلرَّحْمَٰنِ ٱلرَّحِيمِ

قَالَ تَعَالَى:

(أَفَمَنْ أَسَّسَ بُنْيَٰنَهُۥ عَلَىٰ تَقْوَىٰ مِنَ ٱللَّهِ وَرِضْوَٰنٍ خَيْرٌ أَمْ مَّنْ أَسَّسَ بُنْيَٰنَهُۥ عَلَىٰ شَفَا جُرُفٍ هَارٍ فَٱنْهَارَ بِهِۦ فِى نَارِ جَهَنَّمَ ۗ وَٱللَّهُ لَا يَهْدِى ٱلْقَوْمَ ٱلظَّٰلِمِينَ)

صَدَقَ اللهُ الْعَظِيْمُ

التَّوبَة- الآية 109

DEDICATION

To my lovely

Mother and Father

To my Husband,

To my little kids

Faroug and Faris,

To all members of my family,

To all people in my life

I dedicate this research.

ACKNOWLEDGEMENTS

First of all, thanks for ALLAH, my creator for giving me the health and ability to achieve this work.

I would like to express my deep gratitude and appreciation to my advisor Professor Abdelrahman Elzubair, for offering me the opportunity to carry out this interesting research under his supervision. Prof. Abdelrahman has been keen on patiently providing ongoing support and encouragement, expert guidance and insightful comments made my thesis work possible. It has been an honor for me to be one of his Ph.D. students.

I am very grateful to Proffessor Raizal Saifulnaz and Mohd Basri at Structural Laboratory in University of Putra, for helping me with experimental part of my PhD thesis and his valuable suggestions. Prof. Raizal, thank him for his kind help and assistance with the experiments. I truly appreciate his unconditional help and valuable advices, for generously sharing his broad knowledge and for being patient with my questions.

This work was supported by DAAD Scholarship. Thanks to DAAD for offering me an opportunity of doing my experimental tests.

Finally, My deepest gratitude goes to whom their taking care of me, loving me, understanding my needs, giving me unconditional love and inspiring me to go on academic studies and never letting me down.

Sudan, February 2022 *Mai Abdel Raheem Sofyan*

ABSTRACT

The most accurate and reliable approach to investigating concrete slabs structural behavior under impact loading is to conduct impact experiments. This research has the aim of providing a better understanding of the behavior of Hybrid Fiber Reinforced Concrete (HFRC) slabs under impact loading. Experimental work was conducted to study how to enhance the impact resistance of HFRC slabs which are commonly encountered in modern buildings. The focus is on preventing their collapse by increasing their ductility and energy dissipation by strengthening them with steel and Polypropylene (PP) fibers. In this research a study of the behavior of hybrid fiber reinforced concrete slabs under impact loads was carried out by casting and testing eight hybrid fiber reinforced concrete slabs with dimensions of 1700x1700x100 mm and with two fiber volume ratios of 0.5 % and 1.0 %. The tests were carried out at Structural Laboratory of the University of Putra Malaysia.

The free-fall impact tests were conducted with a 200-kilogram hammer and two different drop heights (1m and 2m). The relationships between impact loads, displacements, and strains were established from the recorded tests results. The dynamic responses gained during tests, as well as the failure modes detected, had been thoroughly analyzed. The tests findings show that, when appropriately built, hybrid-fiber reinforcement can greatly improve the overall impact resistance of concrete slabs, stop crack growth, and thereby reduce the size of the damaged area. Under impact force, the slab specimen with a mix of 1% steel fibers and 0.5% PP fibers performed best improvement of integrity after failure and impact resistance with an increase 30.79%.

The load tests showed that hybrid fiber reinforcement contributes to increasing load capacity and ductility of the slab. In addition, the dissipated energy of the reference slab was doubled in the hybrid reinforced concrete slab. Also, applying the strengthening technique led to a change in the crack pattern from one opened hair crack to multiple cracks in the tension face. However, hybrid fiber reinforcement results in a considerable reduction (by up to 68%) in compressive strength.

المستخلص

إجراء تجارب أحمال الصدم هو النهج الأكثر دقة وموثوقية للتحقيق في السلوك الإنشائى للبلاطات تحت تحميل الصدم. ويهدف هذا البحث إلى توفير فهم أفضل لسلوك البلاطات الخرسانية المسلحة بالألياف الهجينة (HFRC) تحت تحميل الصدم. وقد أُجريت دراسات تجريبية لدراسة كيفية تعزيز مقاومة الصدم لبلاطات HFRC التي تستخدم عادة في المباني الحديثة. وينصب التركيز على منع إنهيارها عن طريق زيادة المطيلية وتبديد الطاقة من خلال تعزيزها بألياف الصلب والبولي بروبلين (PP). وفي هذه الدراسة ، تم تنفيذ سلوك البلاطات الخرسانية المسلحة بالألياف الهجينة تحت أحمال الإرتطام (الصدم) عن طريق الصب والإختبار حيث تم إختبار ثمانية بلاطات خرسانية من الألياف الهجينة ذات أبعاد 1700*1700*100 مم بنسبتين 0.5% و 1% من حجم الألياف. وقد تم عمل هذه الإختبارات فى معمل الإنشاءات لجامعة بوتيرا الماليزية.

أجريت إختبارات تأثير السقوط الحر بمطرقة وزن 200 كيلوغرام وإرتفاعين مختلفين للإسقاط (1 متر و 2 متر). وقد تمَّ إستنباط العلاقات بين أحمال الصدم والإنحرافات والإنفعالات. ومن نتائج الإختبارات تمَّ تحليل الإستجابات الديناميكية المكتسبة ، بالإضافة إلى أوضاع الفشل المكتشفة ، بدقة. وقد أظهرت نتائج الإختبارات أنَّه عند البناء بشكل مناسب ، يمكن للتسليح بالألياف الهجينة أن يحسن بشكل كبير من مقاومة الصدم الكلية للبلاطات الخرسانية ، ويوقف ظهوروتمدد الشقوق ، وبالتالي يقلّل من حجم المنطقة المتضررة. وقد أعطت البلاطة الخرسانية مع مزيج من(1% ألياف الصلب و 0.5 ٪ ألياف البولي بروبلين) أداءاً أفضل فى تحسين سلامة الفشل ومقاومة الصدم بنسبة زيادة 30.69%.

وقد أظهرت إختبارات حمل الصدم أن الألياف الهجينة المعززة تساهم في زيادة سعة الحمولة وليونة البلاطة. بالإضافة إلى ذلك، تضاعفت الطاقة المتبددة في البلاطة الخرسانية المسلحة الهجينة عن البلاطة المرجعية. أيضاً ، أدى تطبيق تقنية التسليح إلى تغيير في نمط التشققات من صدع واحد مفتوح إلى تشققات متعددة دقيقة في الواجهة المعرضة للشد. ولكن نتائج الألياف الهجينة أدَّت الى إنخفاض مقدر(68%) فى مقاومة الضغط.

List of Publications

1- Sofyan, M.A.R. and Mohammed, A.E. (2021). Experimental Investigation on Mechanical Properties of Hybrid Steel and Poly Vinyl Alcohol Fiber Reinforced Concrete. Journal of Engineering and Computer Science (Vol. 22, No 2). PP(52-61).

2- Sofyan, M.A.R. and Mohammed, A.E. (2021). Experimental Study on Hybrid Reinforced Concrete Slabs Subjected to Impact Loading. International Journal of Engineering Sciences & Research Technology (Vol.10, 11). PP(1-15).

TABLE OF CONTENTS

LIST OF TABLES

Table **Page**

LIST OF FIGURES

Figure **Page**

LIST OF ABBREVIATIONS

ACE: Army Corps of Engineers

ACIFC: Association of Concrete Industrial Flooring Contractors

ASTM: American Society of Testing Material

BLS: Basic Life Support

CFRP: Carbon Fiber Reinforced Polymer

CRIEPI: Central Research Institute of Electric Power Industry formula

Cent Second: CS

DIF: Dynamic Increase Factor

DT: Dynamic Tear

DWT: Drop Weight Test

FDM: Finite Difference Method

FEM: Finite Element Method

FRC: Fiber Reinforced Concrete

FRPs: Fiber Reinforced Polymers

GFRP: Glass Fiber Reinforced Polymer

HFRC: Hybrid Fiber Reinforced Concrete

HPC: High Performance Concrete

LS-DYNA: Livermore Software Dynamic

LVDTs: Linear Variable Differential Transformers

NDT: Nil Ductility Temperature

NLFEA: Nonlinear Finite Element Analysis

PC: Plain Concrete

PP: Polypropylene

PPF: Polypropylene Fiber

PVA: Poly Vinyl Alcohol

RC: Reinforced Concrete

SFRC: Steel Fiber Reinforced Concrete

SHCC: Strain Hardening Cementitious Composites

SG: Strain Gauges

SF: Steel Fiber

UFC: Unified Facilities Criteria

UHPC: Ultra High Performance Concrete

CHAPTER ONE

INTRODUCTION

1.1 Background

Over the last few decades, numerous explosion events due to military or terrorist activities have happened over the entire world. Structures in urban areas like government and civilian buildings, such as military camps, airports, historical and strategic building, bridges, parliaments, dams and official buildings, have been targeted to inflict damage and casualties. Oklahoma City (1995), Word Trade Centre in New York City (2001) (Musselman, 2007), UN headquarters in Iraq (2003), Al-Shifa the pharmaceutical factory in Sudan (1998) as shown in figure 1.1, are some examples of the massive damage to the buildings and the loss of civilian lives resulting from such events. Normally conventional buildings are incapable to resist out-of-plane loads and such events have brought the topic of strengthening important buildings against the impact and blast loads to the forefront.

Figure 1.1 Tomahawk Missile Impact on Al-Shifa Factory in Sudan Photo (B McMorrow, 2009)

This goal can be achieved by increasing their strength, ductility or energy absorption. In some cases, especially in residential buildings or shelters, enhancing the ductility and the energy dissipation of the elements may not have any substitute for the safety of the occupants. Whilst many techniques have been introduced to achieve this demand, the cost and the feasibility of any implementation method should also be considered.

Local impact damage can be simplified as the impact damage caused by vehicle/train collision, aircraft/missile, and drop-weights, free falling bodies on concrete structures, except explosion. In local impact damage, vehicles, trains, aircrafts, missiles, drop-weights, and free falling bodies are considered as impact projectiles. Projectiles may exist in a long diversity in sizes, shapes, velocity, weight, density, etc such as bullets, fragments, tornado, missile, explosive bomb, steel rod, flying objects at high speed, etc. The impacting projectile (missile) can be classified as 'hard' and 'soft' in nature, depending upon the implication of its deformation with respect to the deformation of target. Hard missile impact can generate both local impact damages and global damages on concrete structures.

Fiber Reinforced Plastic (FRPs) are accepted to be utilized to enhance the physical properties of the structures by improving their strength, stiffness and ductility or energy absorption capacity (Angelucci et al., 2009, Pichandi et al., 2013). The high strength to weight and corrosion-free behavior of the FRPs make them competitive to be considered as effective retrofitting materials.

However, limited studies have been conducted on using Hybrid Fiber Reinforced Concrete (HFRC), for all forms and approaches to enhance the impact resistance of concrete structures due to the expensive experimental works.

Most of the studies mentioned above have been conducted under quasi-static conditions. Limited research has been conducted to study the response of the structures to impact load (Pichandi et al., 2013). Most of the work to date has focused on increasing the load capacity of new and existing members with very few studies

covering other factors such as failure modes, crack patterns, ductility and energy dissipated in the strengthened member, which are known to be critical in preventing collapse of the whole structure.

Designing reinforced concrete structures to withstand impact loads has traditionally been approached in a highly idealized manner, with procedures typically consisting of empirical formulas used to estimate member damage levels or capacity (Kishi et al., 2002) and simple macro-models which reduce structural members to single-degrees-of-freedom system (UFC3-340-02, 2008). Although the simplicities of such methods make them appealing, they have been shown to be unreliable (El-Dakhakhny et al., 2009; Chen and May, 2009) and they provide limited information regarding the actual dynamic response and post-event state of the structure.

As modern code provisions continue to evolve toward performance-based design methodologies, and as extreme loading scenarios such as impact and blast are considered in the design process more regularly, the need for analytical tools which are capable of accurately modeling the behaviors of complex reinforced concrete structures under a wide range of loading conditions continues to grow (Hrynyk, 2013).

Due to intricacy of the local impact effects and complex behavior of concrete, investigations are generally carried out based on experimental data. Conclusions of the experimental observations are then used to develop engineering models. It is observed from literature that, the local impact effect of hard projectile on concrete targets normally can be studied by three engineering techniques using experimental observations:

*Empirical analysis based on experimental data by fitting curve,

*Idealized analytical modeling based on physical laws, and

*Numerical simulations based on computational mechanics and material models.

Therefore, the present experimental study tends to investigate the behavior of hybrid fiber reinforced concrete slabs under low velocity impact load. Well instrumented test data are to be collected from these tests with intent to comprehend the behavior of Hybrid Fiber Reinforced Concrete (HFRC) slabs under impact loads which can be utilized in further studies and can be a reference point in order to develop impact analysis and design methods.

1.2 Problem Statement

The local adverse impact effect of hard projectile on concrete targets and the influence of adding hybrid fiber reinforcement on the impact effect is a complex engineering problem. This problem can normally be studied by empirical analysis based on experimental results, idealized analytical models or numerical simulations based on computational mechanics. An experimental method to study the effect of impact behavior of plain and hybrid reinforced concrete slabs, i.e., mechanical properties of concrete, crack patterns, local damage mode and deflections under specific mass projectile, impact heights, velocities and fiber ratio contents is of great importance.

1.3 Research Questions and Hypotheses

1. Flexural and tensile strength of concrete under impact load is increased by hybrid reinforcement.

2. Does fiber ratio and type make a difference in the impact response of concrete slabs?

3. Does hybrid fiber reinforcement of concrete slabs affect the compressive strength?

4. Local damage mode in concrete under impact load can be enhanced by hybrid reinforcement.

5. What is the level of hybrid fiber reinforcement that should be used to reduce scabbing and prevent perforation?

1.4 Aim and Objectives of the Research

The aim of this research is to enrich the existing knowledge of the structural impact load resistance of HFRC slabs by conducting experimental programs related to some important aspects that have not been studied in depth before.

The specific objectives of this research are:

- To design and carry-out an experimental testing program focused on the behavior of hybrid fiber reinforced concrete slabs subjected to drop-weight impact loading conditions.
- To assess the applicability of using HFRC/FRC slab elements in impact-resistant design.
- To provide data in the response of HFRCR/FRC slabs elements under low velocity impact load.
- To add a limited database pertaining to numerical modeling of the response of reinforced concrete structures under impact loading.

1.5 Research Methodology

The hybrid fiber system as a strengthening method in Plain Concrete slabs against impact loads was considered in this research to investigate and interpret its behavior under short transient loadings such as impact loadings. The slabs were selected to be strengthened as they represent the weakest and the most vulnerable part in the structure to the impact loading effect due to their wide surface which subjects to the impact pressure for all form of the slabs such as floors, wall panels, cladding panels. Available tests include a limited range of projectile mass, velocity and concrete strength without considering the contribution of reinforcement to the impact resistance of hybrid fiber reinforced concrete slabs.

The methodology of this research approved to reach the objectives, was through the following stages:

- Literature Review:
  Where state of the art and basic concepts of hybrid fiber reinforced concrete and impact load resistance of hybrid fiber reinforced concrete slabs were revised and related Literature and relevant data was collected and studied from library search, collecting various data and information through various sources including books, journals and different

references and historical documentary including previous case studies, international studies and papers, and from internet and other sources. Then the main features of the proposed work will be pointed out.

- Experimental Work:
  As a basic finding from literature reviewed, the laboratory tests are the following:
  - Slump test
  - Tension test
  - Flexural test
  - Impact load test
- Analysis and Discussion of Results.
- Drawing Conclusions and Presenting Recommendations.

1.6 Thesis Outlines

The presented work is comprised of five chapters as follows:

Chapter 1 Introduction presents the introduction, the problem statement, the objective and scope of the work and the structure of thesis.

Chapter 2 Literature Review presents basic concepts about impact loads and background information of impact loading conditions is provided. Both the experimental and the nonlinear simulation studies are presented in this chapter. Finally, a summary of the previous work is presented highlighting the areas that need further work.

Chapter 3 Experimental Program presents the specimen details and testing methodologies used in the experimental program. The instrumentation and data measurement techniques employed are summarized.

Chapter 4 Results Analysis and Discussion presents the measured results from the experimental program and discussed in detail in. Additionally, an assessment of the acquired digital data set is provided.

Lastly, **Chapter 5 Conclusions and Recommendations** is the final part of the represented work which contains a summary and the conclusions from the experimental studies. Some suggestions and recommendations for future research are also indicated.

CHAPTER TWO

LITERITURE REVIEW

2.1 Introduction

This chapter aims to present general information on the impact load and its effects on hybrid/fiber reinforced concrete slabs. Furthermore, to grasp the existing knowledge in this area, a review of the studies that have been done so far on enhancing the structural response to the impact loading is presented in this chapter. Also, their results are discussed highlighting their strengths and limitations. The methods and the materials that have been used in the impact strengthening are highlighted with a focus on the pros and cons of each one. Both experimental and numerical studies that were conducted in this area are covered. The areas that have not been covered well and need further research are identified.

Antoniou, 2018 defined impact load as an exceptionally rapid release of energy in very short period of time, assessed in thousandths of a second, or milliseconds. This varies from earthquakes and wind bursts, which are assessed in seconds, or continued wind or flood situations, which may be measured in hours.

Liu et al., 2020 stated that the concept of using fibers in brittle material to improve resistance to cracking and fragmentation is old and intuitive. Different types of fibers and fiber materials are introduced and are being continuously introduced to the market for new applications. These fibers can be made of metals, natural, glass or organic materials. Fiber reinforced concrete is concrete made of hydraulic cements containing fine aggregate, or fine and coarse aggregate and discontinuous discrete fibers. These fibers are in various shapes and sizes. A convenient numerical parameter describing a fiber and its aspect ratio was defined by Mohajerani et al., 2019 as the fiber length divided by an equivalent fiber diameter. Typical aspect ratios range from about 30 to 150 for length dimensions of 6.4 mm to 76 mm. Each type of fiber has its own physical properties.

2.2 Response of Structures to Different Types of Loads

As stated by Al Nussairi, 2018, loads on structures are mostly classified into two categories: static load and dynamic load. The static load is insensitive to the time effect, while the dynamic load is sensitive to the time effect. According to that, the static load may be defined as any load which is applied constantly for relatively long time (compared to the natural period of the member), while dynamic load may be defined as the transient and changeable load that occurs within a short duration (milliseconds) such as vibration, seismic, impact and blast load.

Manibalan & Baskar, 2019 reached the conclusion that: applying the load within very short time results in a higher loading rate which leads to an increase in the deflection rate of the loaded member, and as a result, increasing the strain rate of the structural materials inside the member. Typically, blast and impact loads produce high strain rates due to the high loading rates associated.

According to Ngo et al., 2007 some materials have different mechanical properties under different strain rate values. These are referred to as strain rate dependent materials and the strain rate effect of the dynamic loads, especially with high strain rates, should be considered well in any design procedure. Figure 2.1, presented by Adhikary, 2013, shows the approximate ranges of the expected strain rates for different loading conditions. It can be seen that ordinary static strain rate is located in the range: 10^{-6}-10^{-5} s^{-1}, while impact load normally yield loads associated with strain rates in the range: 10^{0}-10^{2} s^{-1}. For reinforced concrete structures subjected to blast effects the strength of concrete and steel reinforcing bars can increase significantly due to strain rate effects.

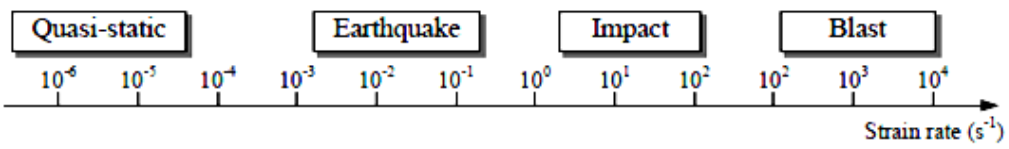

Figure 2.1 Strain Rates Associated with Different Types of Loading (Adhikary, 2013)

Ngo et al., 2007 claimed that it was shown experimentally that steel yield strength is more sensitive to rate effects than the ultimate strength, and it was noted that the dynamic increase factors for the steel yield strength are much higher than for the ultimate strength. As presented in UFC, 2008, also illustrated in Figure 2.2, for concrete, the entire static stress-strain curve is scaled by the appropriate dynamic increase factor. However, for steel, the yield strength is scaled by one factor (see Figure 2.3). Additionally further refinements to the dynamic increase factor values were presented by Krauthammer, 2008 and Kassahun, 2012 as shown in Table 2.1. Where: f'_c is static ultimate compressive strength of concrete, f'_{dc} is dynamic ultimate compressive strength of concrete, f_y is static yield stress of reinforcing steel, f_{dy} is dynamic yield stress of reinforcing steel, f_u is static ultimate stress of reinforcing steel, f_{du} is dynamic ultimate stress of reinforcing steel, E_s is modulus of elasticity for reinforcing steel, E_c is secant modulus of elasticity of concrete and ε_u is rupture strain.

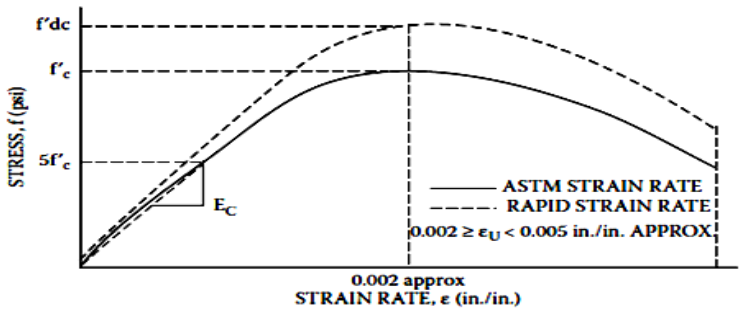

Figure 2.2 Effect of Strain Rate on Stress-Strain Curve for Concrete (UFC, 2008)

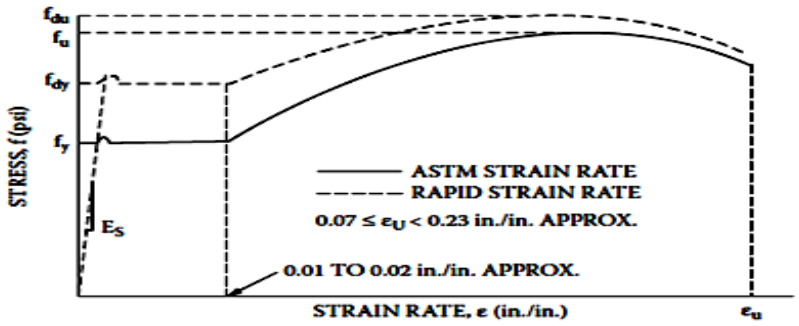

Figure 2.3 Effect of Strain Rate on Stress-Strain Curve for Steel(UFC, 2008)

Table 2.1 Reinforced Concrete Design Dynamic Increase Factors(Krauthammer, 2008) and (Kassahun, 2012)

Type of Stress	Far Design Range			Close-In Design Range		
	Reinforcing Bars		Concrete	Reinforcing Bars		Concrete
	f_{dy}/f_y	f_{du}/f_u	f'_{dc}/f'_c	f_{dy}/f_y	f_{du}/f_u	f'_{dc}/f'_c
Bending	1.17	1.05	1.19	1.23	1.05	1.25
Diagonal Tension	1	-	1	1.1	1	1
Direct Shear	1.1	1	1.1	1.1	1	1.1
Bond	1.17	1.05	1	1.23	1.05	1
Compression	1.1	-	1.12	1.13	-	1.16

2.3 Strain Rate Effect on the Response of Structures

With the strain rate dependent materials, an enhancement in the mechanical properties, such as yielding and ultimate strength, is achieved when they deform with high strain rate values. Silva & Lu, 2007 defined the enhancing factor of these materials, called the dynamic increase factor (DIF), as the ratio of the dynamic to the static strength value. For the structural buildings, both concrete and steel are found to be strain rate dependent materials, where the DIF of steel and concrete each was found to be proportional to the strain rate value. The enhancing factor of the concrete compression strength could exceed 4 under high strain rate values as shown in Figure 2.4. Figure 2.5 shows the DIF of both the concrete and the steel with various strain rate values. It shows that a linear function is obtained for the steel and multi-linear function for the compression strength of concrete. This had also, been confirmed by Al Nussairi, 2018.

Langdon et al., 2014 stated that fiber reinforced composites are essentially strain rate dependent materials where the stress-strain relationship varies with the varying of the strain rates. They had shown that the strain rate dependency depends on the type of the composite material. For Glass Fiber Reinforced Polymer (GFRP) and Carbon Fiber Reinforced Polymer (CFRP), they asserted that increasing the strain rates induces enhancing the ultimate strength

for both the tension and the compression stresses while the modulus of elasticity stays constant.

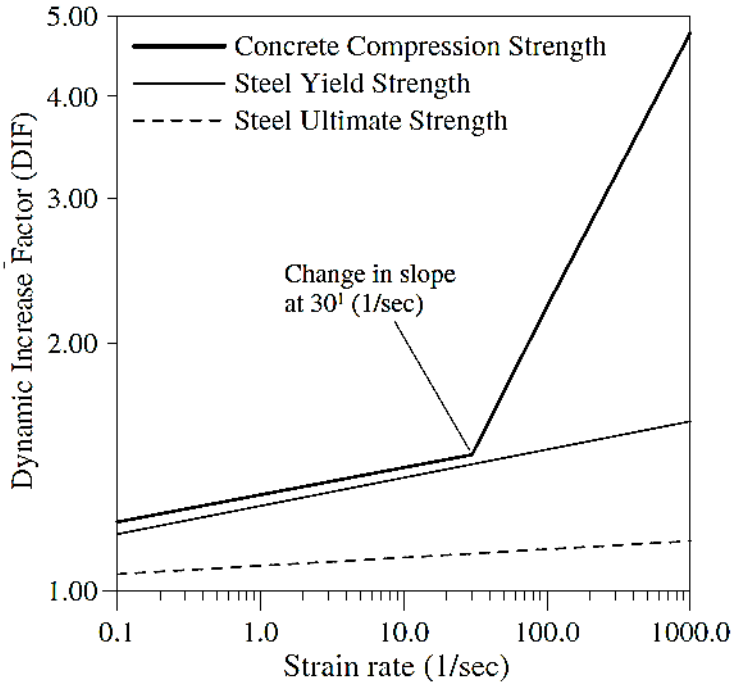

Figure 2.4 DIF of Concrete and Steel under Various Strain Rates(Silva & Lu, 2007)

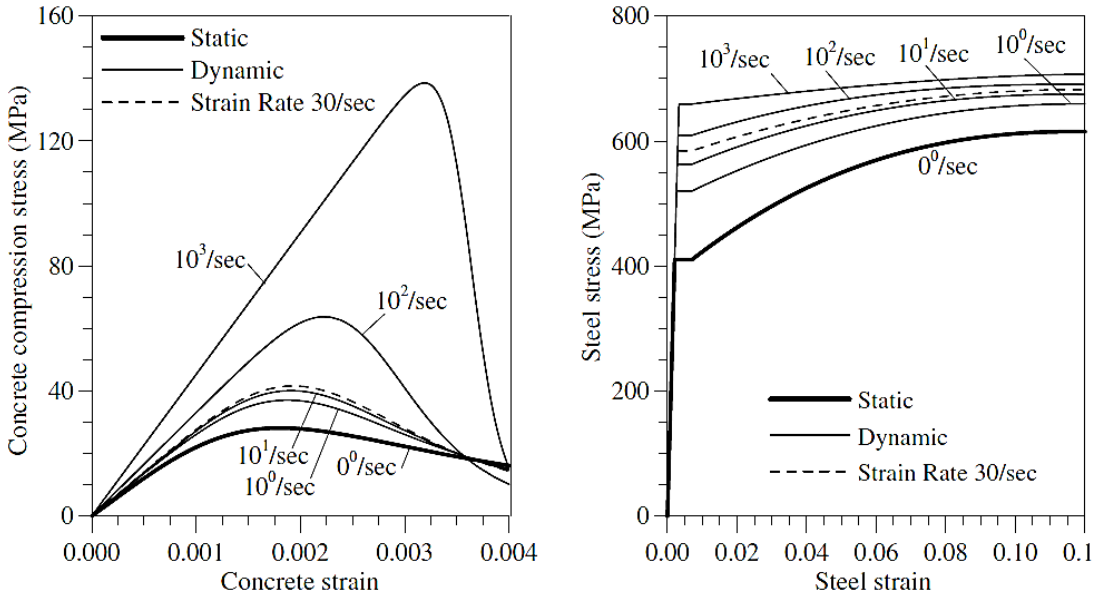

Figure 2.5 Stress-Strain Relationship of Concrete and Steel under Various Strain Rates(Silva & Lu, 2007)

Alhadid et al., 2014 proposed that, when a structural reinforced concrete member is subjected to a very short transient load, such as blast and impact load, the reinforced concrete member oscillates producing a periodic displacement-time function with multiple peaks. They found that the first peak of the displacement which occurs in the first phase of the displacement wave had the highest magnitude and the highest effect on the member as the peak deflection reduced in the consequent phases of the oscillation due to the damping effect. So, only the first peak of the displacement could be considered in analyzing the structural response to the blast and impact loading.

2.4 Assessment Methods of the Behavior of Concrete Structures under Impact Loading:

There are three methods for assessing namely: Experimental investigation, Simplified design methods and Numerical methods. These are briefly outlined in the following sub-sections.

2.4.1 Experimental investigation of Concrete Structures under Impact Loading:

As stated by Zielinski, 1984 this method requires special laboratory facilities and is very laborious. Experiments provide sufficient insight into global force-displacement-time relations and bearing capacity of the structural member or the entire structure considered. This method is of particular importance for studying the local response of concrete structures due to impact, which cannot as yet be properly investigated by other methods. With the respect to the overall response of concrete structures the results of experiments are normally applied to the verification of analytical and numerical solutions.

2.4.2 Simplified Design Methods of Concrete Structures under Impact Loading

According to Antoniou, 2018 the fundamental principle of structural design is to guarantee safety for the community with an economical solution. Thus structures would be capable to preserve their form until ultimate resistance capacity. Concrete is widely

used in protection systems of sensitive infrastructures such as nuclear power plants. The increasing risk of accidental conditions (aircraft impact) or military conditions (missile impact) requires assessing the vulnerability and durability of concrete structures under impulsive loadings. Existing design methods for protection systems under impacts are mainly based on full-size experiments and empirical formulae that are not economical. The impacts are classified as soft impacts and hard impacts as follows:

1. Soft Impacts

Riera, 1980 studied the reaction force (t) of a collapsing aircraft on a rigid surface. He considered the impacted structure to be stiff with negligible deformations in comparison with those of the collapsing aircraft. He developed Equation (2.1) which gives the contact force at the interface between the two colliding bodies:

$$P(t) = P_b(x(t)) + \mu(x(t))\, V^2(t) \qquad (2.1)$$

In which $x(t)$ is length of the aircraft, $P_b(x)$ is the necessary buckling force to crush or deform the fuselage of the aircraft, $\mu(x)$ is the mass of the aircraft per unit length and $V(t)$ is the velocity of uncrashed aircraft. The elastoplastic buckling force $P_b(x)$ can be considered as independent of (t).

2. Hard impacts

Pétry, 1910 developed originally formula (2.2) to account for the penetration depth x (inches) of a rigid missile into a massive target; with Kp the concrete penetrability coefficient, A_p (lb/ft^2) the missile section pressure and V_0 (ft/s) the impact velocity of the projectile. For massive plain concrete K_p= 0.00799, for normal reinforced concrete 0.00426 and 0.00284 for specially reinforced concrete in which the front and rear face steel are laced together with special ties.

$$x = 12\, K_p A_p log_{10}\left(1 + \frac{{V_0}^2}{215}\right) \qquad (2.2)$$

Different authors modified this formula; (Amirikian, 1950) reformed the coefficient Kp to account for the effect of the

compressive strength of concrete target fc, this is illustrated by (Li et al., 2005), as shown in Figure 2.6. Pétry, 1910 also proposed the perforation thickness e (2.3) and scabbing thickness h_s (2.4).

$$e=2x \tag{2.3}$$

$$h_s=2.2\ x \tag{2.4}$$

Walter and Wolde-Tinsae, 1984 presented the coefficient K_p as in the equation (2.5).

$$K_p=6.34\times 10^{-3}(-0.2973\times 10^{-7} f_c) \tag{2.5}$$

The Army Corps of Engineers formula (2.6) (ACE, 1946) was developed based on statistical fitting of experimental results from the Ordnance Department of the United State Army and the BLS to predict the penetration depth.

$$\frac{x}{d}=\frac{282.6}{\sqrt{\mathrm{fc}}}\left(\frac{\mathrm{M}}{d^3}\right)d^{0.2}\left(\frac{\mathrm{V0}}{1000}\right)^{1.5}+0.5 \tag{2.6}$$

Perforation e and scabbing h_s limits are based on ballistic tests with 37, 75, 76.2 and 155 mm steel projectiles as mentioned by Li et al., 2005 as:

$$\frac{e}{d}=1.32+1.24\frac{x}{d}\quad \text{for } 3<\frac{e}{d}<18 \tag{2.7}$$

$$\frac{\mathrm{hs}}{d}=2.12+1.36\frac{x}{d}\quad \text{for } 3<\frac{e}{d}<18 \tag{2.8}$$

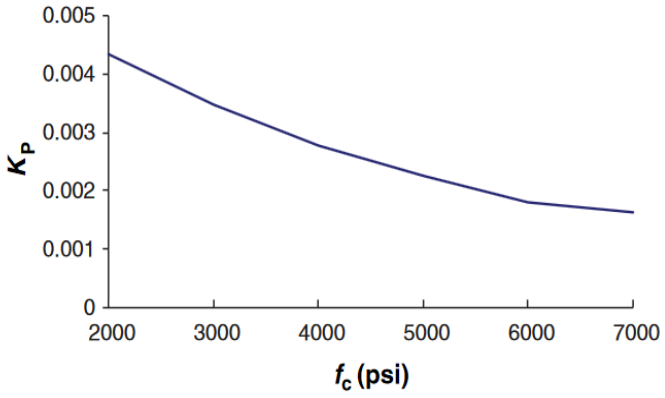

Figure 2.6 Variation of Concrete Penetrability Kp with Unconfined Compressive Strength of Concrete fc (Li et al., 2005)

2.4.3 Numerical Methods of Concrete Structures under Impact Loading

As presented by Zielinski, 1984 many cases of idealized structures subjected to impact loading had been described by writing the governing equations of continuum dynamics into differential form and solving them with the aid of computer. Besides the finite difference method (FDM) the finite element method (FEM) should be mentioned as most widely applied in the advanced analysis of concrete structures. In the FEM an actual structure is idealized by a system of discrete elements of defined loaf-deformation characteristics. The elements are interconnected at nodal points and the behavior of the assembly of these finite elements approximates the behavior of the actual structure.

Zielinski, 1984 mentioned that the governing equations of continuum dynamics can be expressed in the FEM as follows:

$$[M]\ \ddot{\Delta} + [K]\ \Delta = F(t) - F_d(t) \qquad (2.9)$$

Where:

$[M]$ = mass matrix

Δ = displacement vector

$\dot{\Delta}$ = velocity vector

$\ddot{\Delta}$ = acceleration vector

$[K]$ = stiffness matrix

$F(t)$ = external load vector

$F_d(t)$ = damping load vector $(\alpha\ [M]\ [\dot{\Delta}])$

As had been presented by Zielinski, 1984 various techniques had been used for mesh description (Langragian, Eulerian or hybrid) and for time integration (implicit, explicit or mixed), depending upon the particular subject of the dynamic analysis and upon capabilities of available computer codes. In Langrangian codes the computational grid is fixed in the material and follows its motions and distortion whereas in Eulerian codes the computational grid is

fixed in space so that the material passes through it. Explicit methods of time integration enable displacements to be determined at any particular time $t + \Delta t$, even if the accelerations at that time step are not known. In implicit methods, the displacements at any particular time $t + \Delta t$ cannot be calculated without knowledge of the accelerations occurring at that time. Implicit methods such as the β-method or the θ-method are unconditionally stable and deserve particular attention for dynamic loading problems. Explicit methods are more appropriate for wave propagation problems (hard impact). These mentioned techniques for dynamic FEM analysis have several advantages and disadvantages. It must therefore be carefully considered which approach is most appropriate for analyzing particular problems of local and overall response of structures to impact loading.

2.5 Classification of Impact

Mortas, 2013 postulated that impact may be defined as the relatively sudden application of an impulsive force, to a limited volume of material or part of a structure. He stated that generally, impacts are categorized into either low or high velocity (or sometimes hyper velocity), but there is not a clear transition between categories and authors disagree on their definition. Mallick, 2007 and Pashah et al., 2008 defined the separation between the low and high velocity impacts on the basis of the plastic deformation near the contact zone. In practice, the impact condition may range from the accidental dropping of hand tools to high speed collisions and the response of a structure may range from localized damage to total disintegration.

According to Kiran et al., 2017 the classification of soft and hard impacts was introduced by Eibl, 1987 and Kœchlin & Potapov, 2009 depending on the deformation of the impactor (projectile) with respect to the deformation of the target. They stated that soft impact is where the resisting structure remains undeformed and the kinetic energy of the striking body is completely converted into deformation. They defined hard impact as where the striking body is rigid and kinetic energy of the striking body is completely or partially converted to the deformation of the resisting structure.

Alternatively, Yao, 2016 categorized the impact problem can be categorized as low velocity (1~10 m/s), medium velocity (10~100 m/s), and high velocity (100~1000 m/s) impact problems. These velocity ranges were also used to define low, medium, and high velocity experiments. Based on these experimental results, different types of empirical equations had been proposed for estimating local damage to reinforced concrete members in terms of penetration depth, scabbing limit, and perforation limit. He conducted that the most accurate and reliable approach to investigating structural behavior under impact loading is to conduct impact experiments.

Robinson and Davies, 1992 defined low-velocity impacts as being one in which the through-thickness stress wave plays no significant part in the stress distribution and suggested a simple model to give the transition to high velocity. A cylindrical zone under the impactor was considered to undergo a uniform strain as the stress wave propagates through the plate, giving the compressive strain as shown in equation (2.10) below:

$$\varepsilon_c = \frac{impact\ velocity}{speed\ of\ sound\ in\ the\ material} \tag{2.10}$$

Antoniou, 2018 reminded that a simple system was explained as in (Figure 2.7) by Daudeville and Malécot, 2011 consisting of two colliding bodies, m_1 the projectile with initial striking speed, m_2 the structure which is motionless before the impact, a contact spring with stiffness k_1, in between the two masses to represent the force of the deforming bodies after contact, and another spring with a stiffness k_2 to simulate the resisting capacity of the structure was used to describe the impact. This model separates the two types of impacts by accounting only for the deformability of the two bodies. Nonlinear force-deformation relationships define the two springs.

The following differential equations of motion (2.11) describe the system mentioned by Daudeville and Malécot, 2011:

$$m_1\,\ddot{x_1}(t) + k_1[x_1(t) - x_2(t)] = 0 \qquad (a)$$

$$m_2\,\ddot{x_2}(t) - k_1[x_1(t) - x_2(t)] + k_2\,x_2(t) = 0 \qquad (b)$$

(2.11)

If the structure displacement is negligible compared to the projectile $x_1(t) \gg x_2(t)$ then:

$$F(t)=k_1\, x_1(t) \tag{2.12}$$

Thus, the equations of motion (2.11) were decoupled to give the equation (2.12). It is possible to find $x1$ by solving equation (2.12). Then, the impact force F(t) is computed from the equation (2.12) and finally, equation (2.13) gives the response of the structure:

$$m_1\, \ddot{x_1}(t)+ k_1\, x_1(t)=0 \qquad (a)$$

$$m_2\, \ddot{x_2}(t)+k_2\, x_2(t)=F(t) \qquad (b) \tag{2.13}$$

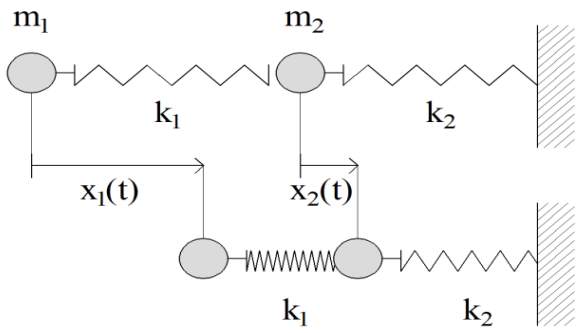

Figure 2.7 Simple Model of an Impact Using a Two-Mass System (Daudeville and Malécot, 2011)

As had been shown by Daudeville & Malécot, 2011 soft impact is defined as the case where the target resists impact with no deformations; hence the kinetic energy of the projectile is wholly transferred to its deformation, see Figure 2.8. Conversely, when $x_1(t) \ll x_2(t)$ the two equations of motion cannot be uncoupled and the impact is called hard, whereas the kinetic energy of the rigid projectile is fully or partially absorbed by deformation of the target Figure 2.9.

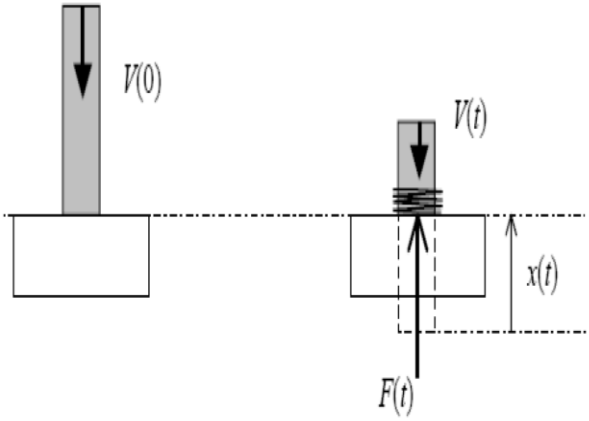

Figure 2.8 Soft Impact(Daudeville and Malécot, 2011)

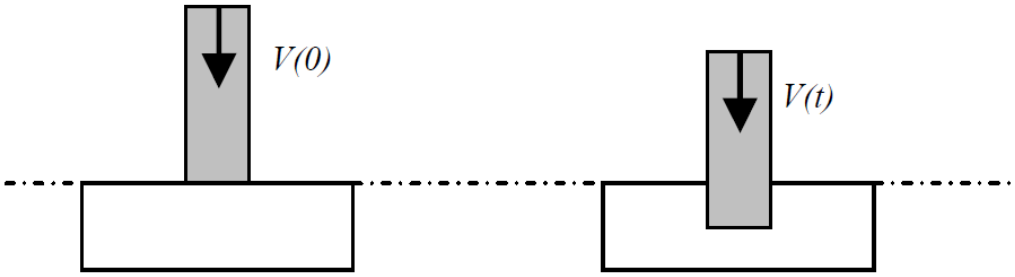

Figure 2.9 Hard Impact(Daudeville and Malécot, 2011)

2.6 Impact Experiments

Bhaduri, 2018 stated that the impact test is a dynamic test, carried out with notched specimen and known as notched-bar impact test. The function of impact loading is to increase the strain rate, whereas the notch not only creates triaxiality but also causes stress concentration, which in turn increases the strain rate many fold.

The impact blow may be applied by means of:

(1) A dropping weight;

(2) A swinging pendulum; or

(3) A rotating flywheel. The rotating flywheel type of machine is capable of providing very high impact velocities.

Again, the specimen is ruptured in impact test by:

• A single blow;

• Repeated blows of constant magnitude; and

• Repeated blows of increasing magnitude, known as 'increment-drop' test, in which the drop-height of the weight is increased gradually until the specimen breaks.

X. Yao, 2016 supposed that reinforced concrete member may respond to impact load locally or globally. When global response dominates, the energy transferred from the impactor to the impacted member is mainly dissipated through the global deformation of the member. When local response dominates, the transferred energy is mainly dissipated through reinforced concrete member's local damage and deformation around the impacted area.

Ruta, 2018 categorized the damage forms of reinforced concrete members under impact loading as shown in Figure 2.10. Figure 2.10 indicates that light local damage on reinforced concrete members occurs where penetration and concrete scabbing happens in the front surface. A more severe impact would cause concrete spalling in the rear surface of the member. By further increasing the impact load, the member may fail in perforation or punching shear. Typical flexural behavior is shown also in Figure 2.10.

As outlined by Sangi, 2011, When subjected to impact, the target structure may respond in several ways depending on the nature of the impact.

Local response: Local damage only, as majority of the impact energy dissipated around the impact zone.

Global response: Bending and deformation of the entire reinforced concrete member.

Combined response: combination of both local and global damage.

The terminology of the different damage modes phenomena was introduced by Kennedy, 1976. The seven phenomena during a hard impact had been defined as:

Penetration: Tunneling into the target by the projectile (the length of the tunnel is called the penetration depth).

Cone cracking and plugging: Formation of a cone-like crack under the projectile and the possible subsequent punching-shear plug.

Spalling: Ejection of target material from the proximal face of the target

Radial cracking: Global cracks radiating from the impact point and appearing on either the proximal or distal face of the concrete slab

Scabbing: Ejection of fragments from the distal face of the target

Perforation: Complete passage of the projectile through the target

Overall structural responses and failures: Global bending, shear and membrane responses as well as their induced failures throughout the target.

From the above impact effects, penetration, spalling, cone cracking, scabbing and perforation had been considered as local impact effects and were generally quantified by the following measurements as defined by Li et al., 2005:

Penetration depth(x): the depth to which a projectile penetrates into a massive concrete target without perforation.

Scabbing limit (h_s): the minimum thickness of the target required to prevent scabbing.

Perforation limit (e): the minimum thickness of the target required to prevent perforation.

Ballistic limit (V_{BL}): the minimum initial impact velocity to perforate the target.

Jonas et al., 1982 and Tamayo, 2017 presented a soft impact perforation scenario on a reinforced concrete slab. They noted that, the duration of a soft impact was more prolonged, whereas the deformation of the projectile generates waves propagating

throughout the structure reflecting on the edges and superimposing on the existing stresses under the impacted area. The response of an impacted concrete structure was a combination of local damage due to a shear mode and global bending.

As had been reported by Yao, 2016 the responses of reinforced concrete structural components under impact loading are affected by many factors such as material properties, contact stiffness, impact energy, reinforcement ratios, contact area, boundary condition, etc. Due to the complex nature of impact problems, many impact experiments were carried out to study how these factors affect structural response.

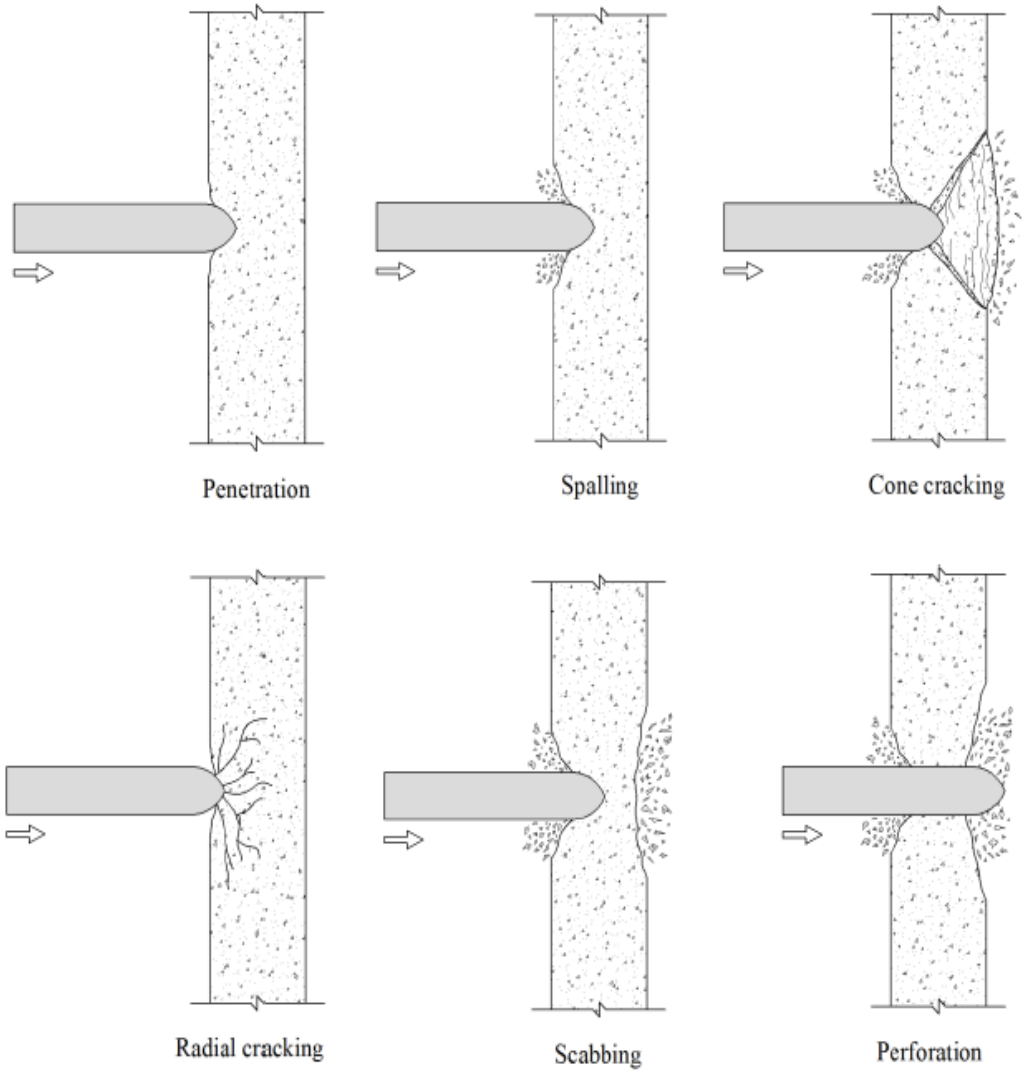

Figure 2.10 Missile Impact Effects on Concrete Target in Case of Hard Impact (Ruta, 2018)

2.7 Types of Impact Tests

Pellini, 1971 had developed tests to be performed on specimens at least 25 mm thick and their rational method of analysis. Some large-scale tests are described below.

2.7.1 Drop Weight Test (DWT)

Bhaduri, 2018 mentioned that: Drop weight test (DWT) was developed by Pellini and Puzak, 1964, particularly to measure the nil ductility temperature (NDT) of 15.9-mm-thick or more thick structural materials with an accuracy of ±5 °C and was quite reproducible. This test is not recommended for steels less than 15.9 mm thick.

According to ASTM, 2018 and Vivas et al., 2020 for this test, there were three standard flat plate-shaped specimens. Centrally located weld bead, approximately 50 mm long and 12.7 mm wide, was deposited on one surface of the plate specimen. At the centre of the length of the weld bead, a minute notch was introduced for initiation of crack. Care had to be taken to ensure that only the weld deposit was notched without cutting the specimen surface. The plate is placed with weld bead face down, as a simple beam in a holder having an anvil stop just below the weld bead and heated in a constant temperature bath to a desired test temperature.

As shown in Figure 2.11 and stated by Bhaduri, 2018, the specimen was impacted with a falling weight on the face opposite to weld bead and as a result, the crack-starter brittle weld bead deposited on the tensile face of the specimen was fractured at near yield stress levels. The impact load is provided by a guided, free-falling weight whose energy varies from 340 to 1630 J depending on the yield strength of the specimen material. The placement of anvil stop had been such as to prevent the specimen from deflecting more than a few tenths of an inch. It was noted that when the specimen was fully bent or deflected under load, the weld bead did not contact the anvil support.

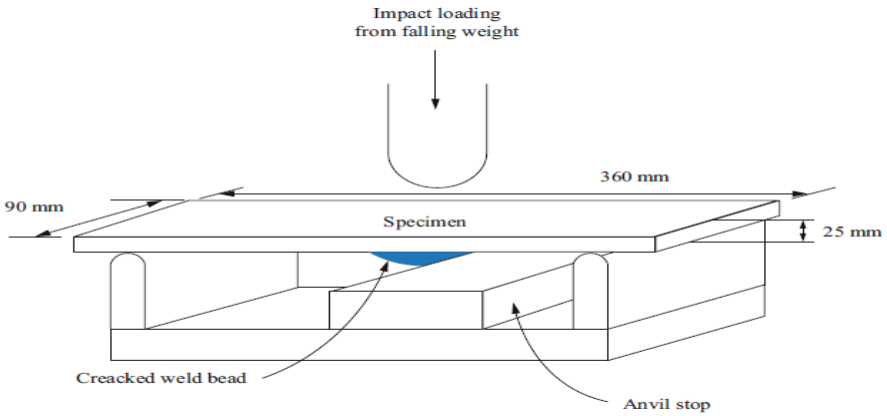

Figure 2.11 Schematic diagram of drop weight test (DWT) (Bhaduri, 2018)

2.7.2 Robertson Crack-Arrest Test

Bhaduri, 2018 carried out a Robertson Crack-Arrest Test that provided the relationship between the magnitude of applied stress and the temperature at which the material is capable of arresting a rapidly propagating crack. In this test, at one side of a 150 mm wide plate specimen, there is a saw cut that acts as a starter crack. The specimen is subjected to a thermal gradient across the plate width by applying heat at one side and using liquid nitrogen coolant at the other side such that the starter crack is at the lowest temperature, as shown in Fig. 2.12.

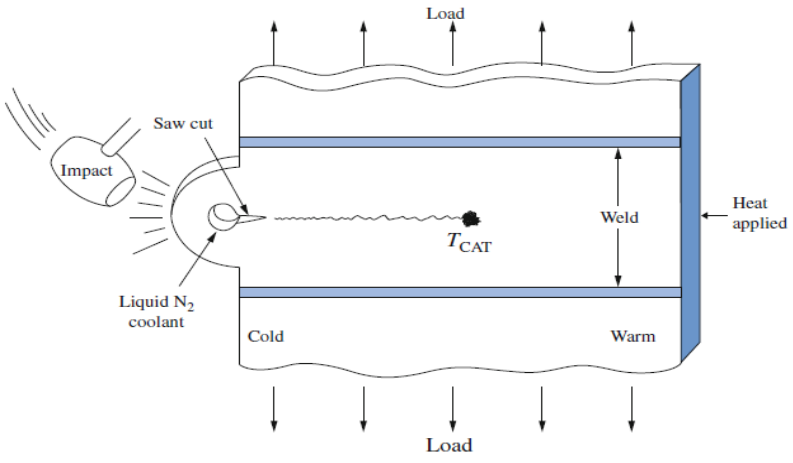

Figure 2.12 Robertson Crack-Arrest Test (Bhaduri, 2018)

2.7.3 Dynamic Tear (DT) Test

Bhaduri, 2018, also stated that the Dynamic tear (DT) test is a large Charpy test carried out on specimens of typically 455×120 and 15–25 mm thick, as shown in Figure 2.13, but the thickness of specimens may be as high as 300 mm.

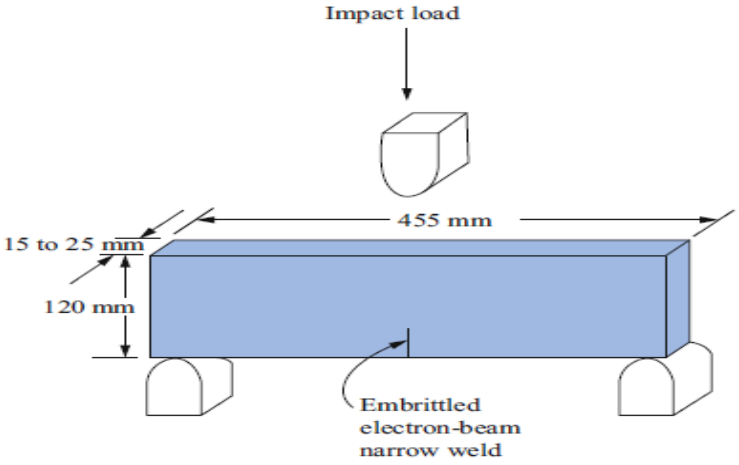

Figure 2.13 Dynamic Tear Test (DT) (Bhaduri, 2018)

2.8 Impacts on Concrete

Antoniou, 2018 defined impact loads as extreme severity loadings with a low probability of occurrence, and very short duration. Natural hazards: avalanches, rock falls or manmade hazards vehicles in a collision with structures, aircraft impacts on nuclear shielding barriers and military missile impacts induced devastating consequences. Therefore, it was necessary to thoroughly comprehend the mechanisms of concrete behavior under impact to develop sufficient design methods.

According to Kœchlin & Potapov, 2009, the study of impacts on structures started from the mid-17th century. For the purpose of safety regulations, national nuclear safety agencies and nuclear energy companies conducted several experimental campaigns to increase the knowledge about the local phenomena and damage modes of concrete structures subjected to impacts considering real-scale experiments and small-scale laboratory tests. They separated

these tests into two limited cases based on the velocity of the impactor and the strength of both impactor and structure.

Adhikary, 2014 motioned that there are typical examples comprised in diversified fields ranging from transportation structures (i.e., bridge piers, guard rails, traffic signal posts and electric poles etc.) subjected to vehicle-crash impact, falling rocks on rock-sheds in mountainous regions, falling heavy loads on industrial facilities due to accidents, marine and offshore structures exposed to ship and ice impact or subjected by tornado or tsunami-borne debris impact, columns in multi-story car park or bridge-pier strike by moving vehicle, protective structures subjected to projectiles or aircraft impact and structures sustaining shock and impact loads during explosions or earthquakes. Figure 2.14 depicts some of the impact loading scenarios on structures.

Also, Adhikary, 2013 stated that impact loading is an extremely severe loading conditions characterized by its application of a force of great intensity within a short duration. Impact loading can be categorized into two basic types: single point impact loading and distributed impact loading. When a structures strike by an impactor or striker at a particular point that is called single point impact; whereas explosions or blasts would bring about distributed impact loading.

Fujikake et al., 2009 had conducted experiments on the behavior of Reinforced Concrete (RC) beam under low velocity impact which consisted of two response phases as shown in Figure 2.15: the local response due to the stress wave that occurs at the impacting point during a very short period after impact; and the overall response that included the free vibration of the whole structural member. Load rate effects and dynamic behavior of the structural components primarily control the overall response. It was recognized that the structural members behaved differently under impact loading as compared to static loading. Furthermore, the effect of impact loading could result in catastrophic and sudden structural failure. So the understanding of the performance and vulnerability of RC structures under drop-weight impact loading has become an emerging topic in recent years.

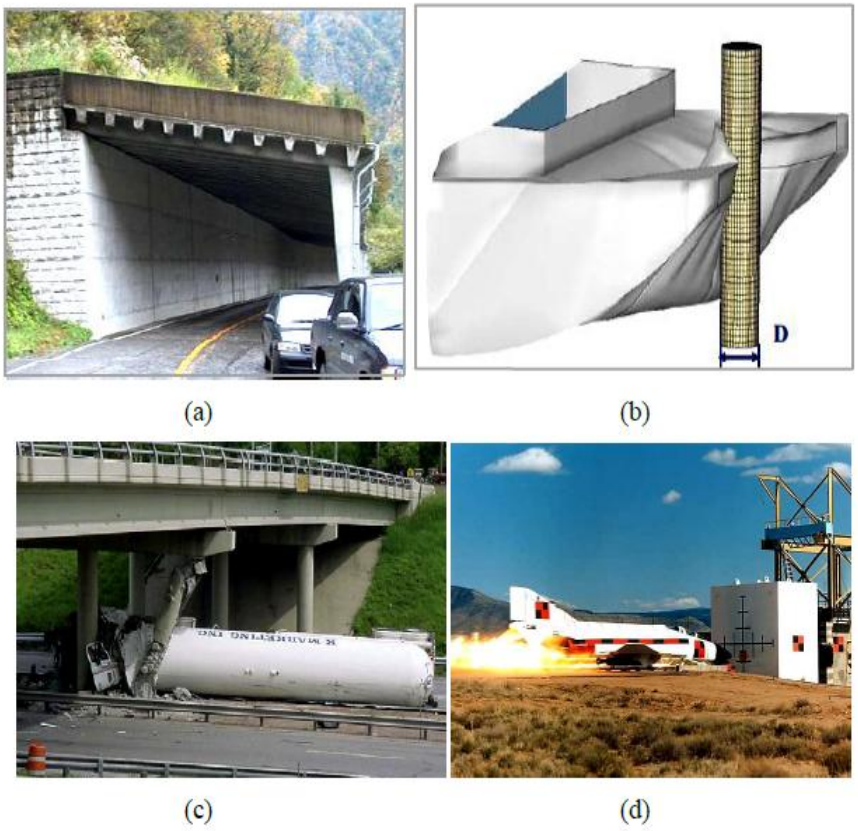

Figure 2.14 Impact Loading Scenarios on Structures:(a)(Yoshida et al., 2007);(b)(Yuan and Harik, 2010);(c) (Dahlberg, 2012); (d) (Sugano et al., 1993) (Adhikary, 2013)

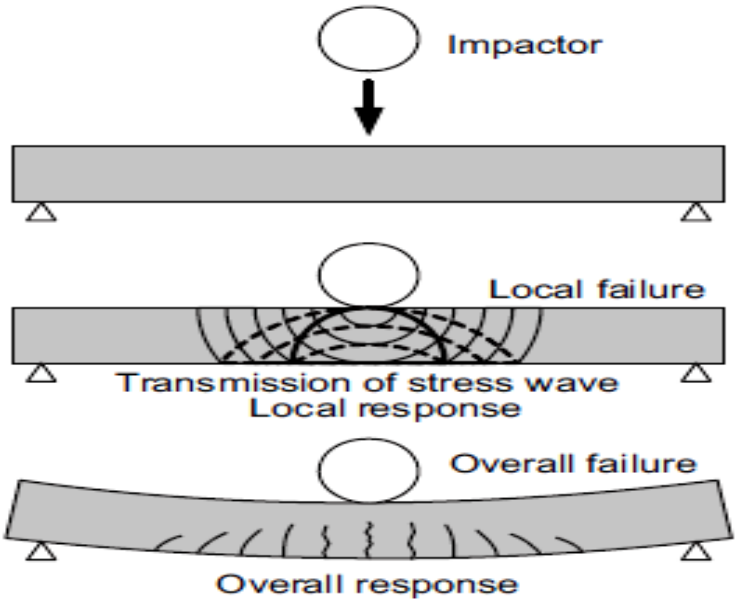

Figure 2.15 Impact Responses of a RC Member (Fujikake et al., 2009)

2.9 Fiber-Hybrid Fiber Reinforced Concrete Behavior under Impact Loading

Groover, 2020 stated that: the word fiber means a single, continuous material whose length is at least 200 times its width or diameter and filaments are endless or continuous fibers. Fibers are filaments of reinforcing material, generally circular in cross-section, although alternative shapes are sometimes used (e.g., tubular, rectangular, hexagonal). Diameters range from less than 0.0025 mm to about 0.13 mm, depending on material.

There are two different classes of fibers mentioned as presented by Mortas, 2014: natural (fibers from mineral, plant and animal sources) and synthetic (man-made) fibers. Within these two classes, synthetics are usually more uniform in size are more economical to use and behave in a more predictable manner. For engineering applications the most commonly employed significant fibers are glass fibers, metallic fibers and organically-derived synthetic fibers. Most strong and stiff fibers (e.g., ceramic fibers of glass, graphite-carbon, boron carbide and silicon carbide) are usually difficult to use as structural materials in bulk. However, embedding such materials in a ductile matrix (such as a polymer or metal) enables them to behave as a stronger, stiffer and tougher material.

Prakash, 2017 defined Fiber Reinforced Concrete (FRC) as a composite material consisting of mixtures of cement, mortar or concrete with discontinuous, discrete, uniformly dispersed suitable fibers. Continuous meshes, woven fabrics and long wires or rods are not considered to be discrete fibers. Also, Fiber reinforced concrete was defined as a concrete containing fibrous material which increases its structural integrity. It contains short discrete fibers that are uniformly distributed and randomly oriented. Fibers were generally classified into two: organic and inorganic. Inorganic fibers included steel fibers and glass fibers, whereas organic fibers included natural fibers like coconut, sisal, wood, bamboo, jute, sugarcane, etc and synthetic fibers were based on acrylic, carbon, polypropylene, polyethylene, nylon, aramid, and polyester. Within these different fibers the character of fiber reinforced concrete changes with varying concretes, fiber materials, geometries,

distribution, orientation and densities. Thus, Figure 2.16 explains tensile loads versus deformation for plain and fiber reinforced concrete.

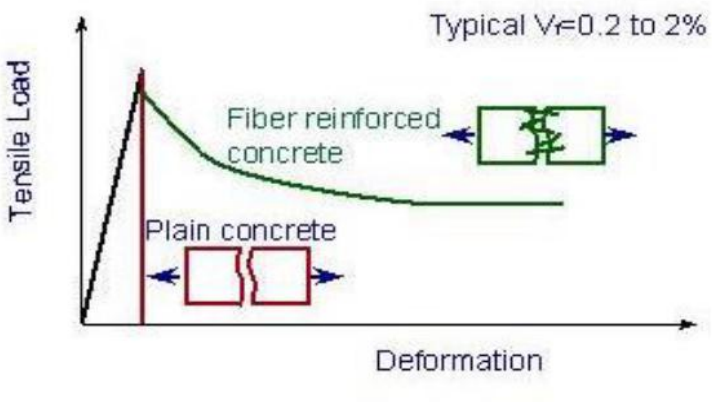

Figure 2.16 Tensile Loads versus Deformation for Plain & Fiber Reinforced Concrete (Prakash, 2017)

Yao et al., 2020 indicated that among the polymer fibers, polypropylene (PP) and polyvinyl alcohol (PVA) fibers had attracted most attention due to the outstanding toughness for concrete reinforced with them. The properties of FRC were improved at a certain level, but not whole levels if reinforced with only one type of fiber. For instance, steel fibers were supposed to strengthen concrete at the coarse aggregate scale, while PP or PVA fibers were suitable for the fine aggregate-scale crack prevention, and carbon nanotubes were proven to improve the strength at the scale of cement grains.

Figueiredo & Ceccato, 2015 mentioned that: the fibers act as a barrier to coarse aggregates movement reducing the materials mobility. So, increasing the aggregate size or the fiber aspect ratio the flowability of the material will be reduced.

2.9.1 Steel Fiber Reinforced Concrete

Latif, 2012 pointed that: steel fibers were the most commonly used in concrete. Their common use was based on the considerations of costs, availability, stability at high temperatures, as well as overall improvement in mechanical properties.

Prakash, 2017 suggested that steel fiber may be produced either by cutting wires, shearing sheets or from a hot melt extract. They may be smooth, or deformed in a variety of ways to improve the mechanical bond with concrete. Steel fibers have high modulus of elasticity which is 10 times that of concrete, reasonably good bond and high elongation at fracture. Steel fibers range in length from 0.25 inches to 3.0 inches (see Figure 2.17). Fiber concentrations in concrete mixes generally range from 0.1 % to 1 % by volume. Present applications of steel fiber reinforced concrete with and without normal reinforcement have been in the areas of factories, pavements, overlays, patching, hydraulic structures, thin shells, and armour for jetties, rock slope stabilization, mine tunnel linings, and precast products. Addition of steel fibers does not significantly increase compressive strength, but it increases the tensile toughness, and ductility. It also increases the ability to withstand stresses after significant cracking (damage tolerance) and shear resistance. It is now well established that one of the important properties of steel fiber reinforced concrete (SFRC) is its superior resistance to cracking and crack propagation. As a result of this ability to arrest cracks, fiber composites possess increased extensibility and tensile strength, both at first crack and at ultimate, particularly under flexural loading; and the fibers are able to hold the matrix together even after extensive cracking. The net result of all these is to impart to the fiber composite pronounced post – cracking ductility which is unheard of in ordinary concrete. The transformation from a brittle to a ductile type of material would increase substantially the energy absorption characteristics of the fiber composite and its ability to withstand repeatedly applied, shock or impact loading.

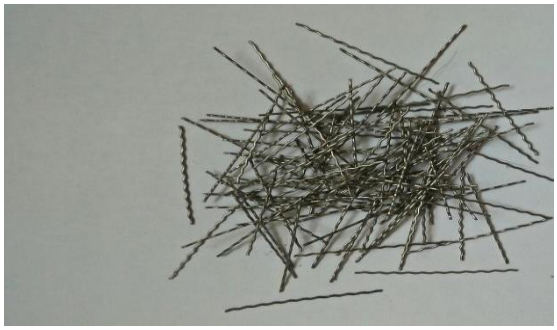

Figure 2.17 Steel Fiber (Prakash, 2017)

Many researchers such as Al Nussairi, 2018, Bazgir, 2016, Pichandi et al., 2013 and Brandt, 2008 mentioned that there were several types of steel fibers that have been used in the past. Apart from other mix constituents, there were four important features of steel fiber that were found to have an effect on the properties of the composite, namely: type (i.e. shape), volume fraction, aspect ratio (the ratio of length to the diameter of the steel fiber) and orientation of fibers in the matrix. Recently, optimization of these parameters had been studied to improve the fiber matrix bond characteristics and to enhance fiber dispensability. It was found that SFRC containing hooked end stainless steel wires had superior physical properties compared to straight fibers. This was attributed to the improved anchorage provided and higher effective aspect ratio than that of the equivalent length of the straight fiber. Also, the size, the shape and the content of the coarse aggregates as well as the geometry and the volume fraction of steel fibers affected the workability of concrete. At a given fiber diameter and volume fraction, compatibility was linearly related with the aspect ratio (l_f/d_f) of the fibers. The relative fiber to coarse aggregate volume and the 'balling up' phenomenon governed the maximum possible content of steel fibers.

Bazgir, 2016 characterized the performance of different types of steel fibers by the following three parameters (Figure 2.18):

- The aspect ratio (L/D)
- The tensile strength
- The bond between fibers and the matrix (dependant on fiber type)

ACIFC, 1999 compared steel fibers to traditional fabric reinforcement, and noted that they have a tensile strength typically 2-3 times greater and a significantly greater surface area to develop bond with the concrete matrix.

Bazgir, 2016 also, supposed that these parameters will affect the performance of steel fiber in concrete as well as the interaction between fibers and concrete matrix. For example, a steel fiber with high tensile strength which has bad bond in concrete most likely will not perform as the steel tensile strength could permit. The combination of these three parameters will give a toughness value at a certain dosage. However, for different dosages (volume fraction of fibers in concrete), the toughness value for a specific steel fiber will vary.

Knapton, 2003 found that the stresses induced on a concrete slab were complex depending on the load that was applied to the

member. In addition, there were number of stresses which were difficult to measure, arising from a number of causes such as shrinkage and thermal effects, sharp turns from fork lift trucks, and impact loads.

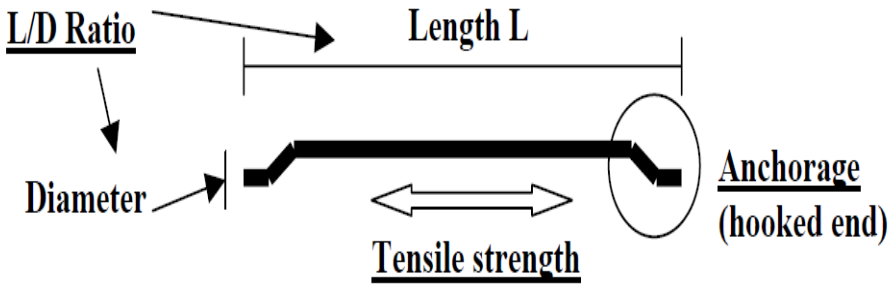

Figure 2.18 The three Important Parameters of a Steel Fiber (Bazgir, 2016)

Knapton, 2003 summarized the advantage of using steel fiber as follows:

- Producing more ductile concrete with a smaller number of cracking
- Reduction of the influence of shrinkage cracking
- High tensile strength
- High compressive strength
- Higher economically efficient compared to conventional steel solutions and enhance costs with lesser fiber amount
- Reducing schedule time due to fast installation
- Reducing the permeability in concrete, which ensures protection of concrete due to the negative effects of moisture
- Easy material handling
- High durability
- Can replace wire mesh in most elevated slabs.

Also, he presented the disadvantages as:

- There are problems involved in attaining uniform distribution of fibers and dependable concrete properties
- At aggressive exposure conditions the corrosion of the surface could take place, influencing the look of the surface
- The use of Steel Fiber Reinforced Concrete (SFRC) required more accurate configuration as opposed to normal concrete
- Reduced workability

2.9.2 Polyvinyl Alcohol (PVA) Fiber

Wang, 2017 reached that polyvinyl alcohol (PVA) fiber had very high elastic modulus and tensile strength that can improve the strength and stiffness of concrete. Polyvinyl alcohol – engineered cementitious composite (PVA – ECC) had a strain – hardening behavior and the capacity of tensile strain can reach 4%. The tensile strength of polyvinyl alcohol (PVA) fiber was between 1600 and 2500 MPa and the cost of PVA fiber was even lower than that of steel fiber based on an equal volume. However, numerous researches represented that PVA fiber reinforced cementitious composites had shown relatively low strain capacities, evenly lower than 0.5%. They were not defined as high – performance based on the aforementioned criteria. The reason for this situation was explained by the sturdy interfacial chemical bond between PVA fiber and cement paste. In order to solve this problem, they introduced an oil agent to modify the extra bonding strength, which improved the performance of PVA – ECC materials.

2.9.3 Forta ECONO-MONO Fiber

It is easy to finish micro synthetic fiber, made of 100% virgin Homopolymer polypropylene monofilament. This economy-grade fiber functions as a plastic shrinkage reinforcement intended to reduce the formation of shrinkage cracks prior to initial set and to reduce settlement shrinkage. ECONO-MONO is non-corrosive, chemically inert, and 100% acid and alkali proof. ECONO-MONO is used in concrete applications such as slabs-on-ground, curbs, driveways, sidewalks, basement floors, garage floors, colored concrete, and small precast products – anywhere that the objective is to control plastic shrinkage cracking while improving basic durability properties. It requires no mix design or placement changes.

2.9.4 Hybrid Fiber Reinforced Concrete (HFRC)

In practice, hybrid fibers were incorporated in a common cement matrix, and the hybrid fiber-reinforced concrete (HFRC) could offer more attractive engineering properties because the hybrid composite derives benefits from each individual fiber and exhibits a synergetic response. In addition, HFRC showed improved structural behavior compared to conventional concrete, such as less spalling and scabbing under impact loadings. Previously, most of

the fiber reinforcement research had been carried out to examine tensile strength, flexural strength and drop-weight impact toughness. Only some work dealt with the blast or impact resistance performance affected by fiber content and type, since the extreme loading tests were costly and even dangerous.

As stated by Sivakumar et al, 2021 :there is a hardly anyone type of fiber that can improve all the desired properties of fresh and hardened concrete. To improve all properties of concrete the combination of two or more types of fibers is required and the composite is known as "hybrid fiber reinforced concrete". The basic purpose of using hybrid fibers is to control cracks at different size levels in different zones of concrete, stress levels and to enhance the properties of concrete by combining the benefits that each particular fiber type can impart.

In most cases, fiber reinforced concrete (FRC) contains only one type of fiber. The use of two or more types of fibers in a suitable combination has the potential to improve the mechanical properties of concrete, and result in performance synergy. This combining of fibers, often called hybridization (Banthia et. al, 2014).

Almusallam et al., 2013 suggested that: to improve the impact resistance and ductility of slabs, addition of hybrid-fibers (i.e. fibers containing steel and plastic fibers in different proportions) in the preparation of concrete mix could be an efficient technique.

The combination of fibers up to a certain ratio in the mixtures triggers high tensile ductility (approximately 3% axial tensile strain capacity) along with narrow crack openings [Özkan & Demir, 2020 , Hu et al.,2019].

Moreover, the hybridisation of steel and PP can improve the load bearing capacity [Qian & Stroeven, 2000], impact resistance [Song et al., 2005].

2.10 Previous Work Related to Behavior of Fiber Reinforced Concrete under Impact Load

Although experimental research is important to determine the accurate behavior of the system and to form a deep knowledge

about its variables, it is still expensive and takes a considerable amount of time to perform a comprehensive research. On the other hand, numerical simulation and analysis helps in investigating the effect of each variable on the system and in studying an unlimited number of cases while saving time and money. Therefore, accurate modeling of the system increases the confidence in adopting it and consequently helps its development and the spread of its use.

As stated by Sangi, 2011 reinforced concrete slabs are mostly subjected to local damage due to impact loads. There had been a number of experimental studies on the local effect of hard projectiles on reinforced concrete targets (mainly slabs), which had resulted in a large number of empirical formulae.

Kishi et al., 1997 investigated the dynamic behavior of slabs; large scale reinforced concrete slabs were tested under impact loading. Nine rectangular specimens measuring 4 m wide and 5 m long were repeatedly loaded onto the centre by a steel weight falling freely. Masses of 1000, 3000 and 5000 kg were used depending on slab thickness. The collapse was assumed when the accumulated residual displacement reached $1/200^{th}$ of span length. Variations of the slab thickness (25, 50, 75 cm), reinforcement ratio (0.5, 1.0 %), reinforcement arrangement type (single and double arrangements) and reinforcement material were considered. The impact behavior was considered by recording maximum impact force, reaction force, residual displacements and crack patterns. The experiments showed that the maximum impact force was more affected by slab thickness than reinforcement ratio, material strength and the reinforcement arrangement type. The failure under repeated impact loading was initiated by flexural cracks, but final failure was due to punching failure. They estimated the punching shear capacity assuming a conical shape shear failure neglecting the reinforcement.

Nine slabs with dimensions of 90×1524×3353 mm were tested under impact loading by Zineddin and Krauthammer, 2007. Effects of locations of welded steel wires, the section area of these steel bars and the impact drop height on the impact behavior were investigated in their study. Analyzing the results in terms of failure

mode, crack pattern and peak load, they had shown that the quantity and type of mesh reinforcement and the dropping height had an important role in defining the global slab collapse, i.e. increasing the hammer falling height, the slab failure was characterized by local behavior with punching shear and huge shear cracks on both top and bottom faces (Figure 2.19). The tests were instrumented using load cell, accelerometers, deflection gauges, reinforcement strains and high-speed videos. Figure 2.20 shows the load-time histories of slabs subjected to 610 mm drop.

Another study was made by Kishi et al., 2011, in which slabs with three kinds of support conditions were tested under impact load and the results were compared to numerical analysis (Figure 2.21). It was found that maximum impact forces did not vary with support conditions as well as maximum deflections. Impact forces obtained from numerical analysis were relatively smaller compared to experimental results.

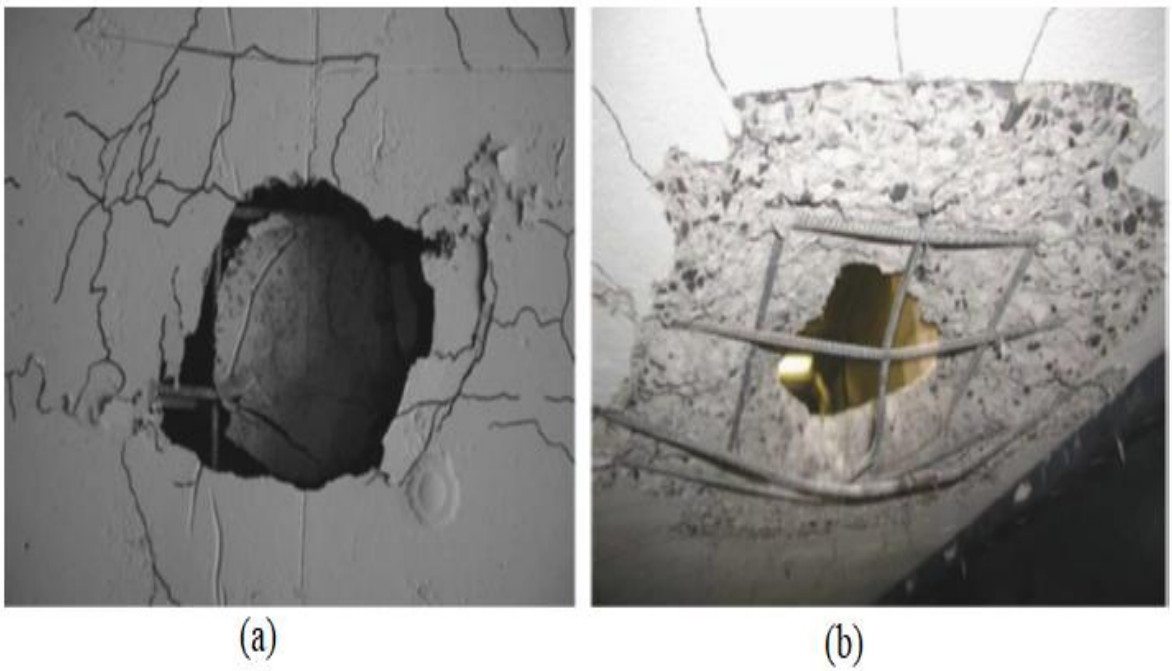

Figure2.19 Experimental Results in Terms of Failure and Crack Propagation for the Slab (610 mm drop height: (a) impact face; (b) bottom face (Zineddin and Krauthammer, 2007)

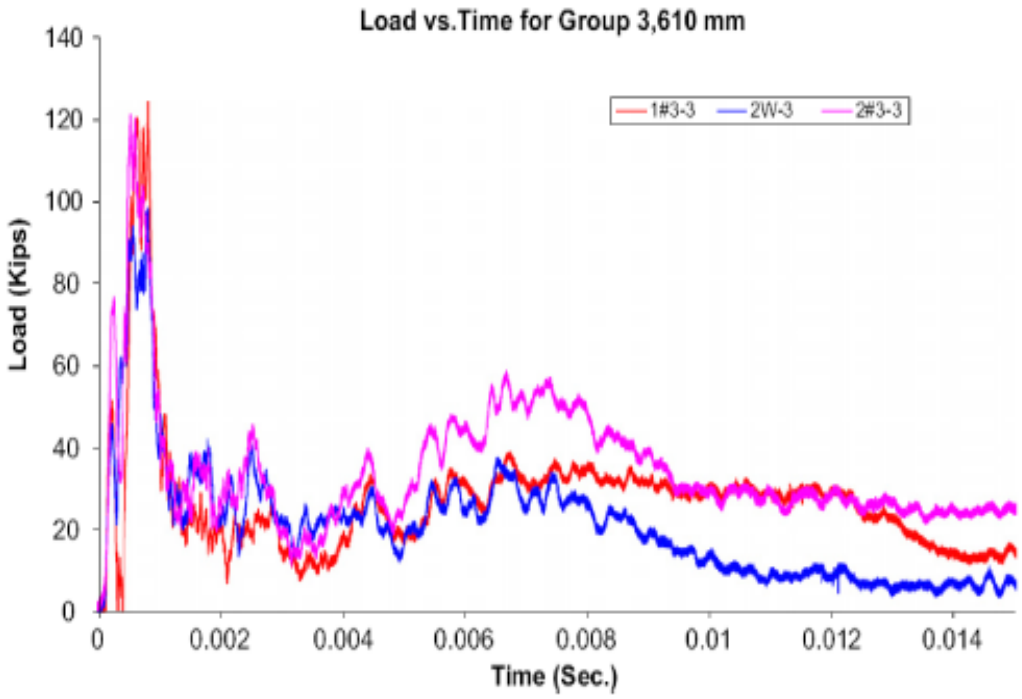

Figure 2.20 Load- Time Histories of Slabs under 610 mm Drop (Zineddin and Krauthammer, 2007)

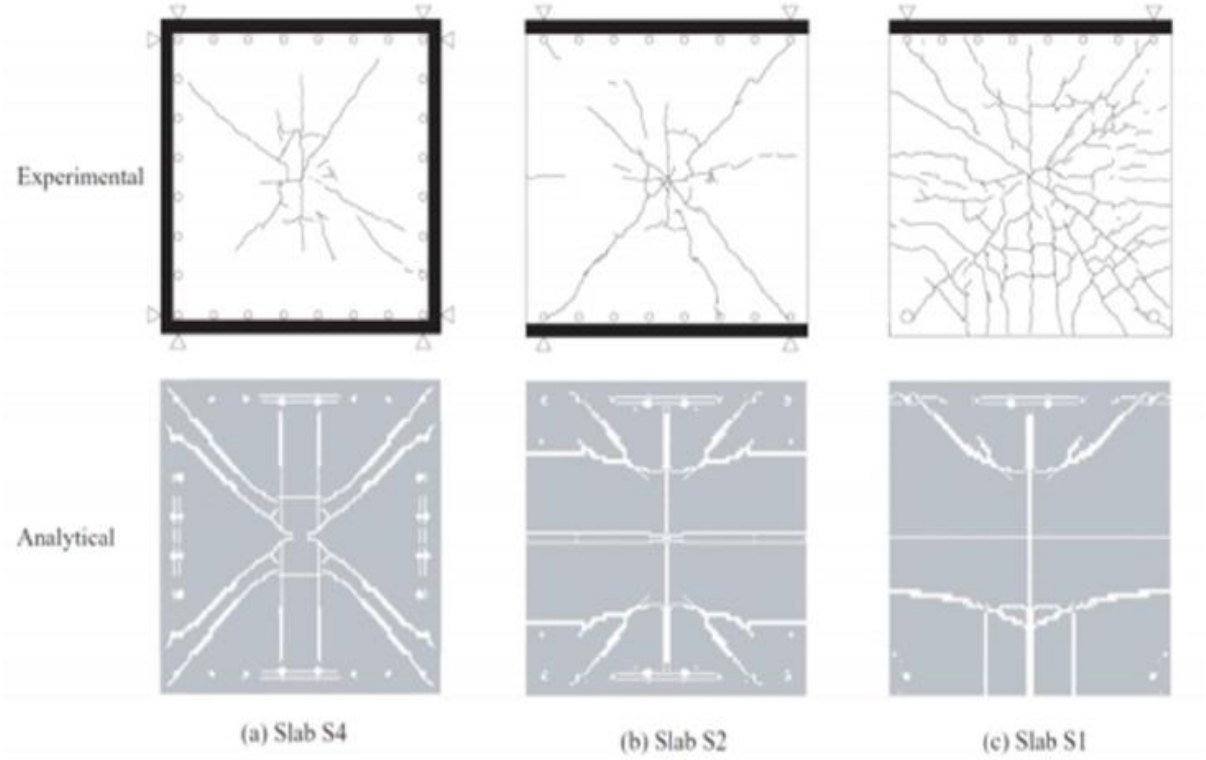

Figure 2.21 Crack Patterns (Kishi et al., 2011)

Experimental studies were carried out by Ong & Paramasivam, 1999 to observe the performance of steel fibers under impact loading. In their study, effectiveness of different kinds of fibers under impact loading was investigated. Mixtures with 1:1.3:2.1, cement: coarse aggregate: Fine aggregate and 0.4 water-cement ratio was used in the study. Three different types of fibers were used in exactly same mixtures. Ordinary Portland cement and crushed aggregate of maximum ten millimeters size were used. Specimens with area of $1m^2$ and depth of 30 mm were cast. Varying amounts of fiber (0.5%, 1.0% and 2.0% by weight) were added to the concrete mix. Slabs were simply supported at all four edges. Impact loading was applied by a fabricated guide (Figure 2.22). The specimens were tested by dropping hemi-spherical nose shaped projectile of mass 43 kg from a height of 4000 mm. Test setup was as presented in Figure 2.22. In case of plain concrete members, the result of the impact event was catastrophic. As presented in Figure 2.23 the projectile penetrated the slab, and then shear cone shaped fracture was formed. Slab lost its integrity and gained momentum as a result of radial crack formation. As presented in Figure 2.24 similar results were obtained in the specimens with the fraction of 0.5% fiber for both polyolefin and polyvinyl alcohol fibers (PVA) fibers. But in case of steel fibers, no such catastrophic results were observed; no penetration occurred in concrete members with steel fibers.

In case of members with polyolefin 0.5% in volume, penetration occurred. By adding the fiber between the amounts of 0.5% to 2.0% some improvements, such as improvement in integrity, number of cracks or width of cracks, were obtained. Members with PVA fibers could not keep their integrity after impact event. They failed in a manner similar to plain concrete members.

Members with steel fibers performed significantly better than other members. In case 0.5% steel fiber addition, penetration, shear cone and radial cracks occurred. In case of 1.0% and 2.0% steel fiber case, size of shear cone and the width of cracks decreased compared to these in specimens with 0.5% fiber contents. For 0.5%, 1.0% and 2.0% steel fiber contents, 24 mm, 12 mm and 4.5

mm residual displacements were obtained. Thus, by adding more steel fiber the stiffness of the member could be increased. Furthermore, in case of 2.0% steel fiber no crack was observed on bottom side.

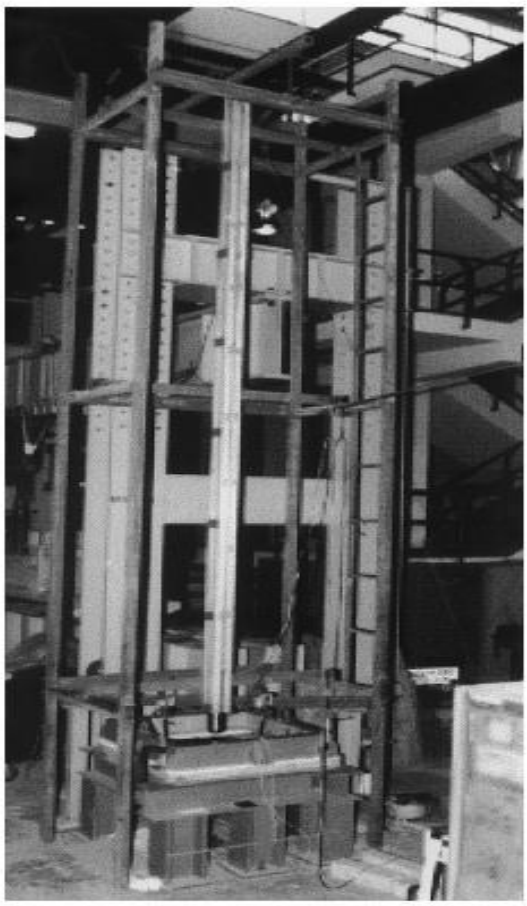

Figure 2.22 Drop-Weight Impact Test Setup (Ong & Paramasivam, 1999)

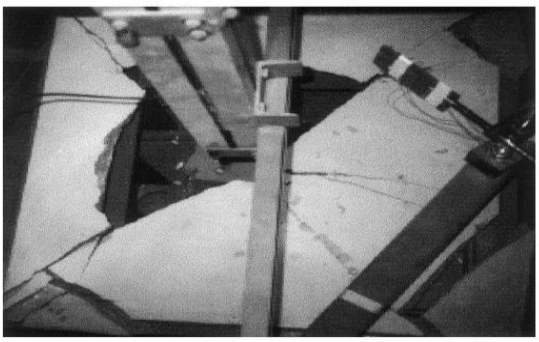

Figure 2.23 Failure of Plain Concrete Slab (Ong & Paramasivam, 1999)

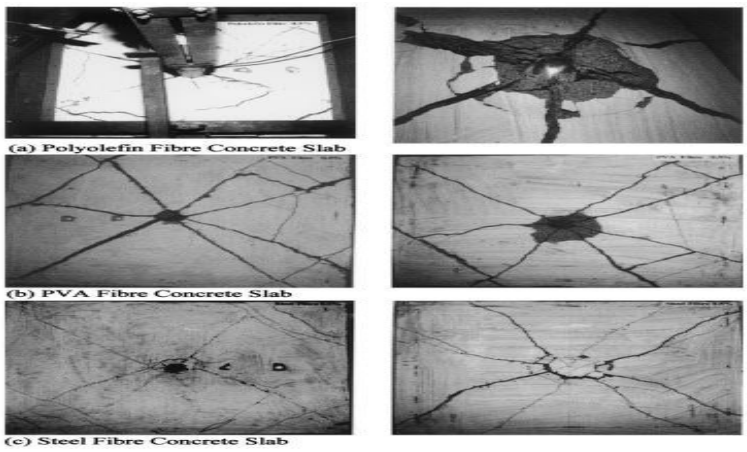

Figure 2.24 Failure Patterns of Slabs Containing 0.5% Volume Fraction of Fibers (Ong & Paramasivam, 1999)

Ong & Paramasivam, 1999 observed the formation of frustum shaped fracture zone and then formation of flexure cracks from center to corners before failure. Polyolefin fibers specimens failed due to pullout and rupture, whereas both steel and PVA fibers failed due to only pullout effect only along fracture surfaces. From Figure 2.25 it can be seen that, adding 2.0% fibers resulted in well behavior compared to 0.5% and 1.0% ones. As a result of increased fiber content both the duration of impact event and maximum peak load of the specimens were reduced. Thus stiffer response was obtained by adding more fibers. For example 36% and 56% reduction in displacement were obtained by increasing volume fraction of steel fiber from 0.5% to 1.0% and 1.0% to 2.0% respectively. Furthermore the duration of impact in 2.0% steel fiber was 50% of that of 0.5% steel fiber member. On increasing fiber fraction from 0.5% to 2.0%, was observed damage after the impact event was decreased. Difference of the damage could be seen from the comparison of results in Figure 2.25.

Hummeltenberg et al., 2011 investigated the behavior of normal concrete, high performance concrete (HPC) and ultra-high performance concrete (UHPC) with several types of longitudinal and shear reinforcement under impact. In the tests, concrete slabs with dimension of 1000×1000×150 mm were impacted with cylindrical steel projectiles(with 10 and 20 cm diameter) dropped

down from different heights (from 3 to 9 m). All the 15 tested slabs had the same longitudinal reinforcement formed by a layer of steel mesh of 150 mm spacing bars of 10 mm diameter. In addition, some slabs had also C shaped stirrups and some other additional fiber meshes reinforcement. The obtained results were then compared in terms of slab perforation (Figure 2.26), velocity and deformation histories. It was found that all the slabs with normal concrete and standard reinforcement, both with and without shear reinforcement, were almost completely perforated during the impacts. In case of HPC slabs, with and without fabric reinforcements, the entity of the perforation was much lower with a huge contribution of the additional reinforcement in contrasting the projectile penetration.

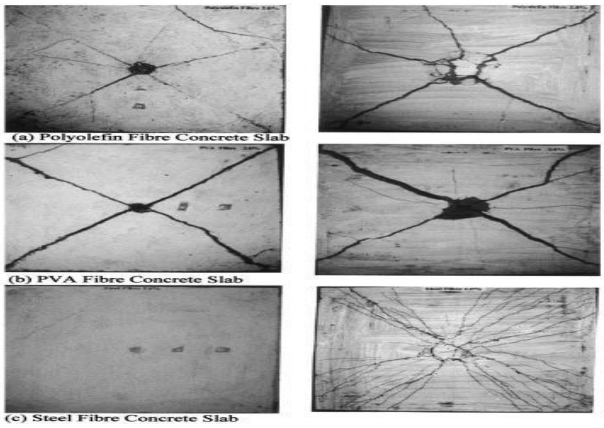

Figure 2.25 Failure Patterns of Slabs Containing 2.0% Volume Fraction of Fibers (Ong & Paramasivam, 1999)

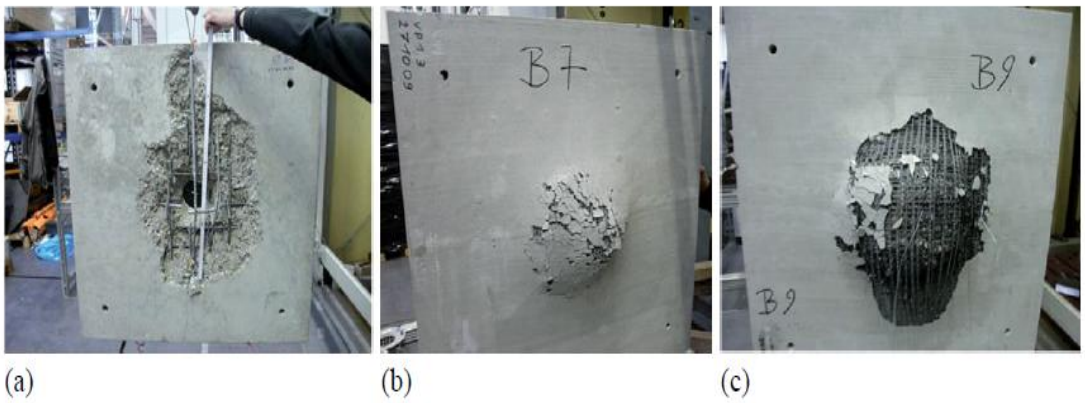

Figure 2.26 Slabs Perforation in Case of Normal Concrete with: (a) Additional Stirrups Reinforcement; (b) Additional Steel Fabric; (c) Additional Carbon Fabric (Hummeltenberg et al., 2011)

Parmar et al., 2014 carried out an experimental program where in a total number of eight reinforced concrete structures were tested under different loading conditions. Two tests were carried out on RC fire damaged frames and six tests on RC slabs with different thicknesses and combinations of thermal and impact loads. The six reinforced concrete slabs were characterized by plan dimensions of 1700×2000 mm. Two different reinforcement ratios and thicknesses corresponding to d equal to 200 and 150 mm were tested under variable impact conditions. During the impact tests all slabs were supported with the help of a supporting structure consisting of two steel frames, one below and the other above the slab. The impact on the center of the slab was achieved with the use of a steel punch designed to increase or decrease its weight by adding or removing standard weight circular plates from its head. Figure 2.27 shows the RC slab damage profile at the end of the impact test, with damage at the top and bottom slab surfaces. The steel punch stopped inside the slab, between the top and the bottom reinforcement layers without passing completely through the slab. The bottom concrete surface was damaged and scabbing phenomena occurred with concrete fragments expelled from the side. They stated that this was mainly due to the fact that the total impact energy was dissipated during the partial initial perforation of the slab and breaking of the top reinforcement.

Figure 2.27 Slab Damage Profile: (a) at the end of the impact test; details of (b) top and (c) bottom slab surface (Parmar et al., 2014)

Also, Dancygier, 2017 investigated the impact resistance of high-performance layered protective barriers. In particular the effects of the different concrete mix ingredients such as aggregate types and sizes, application of steel fibers were experimentally analyzed considering the main resistance parameters which included the extent of rear and front damage surfaces, the overall damage and the impact energy at the ballistic limit. He claimed that the results clearly showed that increasing the concrete compressive strength led to increased perforation resistance with a further increment by using large and hard aggregates that also caused a more extended rear and front damage. Moreover, it was seen that the damage was mitigated by application of steel fibers. The findings reported in the paper, suggested that a protective barrier be engineered to have layers that use these effects to produce better performance under impact.

Yoo et al., 2012 investigated the effect of fiber reinforced polymers (FRPS) strengthening and steel fibers on the enhancement of impact resistance of concrete slabs. Their research investigated the compressive and flexural behaviors under static loading conditions for normal strength concrete as well as steel fiber reinforced concrete (SFRC), including 30mm long end-hooked steel fibers in different volume fractions varying from 0.5 to 1.5%. The flexural strengthening effect of externally bonded Fiber Reinforced Polymer (FRP) sheets and steel fibers on one-way slabs was investigated in a high strain rate range conditions (i.e. impact tests) using a drop-weight impact testing machine. For this test prismatic specimens with dimension of 50mm×100mm×350mm were used (see Figure 2.28). Test results indicated that the flexural resistance of concrete is significantly improved by strengthening with FRP sheets and steel fibers.

Hrynyk & Vecchio, 2014 studied the behavior of steel fiber reinforced concrete slabs under impact load, (Figure 2.29). In their study seven intermediate-scale slabs were constructed and tested to failure under sequential drop-weight impacts. Three slabs were constructed using plain concrete and four slabs were constructed from a steel fiber-reinforced concrete (SFRC) mixture design with varied volumes 0.0, 0.5, 1.0 and 1.5% by volume of concrete of end-hooked steel fibers. The data from the testing program were used to further assess the performance of steel fiber reinforced

concretes in impact-resistant applications and to provide a well-documented data set. The test results showed that the addition of the steel fibers was effective in increasing slab capacity, reducing crack widths and spacing, and mitigating local damage under impact.

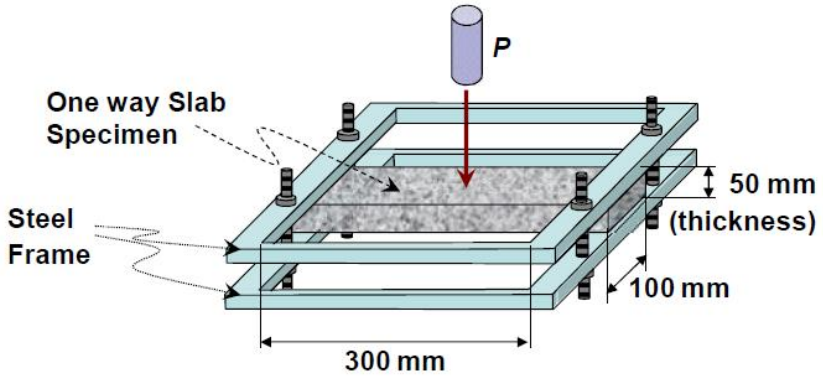

Figure 2.28 Test Set Up for One-Way Slab Specimens (Yoo et al., 2012)

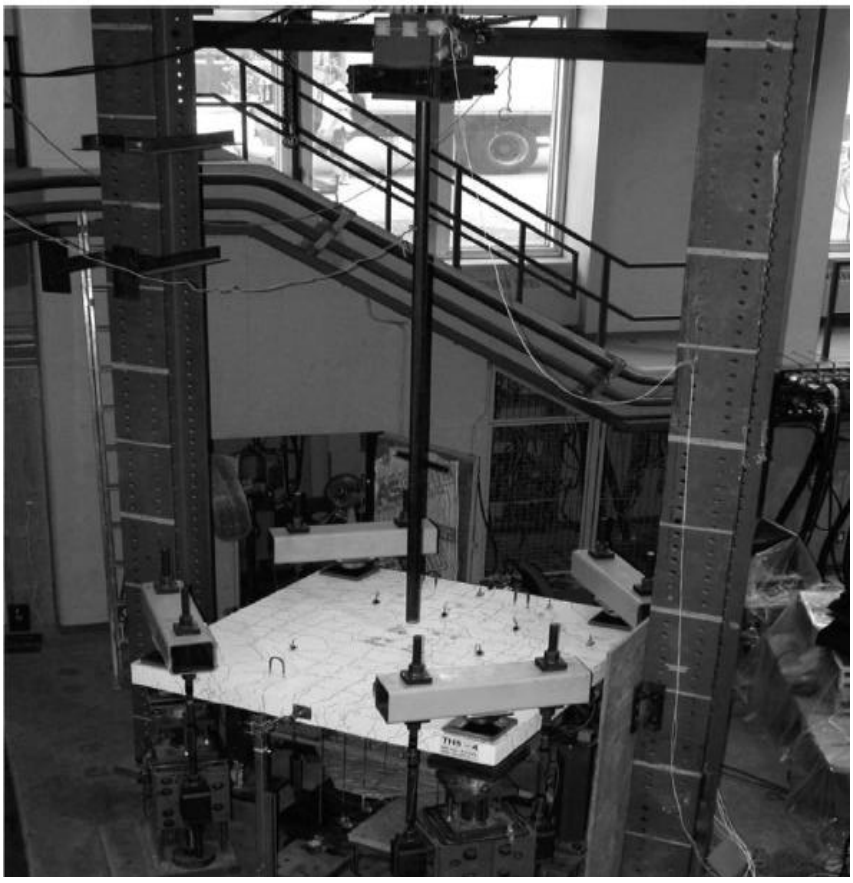

Figure 2.29 Experimental Set-Ups for Impact Test (Hrynyk & Vecchio, 2014)

Elavenil & Knight, 2012 also tested plates under drop weight impact. Dynamic behavior of eighteen plates with varying thicknesses of 20, 25 and 30mm with three different steel fiber contents of 0.5, 0.75 and 1% were studied. The drop weight steel ball of 0.5 kg was used with a cylindrical drop weight of 4.5 kg connected to a tensile wire, as shown in Figure 2.30. The supports considered in their work for the plates were fixed and simply supported. The energy absorption and number of blows were increased drastically when the fiber content increased from 0.5% to 1%. Also the higher aspect ratio (i.e. l/d) of fibers resulted in higher energy absorption, while this factor didn't affect the number of blows. Regarding the crack pattern slabs with support for edges showed radiating cracks while plates with two sides fixed showed cracks parallel to the supports (Figure 2.30). From the test results, it was concluded that the effect of fibers were more pronounced for plates with thickness of 25 and 30 and randomly distributed steel fibers in concrete stopped the propagation of cracks in the post cracking stage of concrete hence less crack width were apparent.

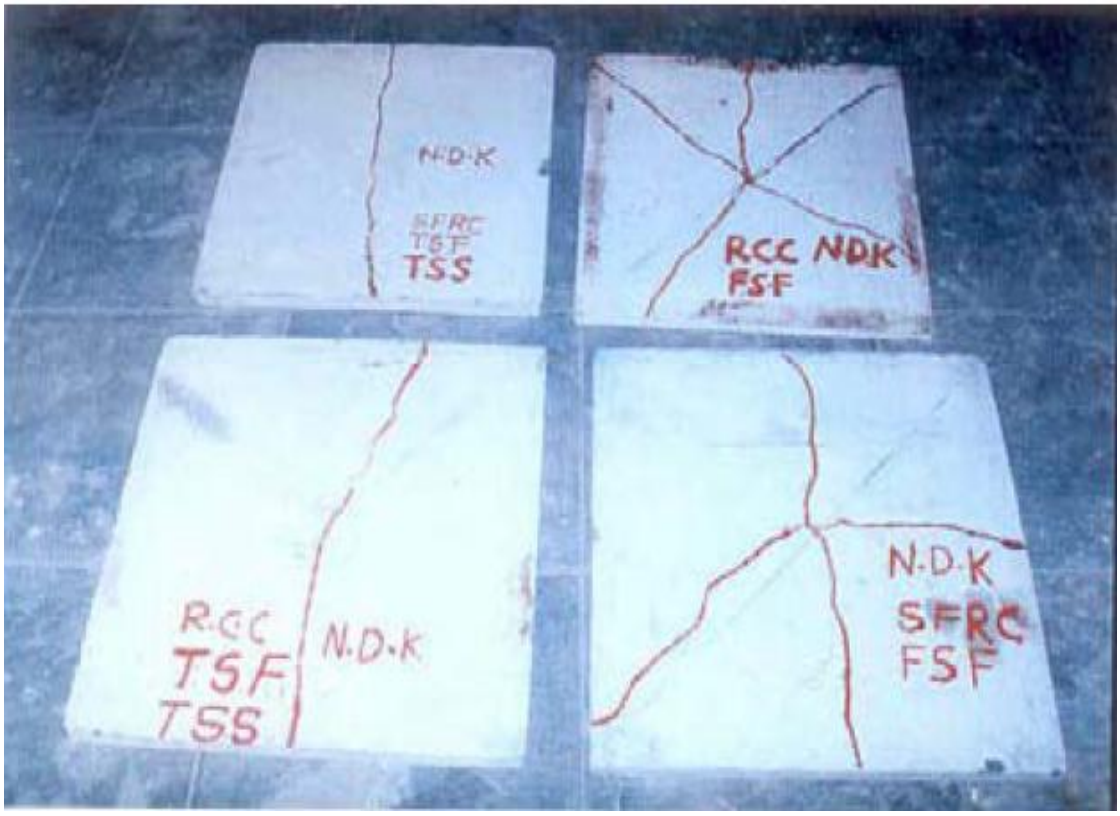

Figure 2.30 Cracking Patterns of Plates (Elavenil & Knight, 2012)

With the development of numerical methods, the study of local effects on concrete targets using such methods has several advantages over empirical and analytical methods. Guo et al., 2020 stated that: the use of finite element method along with other numerical methods, not only determines the local effects, but also predicts the influence of global response. To validate the numerical models, several experimental studies had been carried out.

Sadraie et al., 2019 investigated the effect of rebar's material, amount and arrangement, concrete strength and slab thickness on dynamic behavior of reinforced concrete (RC) slabs using both laboratory experiments and numerical simulations. Performance of fifteen 1000×1000mm concrete slabs, including two 75mm thick plain slabs, five 75mm thick steel reinforced concrete slabs, six 75mm thick reinforced concrete slabs with Glass Fiber Reinforced Polymer (GFRP) bars and two 100mm thick steel reinforced concrete slabs under drop weight impact loads were experimentally investigated. Failure mode, crack development, displacement-time, strain-time, and acceleration-time responses were studied and compared for various slabs. To assess the response of slabs subjected to impact loads, several slabs showed local response including perforation, spalling and scabbing and other samples showed global response as shown in Figure 2.31. By adjusting the amount and arrangement of GFRP, better performance in GFRP slabs than steel reinforced slabs was achieved, which considering the corrosion resistance of this material, can make it an appropriate selection of reinforcement material. Finite element analyses and simulation of specimens were conducted using LS-DYNA explicit software. The results obtained from experiments and numerical models were in good agreement, and they indicate that increasing the reinforcement ratio or the slab thickness enhanced the behavior of RC slabs under impact loads.

Elnagar et al., 2019 prepared and tested 63 RC slabs (with dimensions 500×500×50mm) under the effect of drop weight falling from three different heights; 1, 1.5 and 2 m. A thin layer of Strain-Hardening Cementitious Composites (SHCC) was provided in either tension or compression side of RC slabs aiming to improve their impact resistance. It was found that the SHCC strengthening layer enhanced the impact resistance of the strengthened slab when added at either tension or compression side

(see Figure 2.32). Furthermore, numerical simulations based on ABAQUS software package were performed on the strengthened slabs. Their results showed good agreement with the experimental findings from the viewpoint of the kinetic energy.

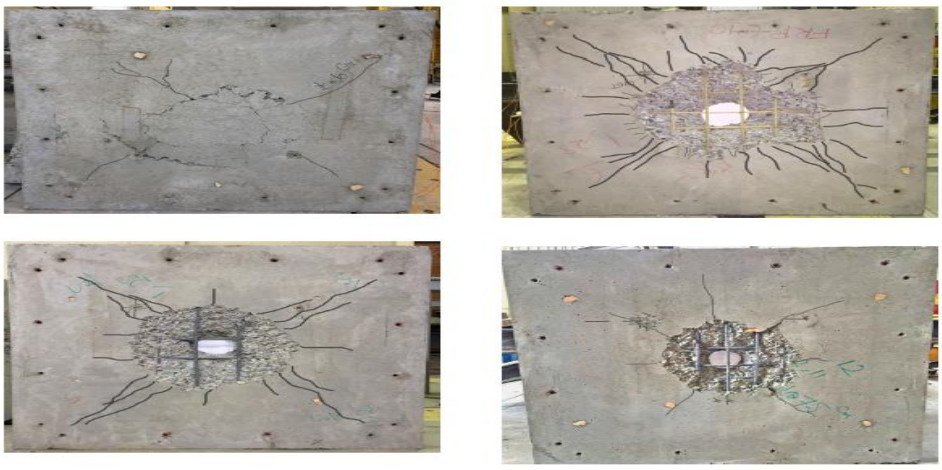

Figure 2.31 Failure and Cracking Pattern of Bottom of Slabs (Sadraie et al., 2019)

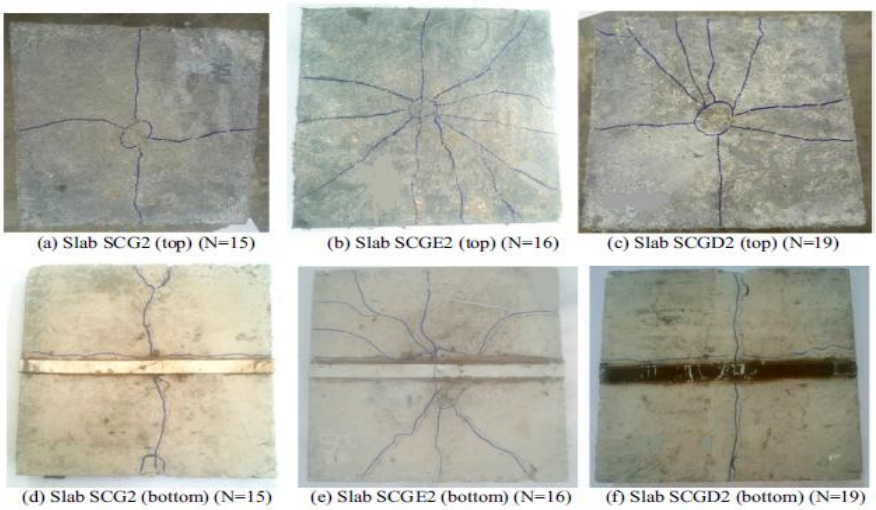

Figure 2.32 Developed Cracks and Failure Zone of SHCC-strengthened Slabs (Elnagar et al., 2019)

Almusallam et al., 2013 studied the effectiveness of hybrid-fibers (a combination of steel and plastic fibers) in improving the impact resistance of slabs. A total of 54 hybrid-fiber reinforced slabs were cast in two groups; each group containing 27 slabs. The specimens of the first group were cast using normal strength concrete, whereas specimens of second group were cast using high strength concrete.

All the slabs were 600×600×90 mm and contained different proportions of steel and plastic fibers. Out of a total number of 54 slabs, three slabs in each group were used as control specimens i.e. without fibers. The test results showed that the hybrid-fibers in the concrete lead to smaller crater volumes and reduced spalling and scabbing damage (see Figure 2.33). The hybrid-fibers arrested the crack development and thus minimized the size of the damaged area.

(a) Front face (b) Rear face

Figure 2.33 Failure Pattern Observed in the Front and the Rear Faces of Slab Specimen (Almusallam et al., 2013)

Kumar et al., 2017 investigated the behavior of micro steel (1%) and polypropylene fibers (0.25% and 0.50%) in concrete under the impact load. They found that the impact strength and splitting tensile strength were increased with the incorporation of steel and polypropylene fibers. The steel and polypropylene fibers bridge the matrix in the cracks when the impact load was applied acting as a reinforcing agent in the concrete. An empirical relationship was obtained between splitting tensile strength and impact energy to predict the impact energy of the concrete through splitting tensile strength. The empirical relationship exhibited good relationship with the percentage difference between experimental and predicted value less than 6%.

Nia et al., 2012 compared impact loading results from numerical simulations of plain concrete (PC) and fiber reinforced concrete (FRC) using version 971 LS-DYNA explicit software with experimental testing data, which were based on a testing procedure recommended by ACI committee 544. Concrete specimens were prepared with two water-cement ratios 0.36 and 0.46. Hooked-end steel fibers with an aspect ratio equal to 80 at 0.5% and 1% volume fractions and polypropylene fibers at 0.2%, 0.3% and 0.5% volume fractions were used. Both the numerical and experimental analysis results indicated that increasing the fiber volume fraction increased the impact resistance of the concrete specimens. The impact resistance increase was greater for normal strength than that for high-strength concrete. The results also demonstrated that steel fibers are more effective at increasing impact resistance than polypropylene fibers (see Figure 2.34).

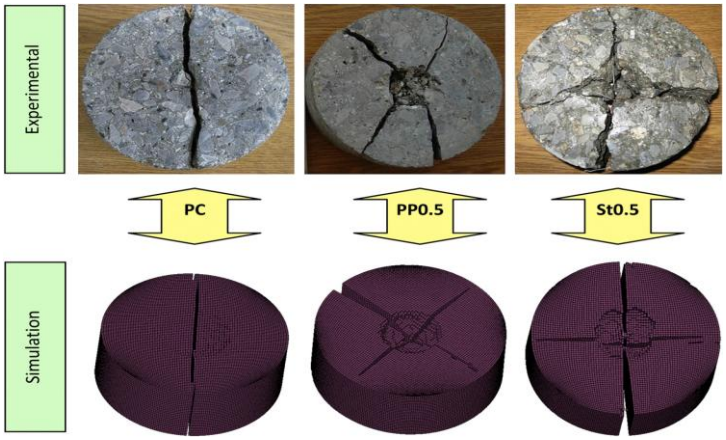

Figure 2.34 Comparison of Fracture Modes of Concrete Specimens (Nia et al., 2012)

Based on the observed damage and crack development in tested specimens, Othman & Marzouk, 2016 found crack pattern to be depending on the reinforcement layout rather than reinforcement ratio. For example as shown in Figure 2.35, the single reinforced specimen HS-3-S failed by localized sudden punching because shear cracks were observed before any significant bending cracks developed. While doubly reinforced specimen HS-3-D failed in a ductile punching mode because the crack pattern indicated that

both bending and shear cracks were developed. Additionally, results showed that the change of reinforcement ratio and/or reinforcement arrangement had no significant effect on impulse and absorbed energy values for the same impact loading condition.

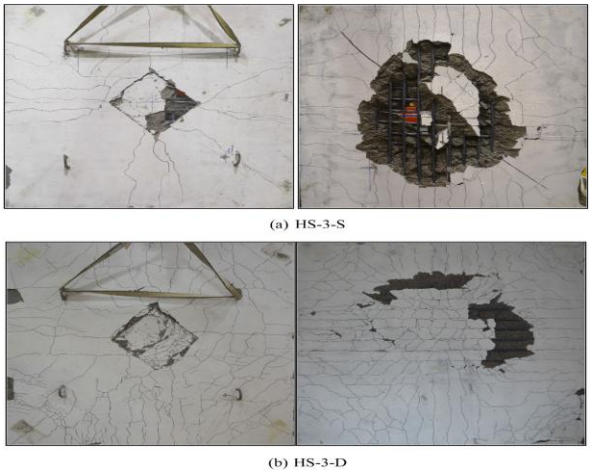

Figure 2.35 Final Crack Patterns (Othman & Marzouk, 2016)

An experimental investigation had been conducted by Othman & Marzouk, 2016 to address the effect of steel reinforcement ratio and arrangement on the impact force characteristics and the impact behaviors of 10 RC plates with dimensions 1950mm^2 with a thickness of 100 mm. As well as generating precision impact test data, special frame had been designed and fabricated to generate the required impact energy. An appropriate method to S filter noisy accelerometer data was presented. A special tie-down steel frame anchored to the strong floor of the Laboratory at both ends was used to prevent the uplift of each corner (Figure 2.36).

Iqbal & Rajput, 2017 studied the ballistic properties of ordinary concrete and reinforced concrete slabs with a size of (450×450) mm^2 and a thickness of 60 mm with an unrestricted compressive strength of 40 MPa. They obtained the amount and area of damage, volume of spalling and scabbing as well as the ballistic limit of plain and reinforced concrete and their results had been compared and discussed. From Figure 2.37 they had shown the ballistic limit of reinforced concrete target was 20% higher than plain concrete target for 60 mm thickness.

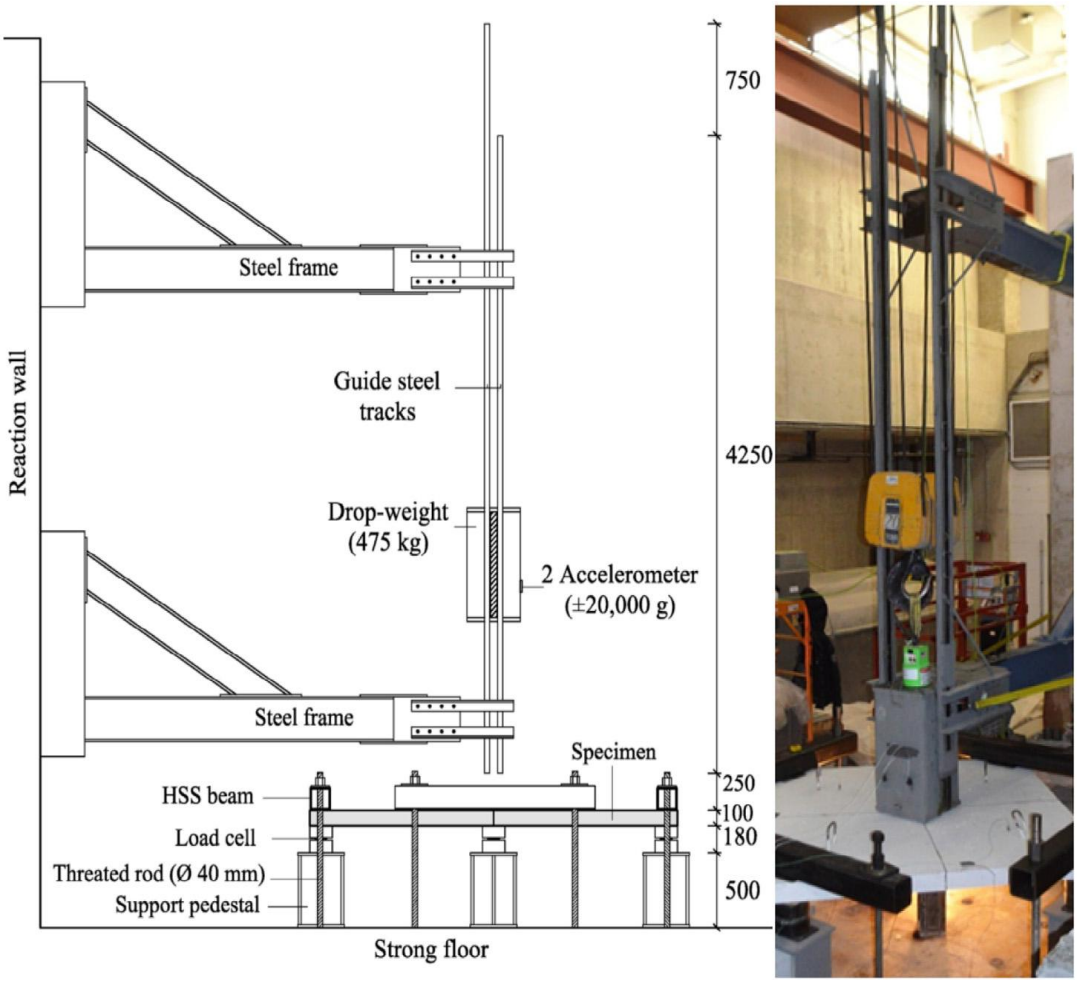

Figure 2.36 Drop-Weight Impact Test Setup (Othman & Marzouk, 2016)

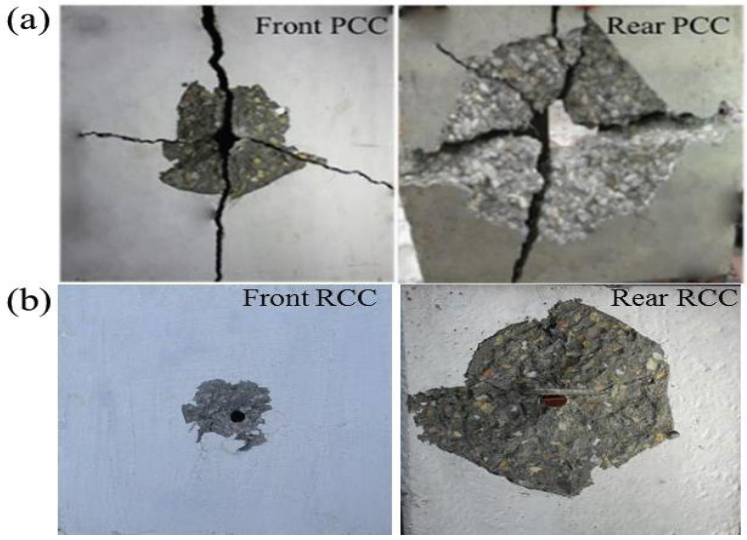

Figure 2.37 Target After Projectile Impact (a) Plain and (b) Reinforced Concrete (Iqbal & Rajput, 2017)

Batarlar et al., 2021 investigated the performance of strengthening layers of carbon textile reinforcement for five reinforced concrete (RC) slabs with dimensions of 1.5 m × 1.5 m × 0.20 m under repeated impact loads. To understand failure mechanisms of RC slabs under impact loadings, they divided the specimens as: two specimens unstrengthened and tested under different impact velocities and the other three specimens were strengthened with three different carbon textile reinforcements embedded in an additional 2 cm fine-grained concrete layer and subjected to impact loads with the same striker velocity. As shown in Figure 2.38 all tested slab specimens were cut into two equal pieces to observe the actual punching cone geometry. From observed test results they found that: the carbon textile reinforcement was very effective at increasing the impact capacities of the specimens. Additionally, displacement–time histories and crack profiles are highly affected due to the carbon textile reinforcement types and ratios during the impact loadings (see Figure 2.39).

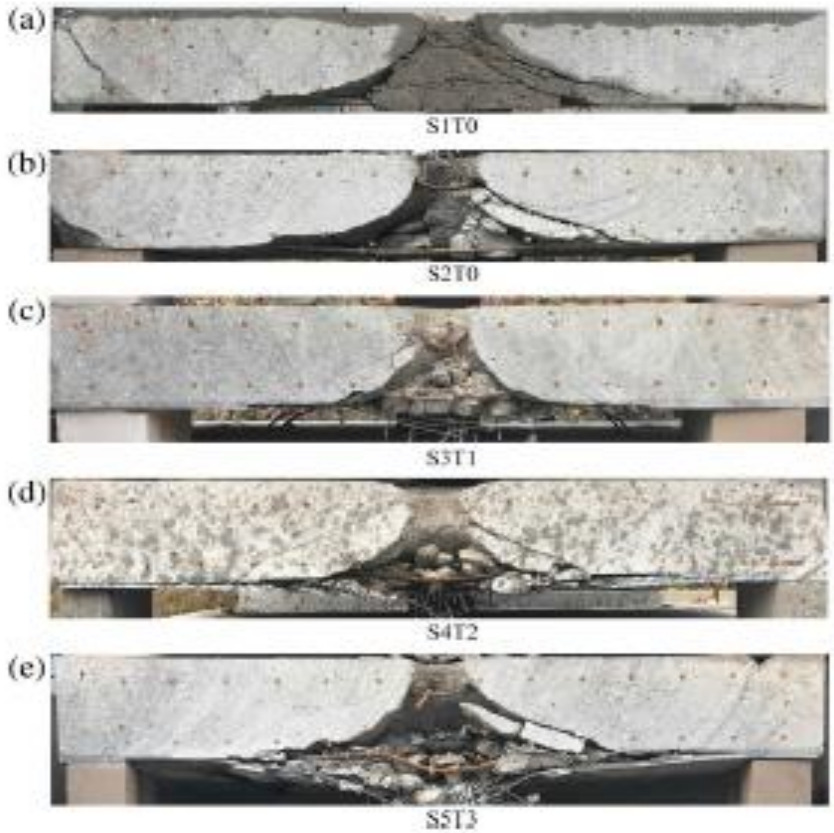

Figure 2.38 Final State of the specimens after Cuts (Batarlar et al., 2021)

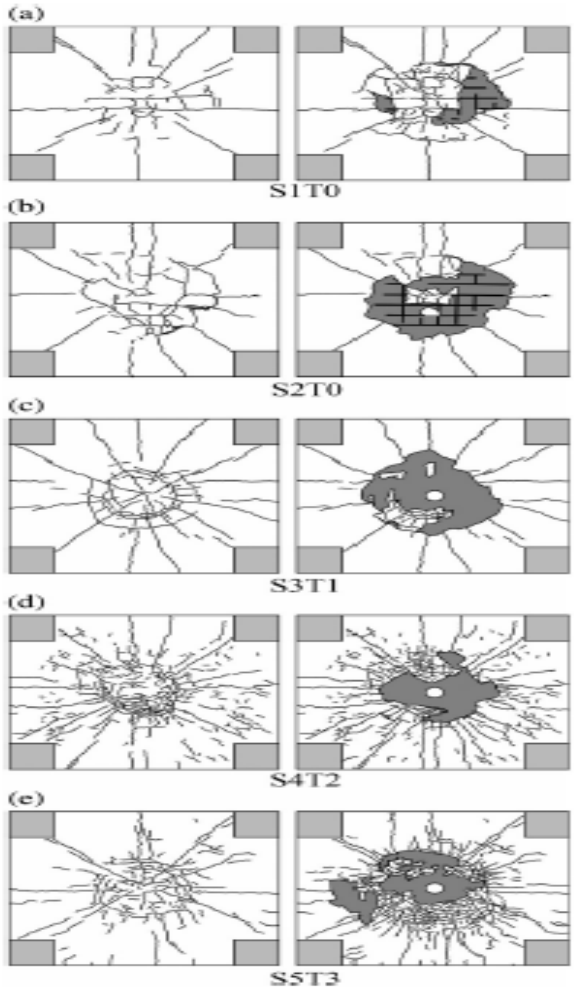

Figure 2.39 Crack Profiles of Bottom Surfaces After First and Final Impacts (left: First impacts; right: Final Impacts) (Batarlar et al., 2021)

Al-Rousan, 2018 investigated the punching shear capacity of reinforced concrete (RC) two-way slabs subjected to drop-weight impacts using Nonlinear Finite Element Analysis (NLFEA). The NLFEA program package (ANSYS) was used. The simulated models were validated against fifteen RC slabs with Polypropylene Fiber (PF) volume (V_f) of 0, 0.3, 0.6, and 0.9 % and subjected to impact load from the height of 0, 1.2, and 2.4 m. Then, the simulated slabs were expanded to cover slabs not subjected to impact load (impact height (HI) of 0 m) and slabs with V_f of 0 % to 1.2 % and subjected to impact load at the height of zero (No Impact) to 11 m (Failure of all slabs), resulting in a total of 182 RC slabs. The behavior of each slab was evaluated in terms of the

crack patterns, ultimate punching shear capacity, and deflection profile. The results were compared with the results from the experimental investigation and NLFEA compared in terms of the load-deflection curves (Figure 2.40). Inspection of Figure 2.41 revealed that the NLFEA load-deflection curves had an excellent agreement with the experimental results in terms of mode of failure. Also, his results (Figure 2.42) showed that adding the PF at a dosage of 0.1 to 1.2 % by volume of concrete lead to significant enhancement in the overall structural behavior of the slabs and their resistance to impact loading.

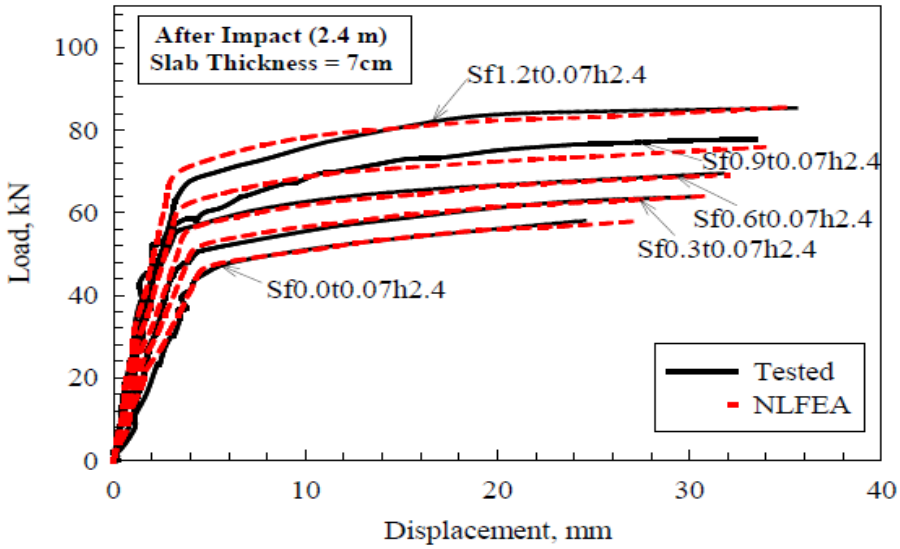

Figure 2.40 Typical Tested and NLFEA Load versus Mid-Span Displacement Curves (Al-Rousan, 2018)

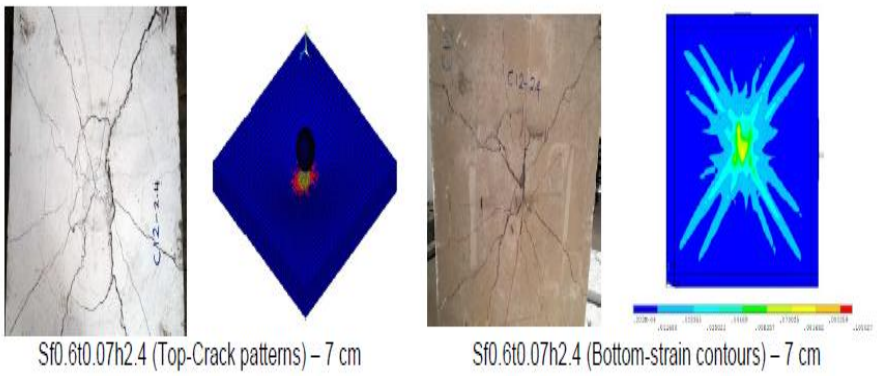

Figure 2.41 Typical Tested and NLFEA Results of RC Slabs (Al-Rousan, 2018)

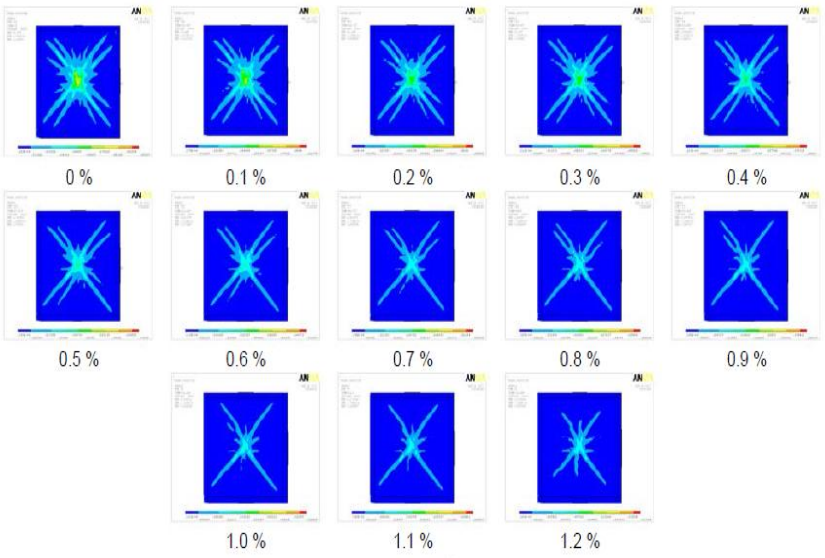

Figure 2.42 Typical Crack Patterns of the Simulated Models for Bottom Side (Al-Rousan, 2018)

Memon et al., 2019 discussed the finite element (FE) modeling of the impact behavior of plain concrete under impact based on LS-DYNA software using three available concrete models i.e. Winfristh Concrete model (MAT 084), Concrete Damage Release 3 model (MAT_072R3) and Continuous Surface Cap model (MAT_159). They obtained experimental data of control specimens from an existing study by (Kantar, Erdem, & Anıl, 2011). The specimens consisted of plain concrete prisms of size 710×150×150 mm^3, with compressive strength 25 MPa. The experimental results showed that maximum vertical acceleration was both dependants on the drop-height and damage level generated by the impact. On overall, it was found that multiple models can be used to compare results but the WIN concrete model showed the most consistent behavior for low velocity impact testing. They suggested further experiments to understand more about the performance of concrete models under low-velocity impact behavior of plain concrete.

Kataoka et al., 2017 investigated the failure characteristics of 12 reinforced concrete slab specimens subjected to moderate-velocity impacts by conducting impact tests and comparing by numerical simulations using ANSYS AUTODYN. Impact motion of the projectile, reaction force, and strain–time history on the back

surface sand reinforcing bars of the reinforced concrete slab were measured to investigate the failure of reinforced concrete slabs. They compared between failures modes obtained experimentally with Central Research Institute of Electric Power Industry formula (CRIEPI) proposed for the local damage of reinforced concrete slabs. They found that reinforcing ratio had no effect on failure status of the reinforced concrete slabs by casting three different reinforcing ratios including plain concrete slab. From the comparison between test and numerical results, the failure of the RC slab subjected to a moderate-velocity impact was the local failure caused by the initial local damage and completed while there was a sharp increase in the reaction force as shown in Figure 2.43.

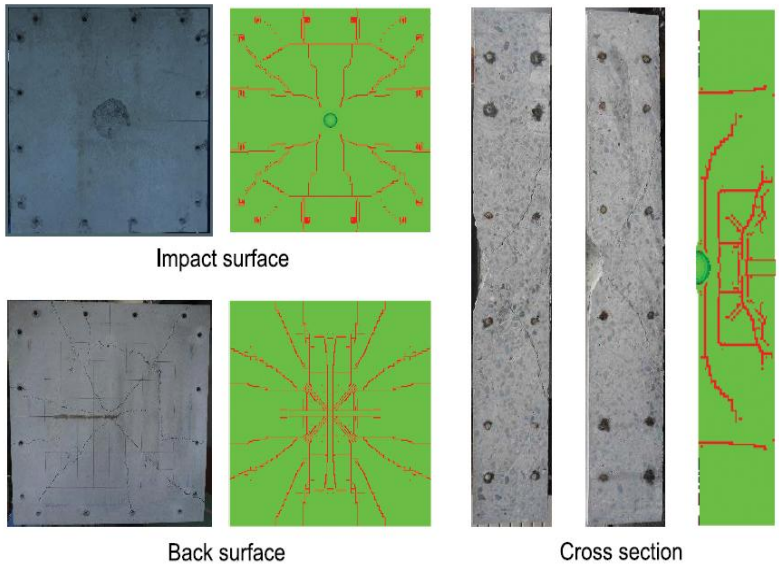

Figure 2.43 Failure State of RC Specimens (Kataoka et al., 2017)

The damage mechanisms of nine Glass Fiber Reinforced Polymer reinforced concrete (GFRP-RC) beams were investigated by conducting a series of impact load tests by Saleh et al., 2020. They observed that increasing the shear capacity of a GFRP-RC beam led to smaller residual deflections and higher residual capacities. Based on experimental observations and existing design specifications, design suggestions were provided to design the GFRP-RC part to withstand these specified input impact loads.

(Hering et al., 2020) conducted research studies to improve impact resistance by using reinforcement layers subsequently applied in mineral-bonded cement composites. Five reinforced concrete reference plates and several similar reinforced concrete plates for strengthening with carbon reinforced concrete with dimensions 1.5 m ×1.5 m × 0.2 m were casted. It was found that (Figure 2.44), the basic type of failure -punching failure- was not changed by the applied strengthening layer, but the intensity of the damage that occurred could be significantly reduced. A systematic consideration of the effect of an impact load on reinforced concrete plates was possible.

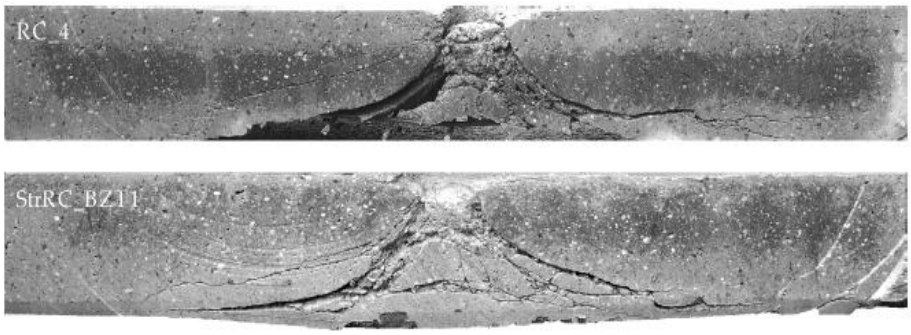

Figure 2.44 Comparison of Two plates (Hering et al., 2020)

Many studies (Pichandi et al., 2013, Brandt, 2008) investigated fibers of different shape such as enlarged end, hooked end, straight, twisted and others to improving the pullout resistance of the fibers (which allows stress redistribution). They suggested that: the hooked end shape is the best for dissipating more energy as the hook help to enhance the bonding between the steel fiber and the concrete which make it more effective in bridging the concrete between the cracks. Because the steel fiber used has a higher bonding strength, improved impact values have been recorded. (Choudhary et al., 2021) found a similar pattern of improved impact strength.

Erdem, 2021 investigated experimentally and numerically dynamic response of two-way reinforced concrete slabs under low velocity impact loading. The relationship between experimental and numerical studies was comparatively examined in terms of crack

patterns (see Figure 2.45) and average ratios of accelerations, displacements, impact loads. He found that the proposed numerical model could be used in the evaluation of experimental results under impact loading.

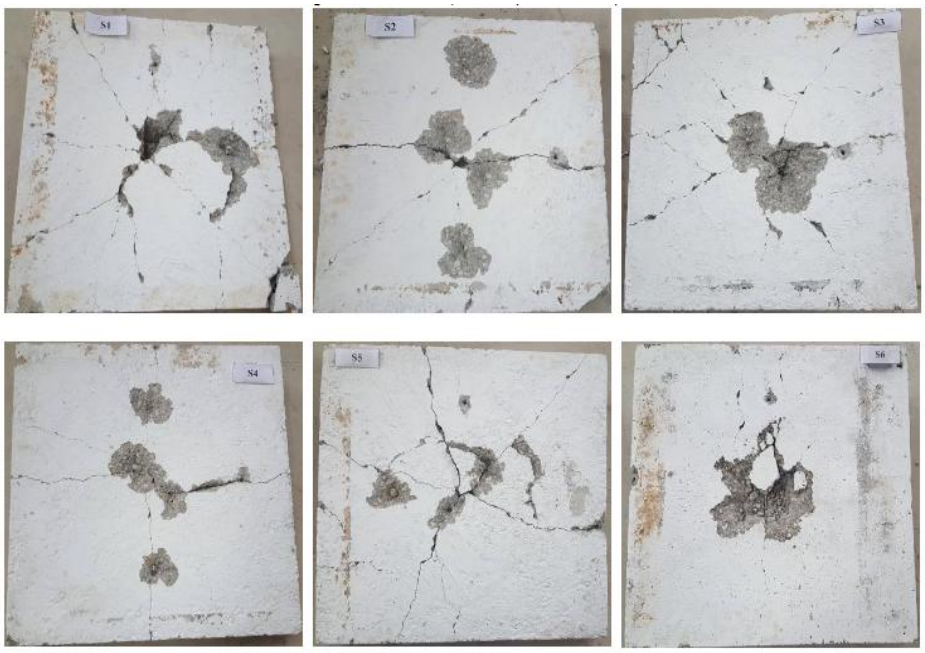

Figure 2.45 Failures of Test Specimens (Erdem, 2021)

2.11 Summary of the Review

Based on the literature review of previous studies, some conclusions can be summarized as follows:

(1) Review of literature related on the performance of fiber reinforced concrete slabs under impact load revealed a paucity of works in this field. A limited number of tests on slabs s3how that the increased flexural strength, stiffness and ductility due to the increase in yield strength of steel reinforcement and (type, shape, dimensions, aspect ratio, tensile strength and quantities) of fiber is a primary reason for change in failure mode of slabs subjected to impact load. Research has revealed the ability of these fibers to enhance strength, ductility and absorbing energy of reinforced concrete slabs to minimize their collapse. Moreover, investigation on effects of low velocity impact load on fiber reinforced concrete slabs is found to be inadequate in literature. Thus, a systematic test

program on fiber reinforced concrete slabs subjected to impact load at their mid-span is worthy of investigation.

(2) It is difficult to make a direct comparison between different studies due to various parametric conditions of the tests, such as different types and weights and velocity of the impact load used. Thus, it is difficult to identify the best type of fibers and the techniques to be adopted.

(3) Since the impact load design is still in its infancy with the lack of any design guidelines, the reviewed literature was aiming to understand the structural performance of fiber reinforced concrete slabs by conducting experimental tests under impact load. Researchers have tried to understand the impact performance of the fiber reinforced concrete slabs by measuring relevant factors such as deflection, ductility, strength, and pattern of failure. But the destructive energy produced from the impact within very short duration (milliseconds) makes it difficult to achieve the desired accuracy by using laboratory instruments whereas it is difficult to quantify the difference or the enhancing factor of the mechanical properties of the slabs against this type of destructive loading. Considering that, in addition to the cost of tests, there is a need to develop theoretical or numerical models with accepted accuracy level. Further, it is not possible to achieve all behaviors by using laboratory instruments to validate the numerical work. Considering that, the need to understand the experimental behavior of the fiber reinforced concrete slabs and developing adequate and validated nonlinear numerical model is in need.

(4) There is a shortage of numerical research on recognizing the effects of different parameters on the behavior of hybrid fiber reinforced slabs under impact load. Therefore, numerical model (three-dimensional) is essential to authorize the experimental results first and further applied to expand the knowledge further on the range of parameters investigated experimentally.

(5) Most of the numerical studies of the impact response have been conducted by using LS-DYNA and ABAQUS explicit codes which were proven to be adequate in simulating the high-velocity impact

problems. However, obtained numerical results highly depend on the constitutive material models which are simulated by using user-defined models with many assumed factors. It is so complicated to provide a comprehensive numerical model to simulate the impact resistance of the hybrid fiber reinforced elements due to the various in the mechanical behavior and the failure criteria of each fiber material which depend on many factors such as the orientation of the fibers, the geometrical shape. While the commercial finite element codes adopt two dimensional failure criteria for the material by neglecting effect of the thickness Also, the mechanical properties of the bonding area provided by the adhesive which vary based on the shape and the type of the fiber add complexity to the numerical modeling, while most of the finite element analysis codes simulate the interfacial area as a cohesive element.

CHAPTER THREE

EXPERIMENTAL PROGRAM AND RESULTS

3.1 Introduction

Reinforced Concrete (RC) member subjected to impact loading is a design concept that has not yet been fully developed. Moreover, current design codes did not suggest a clear method to analyze and predict possible failure mode for RC slabs under impact (Tahmasebinia and Remennikov, 2008).The characteristics of impact loading are different from those of static loading. Since the duration of loading is very short, the effect of strain rate becomes significantly higher than that under quasi-static. As a result, structural response and failure modes will be different (Chen and May, 2009).

There are three ways to study local impact effect on concrete structures. Empirical methods based on experimental data, Analytical methods based on physical laws, and third numerical simulation methods based on computer based material model. Experimental data is always important for understanding and making comparison with other methods (Latif, 2012).

Fibers are usually used in concrete to control plastic shrinkage cracking and drying shrinkage cracking. They also lower the permeability of concrete and thus reduce bleeding of water. Some types of fibers produce greater impact, abrasion and shatter resistance in concrete. The amount of fibers added to a concrete mix is measured as a percentage of the total volume of the composite (concrete and fibers) termed volume fraction (V_f). V_f typically ranges from 0.1 to 3%. Aspect ratio (l/d) is calculated by dividing fiber length (l) by its diameter (d). Fibers with a non-circular cross section use an equivalent diameter for the calculation of aspect ratio. If the modulus of elasticity of the fiber is higher than the matrix (concrete or mortar binder), they help to carry the load by increasing the tensile strength of the material. Fibers which are too long tend to “ball” in the mix and create workability problems (Prakash, 2017).

Studying the behavior of hybrid reinforced concrete slabs subjected to impact loads requires a well-designed experimental program

accompanied by numerical and analytical investigations. Experimental studies are crucial to the verification of analytical and numerical methods to be developed. Therefore, a well-instrumented test program was designed and executed in this study, results of which can be employed in further studies. This chapter explains the details of the test program, including test specimens, test setup and instrumentation.

In this chapter, section 3.2 describes material properties; section 3.3 presents the test specimens and test setup, procedures for impact loading test; section 3.4 and 3.5 describe measurement and instrumentation and analysis of the experimental data. Finally, section 3.6 presents results obtained from mechanical properties tests on specimens and failure mode for representative samples of specimens.

3.2 Material Properties

3.2.1Materials

All the materials used in this research, except for the fibers, were locally produced. The mix design used for this research utilized the same materials, mix design and curing regime as previously used in the University of Purta for the purpose of studying the response of under impact load.

Portland Cement: Ordinary Portland Cement Type 1 (MS 522).

Aggregate: crushed with the nominal maximum aggregate size (NMAS) 20 mm (BS EN 12620).

Fibers:

Steel Fiber: two types of the hooked end steel fiber:

65/35 3D with Geometry: Fiber family: 3Dramix, Length (l): 35 mm, Aspect ratio (l/d): 65

65/60 5D with Geometry: Fiber family: 5Dramix, Length (l): 60 mm, Aspect ratio (l/d): 65

FORTA-ECONO-MONO (Polypropylene) Fiber: is an easy to finish micro synthetic fiber, made of 100% virgin homopolymer polypropylene monofilament. This economy-grade fiber functions as plastic shrinkage reinforcement intended to reduce the settlement shrinkage and increase surface durability. ECONO-MONO is non-corrosive, chemically inert, and 100% acid and alkali proof.

Fibers were added to concrete batch during casting. Although no further investigation was made, it is safe to assume that fibers were randomly distributed inside specimen. Steel fibers can fail due to pull out or rupture effects. The type of the failure of the steel fibers could change the behavior of the specimen significantly. However, due to the difficulties involved in breaking or cutting the specimens after tests, the mode of the failure of the steel fibers could not be investigated.

3.2.2 Concrete Proportions

The concrete specimens were cast from one batch, which were prepared by following the same recipe, as shown in Table 3.1, with a target mean compressive strength $f_{cu,target}$= 40 MPa. As seen in Table 3.1, there are 8 concrete specimens with different hybrid fiber ratios (0, 0.5 and 1) %.

Table 3.1 Concrete Mix Design (for 1 m^3)

Specimen	Cement (kg)	Water (kg)	Course Agg. (kg)	Fine Agg. (kg)	65/35 3D Steel Fiber (kg)	65/60 5D Steel Fiber (kg)	PPF (kg)
C1(Control Specimen)	1138.7	534.7	2866.9	2320.7	0	0	0
M1(1% 65/35 3D)					225.4	0	0
M2(0.5% 65/35 3D + 0.5%PPF)					112.7	0	18.8
M3(1% 65/35 3D high ratio + 0.5% PPF)					225.4	0	18.8
M4(1% 65/60 5D)					0	225.4	0
M5(0.5% 65/60 5D + 0.5%PPF)					0	112.7	18.8
M6(1%65/60 5D high ratio + 0.5%PPF)					0	225.4	18.8
M7(1% PPF)					0	0	37.6

3.2.3 Concrete Properties

In order to determine the compressive and tensile strength of the hardened concrete of each batch, eight concrete combinations were considered, including a control mixture (C1) with no fiber and a 0% volume of SF and PPF. The remaining mixtures (M1 to M7) had 0.5 percent or 1.0 percent volume fractions of two types of SF and PPF. As a result, every batch of concrete contained the same amount of cement, fine particles, and coarse aggregates. For all concrete batches, the water-cement ratio was 0.47. Table 3.2 illustrates the amounts of SF and PPF based on varied percentage proportions.

The control concrete mixture was constructed to meet British Standards BS EN 206-1, 2000 for concrete compressive strength of 40 MPa, which was used to construct the specimens. To assess the concrete compressive strength, compressive tests were performed on three specimens of cubes with a standard size of 150 x 150 x 150 mm on the 28th day for each combination. After 24 hours, the specimens were demolded and stored in a water tank for 28 days (see Figure 3.1). Flexural tests were performed on three prism specimens with a standard size of 100 x 100 x 500 mm on the 28th day to assess the concrete flexural strength, as required by British Standards BS EN 12390-3 and BS EN 12390-5, respectively. The load was recorded during the compressive and flexural testing. Under the loading system, all of the specimens were tested to failure. Figure 3.2 depicts the universal testing machine used to determine the compressive and flexural strengths of concrete, respectively.

Figure 3.1 Curing of Test Specimens

Table 3.2 Mix Proportions %

Mix proportions %			
	65/35 3D SF	**65/60 5D SF**	**PPF**
C1	0	0	0
M1	1	0	0
M2	0.5	0	0.5
M3	1	0	0.5
M4	0	1	0
M5	0	0.5	0.5
M6	0	1	0.5
M7	0	0	1

(a) (b)

Figure 3.2 (a) Compression Test Machine and (b) Flexural Test Machine

3.3 Concrete Tests Results

All of the tests results performed in the concrete laboratory are analyzed and discussed in this section. At the appointed times, the specimens were cured and tested. A total of eight concrete mix specimens (24 cubes and 24 prisms) were tested.

3.3.1 Slump Test

Slump tests were performed on fresh concrete. The Slump class in this investigation was set at (10-30) mm. Figure 3.3 shows how the droop of the concrete was determined by measuring the distance between the top of the slumped concrete and the level of the top of the slump cone. The results of slump tests for all concrete mixes are presented in Table 3.3.

Figure 3.3 Concrete Slump Tests

3.3.2 Concrete Compressive Strength Test Results

The compressive cube strength of concrete was calculated using an average of three cubes for each specimen, as shown in Table 3.4.

Table 3.3 Slump Test Results

Specimen	Slump Average Value (mm)
C1	29
M1	25
M2	15
M3	15
M4	25
M5	15
M6	15
M7	26

Table 3.4 Concrete Compressive Cube Strength Test Results

Specimen	Concrete Compressive Cube Strength Test (N/mm^2)									
	Cube No. 1			Cube No. 2			Cube No. 3			Average
	Weight (kg)	Ult. Load (kN)	Compressive Strength (N/mm^2)	Weight (kg)	Ult. Load (kN)	Compressive Strength (N/mm^2)	Weight (kg)	Ult. Load (kN)	Compressive Strength (N/mm^2)	Compressive Strength (N/mm^2)
C1	8.03	871.0	**38.7**	8.10	920.4	**40.9**	7.91	**934.0**	41.5	**40.4**
M1	8.12	673.5	**29.9**	8.01	634.5	**28.2**	8.07	**736.1**	32.7	**30.3**
M2	7.85	568.8	**25.3**	7.98	574.6	**25.5**	8.26	**567.8**	25.2	**25.3**
M3	7.73	399.6	**17.8**	7.81	394.5	**17.5**	7.78	**364.7**	16.2	**17.2**
M4	8.02	681.2	**30.3**	8.05	720.8	**32.0**	7.92	**593.3**	26.4	**29.6**
M5	7.38	425.1	**18.9**	8.27	433.6	**19.3**	7.52	**417.6**	18.6	**18.9**
M6	7.58	315.4	**14.0**	7.40	244.7	**10.9**	7.45	**287.2**	12.8	**12.6**
M7	7.61	329.2	**14.6**	7.40	314.3	**14.0**	7.49	**348.3**	15.5	**14.7**

3.3.3 Flexural Strength Test on Concrete

Flexural test evaluates the tensile strength of concrete indirectly. It tests the ability of unreinforced concrete beam or slab to withstand failure in bending.

The results of the Concrete Flexural Strength Test are shown in Table 3.5. The greatest value for M4 specimen was 6.5 N/mm^2, which was higher than the maximum value for C1 (4.5 N/mm^2). While M7 (PP fiber alone) yields gives the lowest result.

Table 3.5 Concrete Flexural Strength Test Results

Specimen	Concrete Flexural Strength Test (N/mm^2)									
	Prism No. 1			Prism No. 2			Prism No. 3			Average
	Weight (kg)	Ult. Load (kN)	Flexural Strength (N/mm^2)	Weight (kg)	Ult. Load (kN)	Flexural Strength (N/mm^2)	Weight (kg)	Ult. Load (kN)	Flexural Strength (N/mm^2)	Flexural Strength (N/mm^2)
C1	11.98	14.67	**4.4**	12.07	15.33	**4.6**	12.16	15.00	**4.5**	**4.5**
M1	11.99	12.67	**3.8**	12.32	14.33	**4.3**	12.44	14.33	**4.3**	**4.1**
M2	12.02	15.27	**4.6**	11.58	15.16	**4.5**	12.31	17.38	**5.2**	**4.8**
M3	11.64	18.46	**5.5**	11.75	16.06	**4.8**	11.41	11.36	**3.4**	**4.6**
M4	12.23	22.83	**6.8**	12.02	20.33	**6.1**	12.46	21.63	**6.5**	**6.5**
M5	11.98	12.62	**3.8**	11.33	11.35	**3.4**	11.65	11.42	**3.4**	**3.5**
M6	11.09	14.85	**4.5**	11.01	8.72	**2.6**	11.74	16.93	**5.1**	**4.1**
M7	11.00	9.40	**2.8**	11.05	11.11	**3.3**	11.02	8.08	**2.4**	**2.8**

3.3.4 Cracking Pattern and Mode of Failure

Figures 3.4 to 3.11 demonstrate the cracking pattern and failure mode of concrete prisms. The fracture usually starts at the bottom of the mid-span and extends upwards between the two places of loading. As can be seen in Figure 3.4, there was a rapid decrease in load and breaking for plain concrete. The addition of steel fiber resulted in significant gains in tensile strength, as seen in these results. These increases in fracture energy are dependent on the steel fiber content and diameter. PPF prisms, on the other hand, indicate an increase in failure modes as compared to plain concrete. Increased flexural strength can be used as a proxy for changes in concrete ductility when compared to ordinary concrete.

Prism condition (before tested)

Prism condition (being tested)

Prism No. 1

Prism No. 2

Prism failure (right view) – splitted into two sections

Prism failure (left view) – splitted into two sections

Prism No. 3

Prism failure (plan view) – splitted into two sections

Prism failure (left view) – splitted into two sections

Figure 3.4 Cracking Pattern of C1 Prism at Failure

Prism condition (before tested)

Prism condition (being tested)

Prism No. 1

Prism failure (right view) – almost splitted into two sections

Prism failure (left view) – almost splitted into two sections

Prism No. 2

Prism failure (right view) – almost splitted into two sections

Prism failure (left view) – almost splitted into two sections

Prism No. 3

Prism failure (right view) – almost splitted into two sections

Prism failure (left view) – almost splitted into two sections

Figure 3.5 Cracking Pattern of M1 Prism at Failure

Prism condition (before tested)

Prism condition (being tested)

Prism No. 1

Prism failure (right view) – only cracks appeared

Prism failure (left view) – only cracks appeared

Prism No. 2

Prism failure (right view) – almost splitted into two sections

Prism failure (left view) – almost splitted into two sections

Prism No. 3

Prism failure (right view) – almost splitted into two sections

Prism failure (left view) – almost splitted into two sections

Figure 3.6 Cracking Pattern of M2 Prism at Failure

Prism condition (before tested)

Prism condition (being tested)

Prism No. 1

Prism failure (right view) – almost splitted into two sections

Prism failure (left view) – almost splitted into two sections

Prism No. 2

Prism failure (right view) – only cracks appeared

Prism failure (left view) – only cracks appeared

Prism No. 3

Prism failure (right view) – only cracks appeared

Prism failure (left view) – only cracks appeared

Figure 3.7 Cracking Pattern of M3 Prism at Failure

Prism condition (before tested)

Prism condition (being tested)

Prism No. 1

Prism failure (right view) – only cracks appeared

Prism failure (left view) – only cracks appeared

Prism No. 2

Prism failure (right view) – only cracks appeared

Prism failure (left view) – only cracks appeared

Prism No. 3

Prism failure (right view) – only cracks appeared

Prism failure (left view) – only cracks appeared

Figure 3.8 Cracking Pattern of M4 Prism at Failure

Prism condition (before tested)

Prism condition (being tested)

Prism No. 1

Prism failure (right view) – almost splitted into two sections

Prism failure (left view) – almost splitted into two sections

Prism No. 2

Prism failure (right view) – almost splitted into two sections

Prism failure (left view) – almost splitted into two sections

Prism No. 3

Prism failure (right view) – almost splitted into two sections

Prism failure (left view) – almost splitted into two sections

Figure 3.9 Cracking Pattern of M5 Prism at Failure

Prism condition (before tested)

Prism condition (being tested)

Prism No. 1

Prism failure (right view) – only cracks appeared

Prism failure (left view) – only cracks appeared

Prism No. 2

Prism failure (right view) – almost splitted into two sections

Prism failure (left view) – almost splitted into two sections

Prism No. 3

Prism failure (right view) – almost splitted into two sections

Prism failure (left view) – almost splitted into two sections

Figure 3.10 Cracking Pattern of M6 Prism at Failure

Prism condition (before tested)

Prism condition (being tested)

Prism No. 1

Prism failure (right view) – only cracks appeared

Prism failure (left view) – only cracks appeared

Prism No. 2

Prism failure (right view) – splitted into two sections

Prism failure (left view) – splitted into two sections

Prism No. 3

Prism failure (plan view) – only cracks appeared

Prism failure (left view) – only cracks appeared

Figure 3.11 Cracking Pattern of M7 Prism at Failure

3.4 Impact Loading Tests

3.4.1 Test Specimens

All test specimens were **1700mm*1700mm** square slabs with 100mm thickness, reinforced with different ratios of two types of fibers: steel fiber and PP fiber with one plain concrete (control specimen with no fiber).

Manufacturing of formworks and casting specimens were carried out at the University of Putra Malaysia UPM Civil Engineering laboratory (see Figure 3.12). Mechanical set-up for impact load test is presented in Appendix A.

Eight slab specimens were designed for the test program, which were tested under impact load acted on the center of the front face of each specimen. Figure 3.13 Shows photo of a specimen with support conditions before testing.

Figure 3.12 Manufacturing of Formworks and Casting Specimens

Figure 3.13 Typical Specimen Setup Before Testing

3.4.2 Test Setup

In all slabs, the impact load was applied by means of the free fall of a drop-weight. For free fall, the drop-weight was arranged for sliding between tracks on the drop-tower and impacted the specimens at the mid-point. The free falling drop impact load acted on the center of the front face of each specimen during impact test. Specimens were attached horizontally to the frame set-up. For the impact test, specimens were simply supported along the top and bottom edges. The designed drop-weight test setup allows for dropping steel hammer from a height which is up to 2.0 m. The designed drop-weight test setup is depicted in Figure 3.14. Besides, a steel support setup was designed to provide simply support in the experiments. Drop-height is one of the investigated variables in the test. Impact loading with different level impact energies was conducted by varying the drop-height of the steel hammer. The weight of the hammer and the geometry of the hammer which

contacts with RC slabs were taken as constant in all impact tests. The hammer with the weight of 200 kg had semispherical-head fabricated from high-strength steel material as shown in Figure 3.15 and it was dropped from heights of (1,000 and 2,000) mm.

Figure 3.14 Drop Weight Impact Machine and Test Setup

Figure 3.15 Details of 200 kg Mass Hammer Drop Weight

3.5 Measurement and Instrumentation

To measure the output of the experimental test accurately, several good quality devices were used in the test. Specimen deflections (vertical displacement) were measured from a top face of the specimen at the center and transverse directions of the specimen using 8 linear variable differential transformers LVDTs. The Kyowa LVDTs had measurement uncertainty equal to 0.01 mm and were calibrated before the tests using the calibration procedures No.MSD/0010 Rev.5.0. Also, to measure strains of slab specimens; 8 strain gauges were used. Kyowa strain gauges type KC-70-120-A1-11 with 67 mm length. Interface 1000 high capacity load cell was placed between hydraulic jack and specimen at the center soffit slab, in order to monitor the applied load as shown in Figure 3.16.

Figure 3.16 Load Cell Placed at the Center Soffit Slab

All these sensors were connected to a Strain Smart System EDX-100A data logger from Kyowa factory with a parallel recording frequency of 100 Hz -1 second (100000 cycle/second) to record the output data impact tests respectively (see Figure 3.17). Procedure for installing the strain gauges is described in the following section.

LVDTs, strain gauges and load cell locations on the slab specimens were as shown in Figure 3.18. 8 LVDTs mounted at different locations along the element span to measure the vertical displacement exhibited at these points. All specimens in tests were fitted with 8 strain gauges mounted on the top surface at distance 150mm from mid-span. Despite all the efforts, some strain gauges had been fallen in impact loading.

Figure 3.17 the Instruments Used in the Impact Test; (a) the LVDT and (b) the Data Logger System

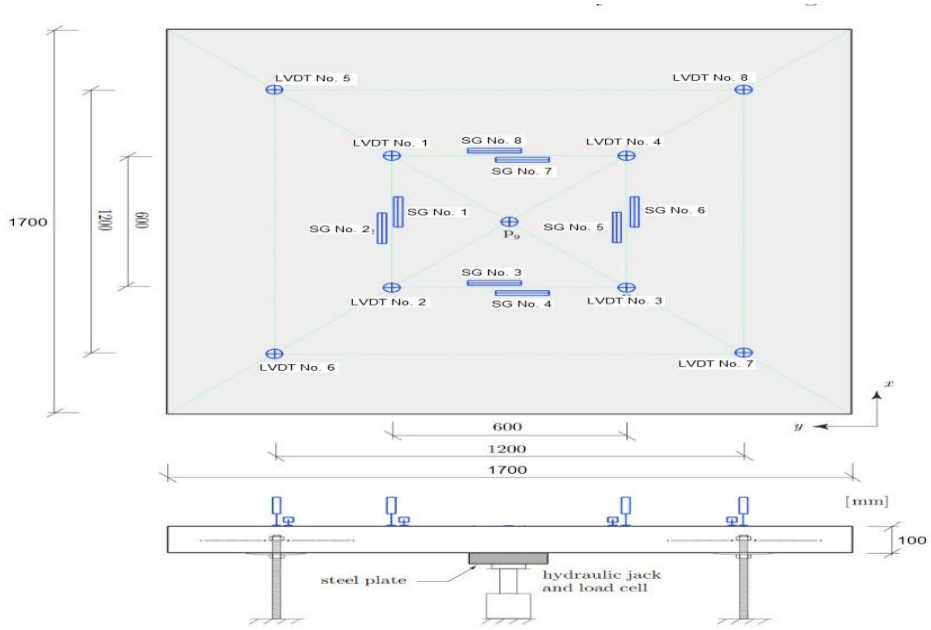

Figure 3.18 Locations of Strain Gauges, LVDs and Load Cell Instrumentations

Strain Gauge Installation: Before bonding the strain gauges, the concrete slabs surfaces were prepared well by following the procedure recommended by the manufacturer. The concrete surfaces are coated by white ordinary paint as recommended for good preparation to observe and marked the cracks that occurred during tests. The paint used has no effects at all to slab specimen specification. Figure 3.19 presents photos of the concrete strain gauges and LVDTs, which show that the concrete strain gauges and LVDTs are positioned in top surface of the specimen to record the potential maximum strain and deflection in the critical section of the element.

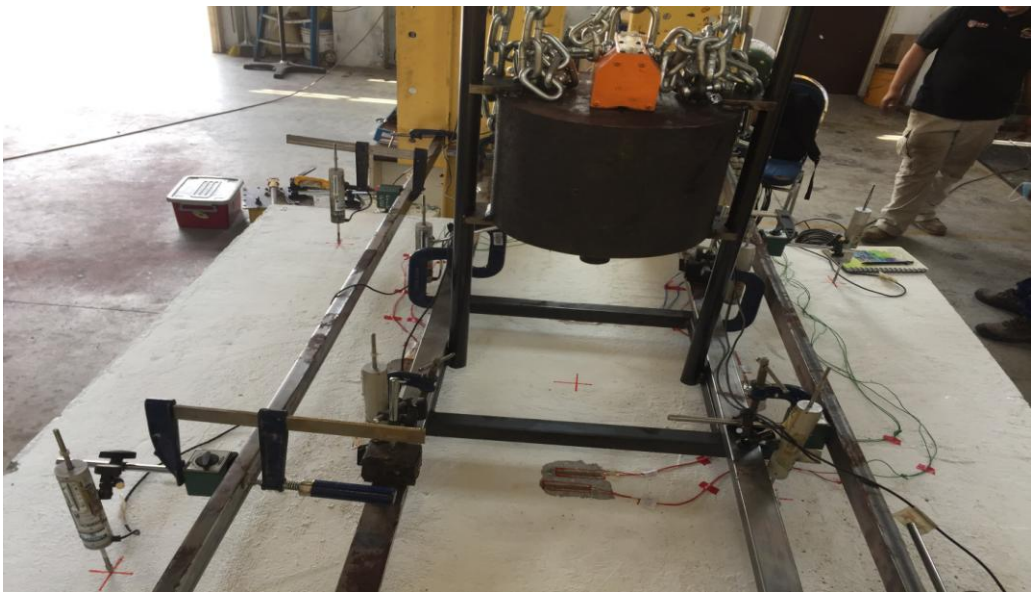

Figure 3.19 Strain Gauges and LVDTs that Used in the Slab Specimens

3.6 Analysis of the Experimental Data

For each type of test, comparisons were made between the control and the hybrid fiber reinforced concrete slabs based on many factors including load capacity, ductility, and the energy dissipation based on the measured data of load, deflection and concrete strains and the post test observation of the crack patterns and the failure mode. For the impact tests, the impact load was considered to compare load capacities.

3.6.1 HFRC Slab Energy Absorption:

The formula used by Kiran et al., 2015 for calculating the HFRC Slabs energy absorption is:

$$E = N \times (w \times h) \text{ joules} \quad (3.1)$$

Where,

E is the energy absorbed in joules,

w is weight of hammer in Newton, $(m \cdot g)$

h is the height of drop in meter and

N is the no. of impact blows.

g is natural acceleration

3.6.2 The impact velocity:

Ignoring frictional effects the impact velocity v is given by:

$$v = \sqrt{2 \cdot g \cdot h} \quad (3.2)$$

3.7 Impact load Test Results

Data from the sensors were collected with a digital data acquisition system at a 100 Hz sampling rate. In other words, continuous analog signals generated by the sensors were read and recorded on computer at a rate of 100 times per second (100000 cycles/second). This process is referred to as digitization. Digitized data is a discrete representation of the original continuous analog signal; therefore, it is only an approximation, from which the original signal can later be recovered. One of the main factors affecting the quality of this approximation, and hence the recovered signal, is the sampling rate.

3.7.1 Deflection Data

There were eight LVDTs used to measure deflection of slab specimens to study the effect of impact load. Tables 3.6 to 3.12 present the maximum values of deflection and residual deflection with time for 8 LVDTs for all slab specimens.

Table 3.6 Maximum Deflection and Residual Deflection Values with Time (LVDT1)

Specimen	Max.+ve.	Time	Max. -ve	Time	Residual	Time
C1	19.7114	9.24	19.712	9.27	-19.712	24.24
M1,1	17.578	7.7	6.413	8.4	-2.142	15.8
M1,2	34.027	15.55	10.840	15.64	0.436	22.99
M2,1	4.539	8.93	37.468	8.98	-24.919	49.94
M2,2	6.653	8.81	11.652	8.86	-1.985	30.54
M3,1	11.911	4.56	7.968	4.67	-0.159	9.29
M3,2	21.885	7.25	17.367	7.19	-1.468	13.54
M4,2	40.136	5.04	10.921	5.51	-2.057	11.14
M5,2	36.039	8.8	8.623	8.94	1.864	15.24
M6,2	33.140	9.26	18.528	9.7	-0.138	15.14
M7,2	19.710	9.29	10.004	9.4	-0.493	17.14

Table 3.7 Maximum Deflection and Residual Deflection Values with Time (LVDT2)

Specimen	Max.+ve.	Time	Max. -ve	Time	Residual	Time
C1	8.782	9.02	19.712	8.19	-19.712	24.24
M1,1	9.105	7.8	6.996	8.2	-2.481	15.8
M1,2	47.039	15.55	10.798	15.71	-0.599	22.99
M2,1	1.940	9.06	37.805	9.00	-19.313	49.94
M2,2	8.008	8.64	5.676	8.58	-0.090	30.54
M3,1	17.427	4.73	14.841	4.76	-0.562	9.29
M3,2	14.838	7.16	16.203	7.34	-2.199	13.54
M4,2	23.741	5.04	17.072	5.13	-5.345	11.14
M5,2	18.504	8.78	7.312	9.27	-0.045	15.24
M6,2	22.438	9.21	27.100	9.61	-1.865	15.14
M7,2	22.748	9.31	18.892	9.4	0.249	17.14

Table 3.8 Maximum Deflection and Residual Deflection Values with Time (LVDT3)

Specimen	Max.+ve.	Time	Max. -ve	Time	Residual	Time
C1	14.016	9.02	19.712	9.14	-19.712	24.24
M1,1	12.584	7.7	6.247	8.1	-0.502	15.8
M1,2	26.562	15.55	13.375	15.75	-0.339	22.99
M2,1	0.553	8.81	34.785	9.07	-20.989	49.94
M2,2	7.089	8.81	7.546	8.82	-0.484	30.54
M3,1	25.494	4.58	15.514	4.74	0.884	9.29
M3,2	24.979	7.18	15.484	7.41	-0.532	13.54
M4,2	32.577	5.06	16.690	5.49	0.478	11.14
M5,2	73.366	8.8	24.604	8.96	-1.684	15.24
M6,2	37.411	9.26	22.868	9.68	0.833	15.14
M7,2	21.211	9.29	14.889	9.69	-4.0154	17.14

Table 3.9 Maximum Deflection and Residual Deflection Values with Time (LVDT4)

Specimen	Max.+ve.	Time	Max. -ve	Time	Residual	Time
C1	6.949	9.02	19.712	9.09	-19.712	24.24
M1,1	15.066	7.7	9.682	7.9	-3.534	15.8
M1,2	25.124	15.59	19.148	15.79	-0.541	22.99
M2,1	13.743	8.91	38.476	9.02	-22.673	49.94
M2,2	5.001	8.66	5.835	8.62	-1.594	30.54
M3,1	32.917	4.56	19.873	5.06	-1.414	9.29
M3,2	22.787	5.57	24.114	7.62	0.012	13.54
M4,2	38.801	5.04	21.226	5.26	-2.003	11.14
M5,2	37.932	8.78	16.751	9.02	-0.262	15.24
M6,2	23.046	9.26	6.617	9.35	0.632	15.14
M7,2	33.537	9.33	15.959	9.55	0.135	17.14

Table 3.10 Maximum Deflection and Residual Deflection Values with Time (LVDT5)

Specimen	Max.+ve.	Time	Max. -ve	Time	Residual	Time
C1	12.543	8.97	9.27	9.06	1.272	24.24
M1,1	8.855	7.6	8.485	7.7	0.117	15.8
M1,2	17.725	15.58	2.809	15.63	6.686	22.99
M2,1	11.851	8.99	5.667	8.96	3.019	49.94
M2,2	2.635	8.69	7.760	8.63	-3.155	30.54
M3,1	12.407	4.59	16.038	4.62	-0.274	9.29
M3,2	28.213	7.15	14.257	7.61	-3.146	13.54
M4,2	22.523	5.05	3.014	5.23	4.232	11.14
M5,2	29.642	8.81	10.001	8.93	1.278	15.24
M6,2	34.764	9.25	14.407	9.56	0.614	15.14
M7,2	22.730	9.3	3.366	9.37	3.419	17.14

Table 3.11 Maximum Deflection and Residual Deflection Values with Time (LVDT6)

Specimen	Max.+ve.	Time	Max. -ve	Time	Residual	Time
C1	19.711	8.48	1.701	9.00	15.134	24.24
M1,1	15.599	7.6	7.775	8.4	-0.559	15.8
M1,2	15.583	15.56	12.916	15.95	0.541	22.99
M2,1	14.964	9.16	1.537	8.96	7.095	49.94
M2,2	3.973	8.84	4.788	8.78	-0.872	30.54
M3,1	13.493	4.57	16.633	4.66	-0.638	9.29
M3,2	17.457	7.17	17.265	7.52	-2.764	13.54
M4,2	26.406	5.03	15.739	5.45	-0.331	11.14
M5,2	15.638	8.92	15.434	8.86	1.017	15.24
M6,2	26.971	9.22	9.965	9.42	1.729	15.14
M7,2	14.606	9.28	1.925	9.33	5.570	17.14

Table 3.12 Maximum Deflection and Residual Deflection Values with Time (LVDT7)

Specimen	Max.+ve.	Time	Max. -ve	Time	Residual	Time
C1	19.711	9.24	4.538	8.98	1.914	24.24
M1,1	12.991	7.60	75.005	8.1	-1.176	15.8
M1,2	19.879	15.62	15.388	15.72	0.211	22.99
M2,1	9.381	9.00	8.655	9.14	1.341	49.94
M2,2	5.282	8.65	2.779	8.75	0.671	30.54
M3,1	27.467	4.61	7.068	4.92	-1.492	9.29
M3,2	27.946	7.15	9.601	7.23	0.054	13.54
M4,2	27.266	5.06	21.307	5.4	-2.069	11.14
M5,2	16.912	8.79	6.936	8.86	-0.057	15.24
M6,2	22.420	9.23	15.668	9.37	-1.943	15.14
M7,2	21.488	9.30	13.737	9.60	0.987	17.14

Table 3.13 Maximum Deflection and Residual Deflection Values with Time (LVDT8)

Specimen	Max.+ve.	Time	Max. -ve	Time	Residual	Time
C1	19.711	9.16	19.712	9.26	-19.712	24.24
M1,1	7.874	7.60	7.294	7.70	0.608	15.8
M1,2	34.626	15.62	19.400	15.95	0.812	22.99
M2,1	12.759	8.91	9.336	9.00	-0.716	49.94
M2,2	4.975	8.60	6.178	8.74	-0.339	30.54
M3,1	33.543	4.62	8.563	5.08	0.800	9.29
M3,2	22.213	7.15	8.103	7.70	-1.835	13.54
M4,2	33.997	5.07	16.886	5.32	0.752	11.14
M5,2	35.101	8.82	15.773	9.04	-4.907	15.24
M6,2	23.073	9.21	12.486	9.56	-0.018	15.14
M7,2	33.937	9.26	9.661	9.46	-1.041	17.14

3.7.2 Strain Data

Similar analysis had been performed for the other sensors as well. To investigate the response of the strain gauges at all slab specimens, Tables 3.14 to 3.21 illustrate maximum strain and residual values with time for all 8 Strain Gauges (SGs).

Table 3.14 Maximum Strain and residual Values with Time (SG1)

Specimen	Max.+ve.	Time	Max. -ve	Time	Residual	Time
C1	1023.969	8.98	-	-	1023.969	24.24
M1,1	2.094	6.8	39.031	12.5	-33.813	15.8
M1,2	263.594	15.54	37.188	15.88	-23.594	22.99
M2,1	1.844	7.96	263.375	8.87	-63.156	49.94
M2,2	53.281	8.57	25.844	8.62	-11.438	30.54
M3,1	74.188	4.68	21.781	4.59	18.844	9.29
M3,2	101.875	7.13	162.313	7.12	-10.969	13.54
M4,2	146.688	4.99	189.094	5.11	-114.406	11.14
M5,2	1023.969	8.74	366.5	8.73	1023.969	15.24
M6,2	189.375	9.18	308.688	9.17	-8.563	15.14
M7,2	151.438	9.24	51.906	9.44	-16.219	17.14

Table 3.15 Maximum Strain and residual Values with Time (SG2)

Specimen	Max.+ve.	Time	Max. -ve	Time	Residual	Time
C1	2.031	8.94	78.906	8.98	-66.25	24.24
M1,1	19.719	7.7	1.344	1.1	7.219	15.8
M1,2	49.343	15.54	51.438	15.88	-10.625	22.99
M2,1	1.063	2.83	344.969	8.87	-65.5	49.94
M2,2	52.063	8.57	36.656	8.62	-17.875	30.54
M3,1	215.531	4.55	26.406	4.58	47.375	9.29
M3,2	148.25	7.13	387.625	7.12	-33.719	13.54
M4,2	758.844	5.00	209.844	5.33	-207.406	11.14
M5,2	1023.969	8.74	550.469	8.73	1023.969	15.24
M6,2	636.219	9.18	584.656	9.17	134.531	15.14
M7,2	84.781	9.24	68.344	9.44	-3.25	17.14

Table 3.16 Maximum Strain and residual Values with Time (SG3)

Specimen	Max.+ve.	Time	Max. -ve	Time	Residual	Time
C1	2.156	8.38	79.406	14.16	-78.875	24.24
M1,1	4.656	7.5	133	13.9	-131.844	15.8
M1,2	95.75	15.55	36.594	15.86	4.031	22.99
M2,1	1023.969	8.88	1024	8.87	1023.969	49.94
M2,2	1023.969	0	-	-	1023.969	30.54
M3,1	1023.969	4.55	5.03	2.97	023.969	9.29
M3,2	1023.969	0	403.906	7.12	1023.969	13.54
M4,2	79.906	5.00	76.125	5.33	2.188	11.14
M5,2	1023.969	8.73	-	-	1023.969	15.24
M6,2	1023.969	9.18	629.813	9.17	443.906	15.14
M7,2	55.188	9.25	174.463	9.24	-70.313	17.14

Table 3.17 Maximum Strain and residual Values with Time (SG4)

Specimen	Max.+ve.	Time	Max. -ve	Time	Residual	Time
C1	1023.969	9.00	60.594	8.96	1023.969	24.24
M1,1	7.125	7.6	1.406	0.9	1.094	15.8
M1,2	1023.969	15.55	-	-	1023.969	22.99
M2,1	1023.969	8.88	616.031	8.87	1023.969	49.94
M2,2	1023.969	0	-	-	1023.969	30.54
M3,1	1023.969	4.55	5.03	2.97	023.969	9.29
M3,2	1023.969	0	-	-	1023.969	13.54
M4,2	1023.969	5.00	-	-	1023.969	11.14
M5,2	57.875	8.73	69.969	9.27	-58.938	15.24
M6,2	479.719	9.18	614.594	9.17	65.438	15.14
M7,2	114.875	9.25	302.469	9.24	-43.625	17.14

Table 3.18 Maximum Strain and residual Values with Time (SG5)

Specimen	Max.+ve.	Time	Max. -ve	Time	Residual	Time
C1	161.25	9.18	19.969	9.02	-12.875	24.24
M1,1	33.563	7.7	2.625	0.6	16.719	15.8
M1,2	344.813	15.56	1.375	12.14	163.781	22.99
M2,1	-	-	376.813	8.87	141.938	49.94
M2,2	77.844	8.57	29.625	8.86	-29.563	30.54
M3,1	86.531	4.68	13.75	4.59	30.281	9.29
M3,2	179.344	7.13	347.219	7.12	47.625	13.54
M4,2	73.125	5.00	103.688	5.33	-14.563	11.14
M5,2	43.656	8.74	78.125	9.15	-29.813	15.24
M6,2	112.094	9.18	70.531	9.17	2.625	15.14
M7,2	29.25	9.45	119.156	9.44	-13.75	17.14

Table 3.19 Maximum Strain and residual Values with Time (SG6)

Specimen	Max.+ve.	Time	Max. -ve	Time	Residual	Time
C1	1023.969	9.22	35.469	9.1	1023.969	24.24
M1,1	40.688	7.7	2.563	6.1	12.844	15.8
M1,2	148.906	15.65	8.344	15.55	43.313	22.99
M2,1	210.156	8.92	361.656	8.87	-92.688	49.94
M2,2	135.844	8.58	4.688	8.63	7.969	30.54
M3,1	63.125	4.55	33.813	4.59	1.188	9.29
M3,2	206.469	7.13	209.219	7.12	36.406	13.54
M4,2	64.063	4.99	110.313	5.33	-40.344	11.14
M5,2	43.656	8.74	78.125	9.15	-29.813	15.24
M6,2	30.406	9.18	124.75	9.17	-32.969	15.14
M7,2	14.156	9.45	113.813	9.44	-21.719	17.14

Table 3.20 Maximum Strain and residual Values with Time (SG7)

Specimen	Max.+ve.	Time	Max. -ve	Time	Residual	Time
C1	1023.969	8.99	587.906	8.98	1023.969	24.24
M1,1	60.906	7.6	26.094	13.3	-25.063	15.8
M1,2	92.031	15.55	155.688	15.56	-91.875	22.99
M2,1	0.688	8.76	444.063	8.87	-122.188	49.94
M2,2	28.063	8.57	20.063	8.75	-13.344	30.54
M3,1	192.469	4.55	83.094	4.76	-29.906	9.29
M3,2	247.469	7.13	531.5	7.12	21.688	13.54
M4,2	1023.969	4.99	0.969	4.98	1023.969	11.14
M5,2	129.25	9.16	31.031	9.27	22.656	15.24
M6,2	66.844	9.18	153.594	9.17	-22.906	15.14
M7,2	171.25	9.25	92.5	9.44	35.469	17.14

Table 3.21 Maximum Strain and residual Values with Time (SG8)

Specimen	Max.+ve.	Time	Max. -ve	Time	Residual	Time
C1	1023.969	9.05	92.438	8.96	1023.969	24.24
M1,1	1.438	7.3	42.813	14.3	-40.875	15.8
M1,2	1023.969	15.55	1.125	15.42	1023.969	22.99
M2,1	-	-	490.156	8.87	-112.438	49.94
M2,2	24.875	8.57	12.75	8.65	-5.438	30.54
M3,1	119.313	4.55	76.25	4.76	-38.844	9.29
M3,2	186.719	7.13	197.25	7.12	15.563	13.54
M4,2	1023.969	4.99	1.625	4.96	1023.969	11.14
M5,2	81.219	8.73	56.218	9.27	26.031	15.24
M6,2	55.063	9.18	138	9.17	-28.063	15.14
M7,2	141.344	9.37	98.438	9.26	72.969	17.14

3.7.3 Load Cell Data

To apply impact loads on slab specimens, impact loads were dropped from 1m and 2m drop heights. Using equations 3.1 and 3.2, the input impact energies and velocities are obtained as follows:

W= m*g= 200*9.81= 1.96 N

E= 1.962*1= 1.962 kJ and v= √2*9.81*1= 13.87 m/s for 1m.

E= 1.962*2= 3.924 kJ and v=√2*9.81*2=19.62 m/s for 2m.

To investigate the data obtained from the load cell, load cell readings were as presented in Table 3.22. Where: negative values means: load cell was being compressed; it means: it measured how

much load from the impact. Positive values means: vice versa (weight was bouncing upward).

Table 3.22 Impact Load of Impact Load Test on HFRC Slab Specimens

Specimen	Positive values kN	Negative values kN
C1	1.5965	209.4162
M1 at 1m	0.3259	7.2218
M1 at 2m	6.9961	63.9098
M2 at 1m	0.37614	64.0853
M2 at 2m	4.7811	116.1845
M3 at 1m	6.4445	13.7666
M3 at 2m	6.3525	273.8944
M4 at 2m	1.2287	57.8331
M5 at 2m	4.0038	194.1283
M6 at 2m	5.3579	273.8944
M7 at 2m	4.1124	194.7469

3.7.4 The Strain Rate of HFRC Slabs

Table 3.23 shows the highest tensile and compressive strain rates of the specimens at the first drop.

Table 3.23 Maximum Tension and Compression Strain Rate (µm/m) of Impact Test HFRC Slab Specimens for Strain Gauges

Specimen	Tension strain rate	Compression strain rate
C1	1023.969	587.9063
M1 at 1m	60.90625	132.1875
M1 at 2m	1023.969	155.6875
M2 at 1m	1023.969	1024
M2 at 2m	135.8438	36.65625
M3 at 1m	1023.969	83.09375
M3 at 2m	1023.969	531.5
M4 at 2m	1023.969	209.8438
M5 at 2m	1023.969	550.4688
M6 at 2m	1023.969	629.8125
M7 at 2m	171.25	302.4688

3.7.5 Load Deflection of Impact Load Test of HFRC Slabs

Table 3.24 illustrates the maximum deflection of impact load test. Where: Positive values means: deflection upward and negative values means: deflection downward.

Table 3.24 Maximum Deflection (mm) of Impact Load Test HFRC Slab Specimens for 8 LVDTs

Specimen	Positive values	Negative values	Residual
C1	19.7114	19.712	-19.712
M1,1	17.57765	8.485038	-2.142
M1,2	47.03917	19.2891	6.686
M2,1	14.96386	38.47593	-24.919
M2,2	8.088006	11.65226	3.155
M3,1	33.54312	19.87261	-1.492
M3,2	28.21328	24.11363	-3.146
M4,2	40.13624	21.30734	-5.345
M5,2	37.93152	24.6039	-4.907
M6,2	37.41117	27.10039	-1.943
M7,2	33.93714	18.89207	5.570

CHAPTER FOUR

ANALYSIS AND DISCUSSION OF RESULTS

4.1 Introduction

The experimental procedure started with using different ratios of steel and PP fibers on concrete to investigate the effect of Hybrid Fiber on mechanical properties of concrete and the dynamic testing of impact load with drop-heights h = 1.0 m and 2.0 m. the results of both mechanical and impact tests on HFRC slabs are given in this chapter. Test set-up, experiments, slab specimens and concrete properties test results are presented in Chapter3.

In this chapter, section 4.2 presents concrete tests results analysis, slump tests for all concrete mixes; concrete compressive strength tests and flexural strength tests. The impact results gathered from the data logger are analyzed in section 4.3. The information treated in this section covers, among others, the strain field of the slab specimens and impact load due to impact, slab deflection over time, as well as the variation of the deflected shape of the slab over time. Whiles, sections 4.4 and 4.5 present the discussion of concrete mechanical properties and the impact load test respectively.

4.2 Concrete Test Results Analysis

4.2.1 Slump Test Results Analysis

Figure 4.1 and Table 4.1 show the results of slump tests for all concrete mixes. The following conclusions can be drawn from these results: The combination of SF and PPF reduces the slump of M2, M3, M5, and M6 specimens from 29 mm for the control specimen C1 to 15 mm (48% reduction). M1 and M4 have a slump value of roughly 25 mm (13.8% reduction), whereas M7 has a slump value of 26 mm (10.3% reduction). The workability of the mixtures stiffens as the percentage of fiber increases from 0.5 percent to 1.0 percent. This implies that adding SF and PPF fibers to concrete will make it less workable. Moreover, due to the higher surface area of hybrid fiber than plain concrete, the matrix absorbs a greater amount of water and thus makes the mixture stiffer

resulting in lower workability. Also, as had been conducted by Mohammadhossieni et al., 2020, the higher the fiber dosage, the lower the workability of concrete.

Table 4.1 % Difference Slump Test Results

Specimen	Slump Value (mm)	Difference %
C1	29	-
M1	25	-13.8
M2	15	-48.3
M3	15	-48.3
M4	25	-13.8
M5	15	-48.3
M6	15	-48.3
M7	26	-10.3

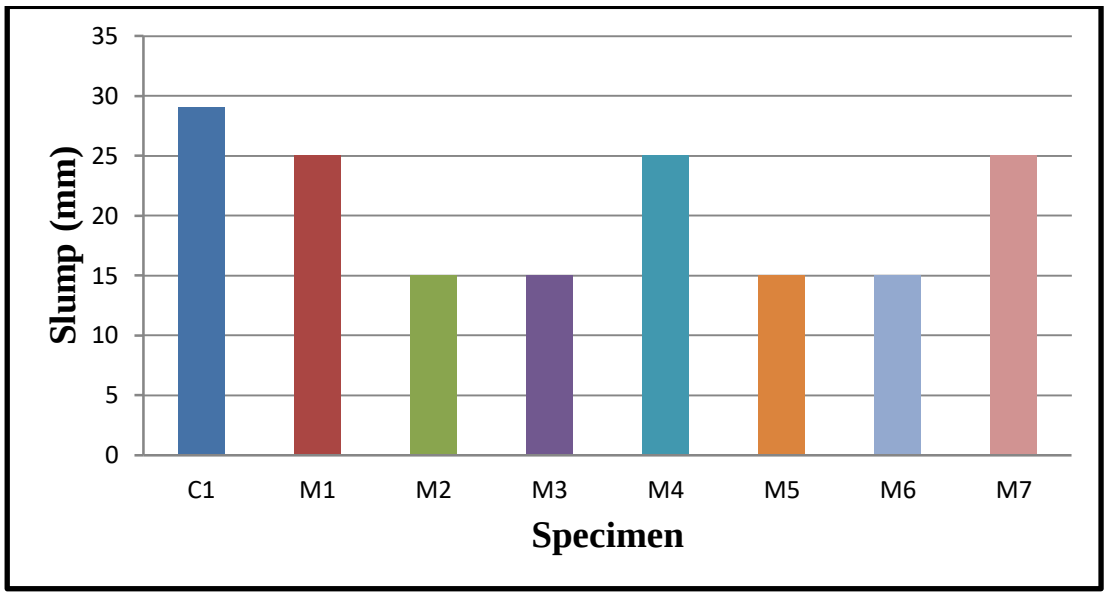

Figure 4.1 Slump Test Results of Concrete Mixtures

4.2.2 Concrete Compressive Strength Test Results

As shown result from Table 4.2 and Figure 4.2, it may be concluded that: Control specimen C1 obtained a compressive strength of 40.4 MPa, which is 1% higher than the specified compressive strength of 40 MPa. With a 24% difference, M1 equals 30.3 MPa. Other specimens also had lower concrete compressive strength ratings. M1 and M4 (65/35 3D and 65/60 5D steel fiber) have the highest value, while M6 (65/60 5D steel fiber

with PP fiber) has the lowest. This indicates that when two fibers are combined, their compressive strength decreases. M7 (PP fiber alone) has a greater value than M6.

Table 4.2 % Difference in Compressive Strengths

Specimen	Strength (N/mm^2)	Difference relative to C1 %	Difference relative to Designed Strength %
C1	40.4	-	+1.0
M1	30.4	-24.8	-24
M2	25.3	-37.4	-36.8
M3	17.2	-57.4	-57
M4	29.6	-26.7	-26
M5	18.9	-53.2	-52.8
M6	12.6	-68.8	-68.5
M7	14.7	-63.6	-63.3

4.2.3 Flexural Strength Test

The results of the Concrete Flexural Strength Test are shown in Figure 4.3. As all of the results of concrete mixture specimens are analyzed, it can be shown that there is a 44.4% improvement in the behavior of concrete specimens with 1% of 65/60 5D steel fiber when compared to C1 (control concrete specimens), as shown in Table 4.3. In other words, steel fibers enhanced flexural strength by 44.44% for M4 specimens with 65/60 5D Steel Fiber and 6.66% for M2 specimens with 65/60 5D Steel Fiber (0.5 percent steel fiber and 0.5 percent PP fiber). The change in failure mode from brittle to ductile revealed that the sudden loss in concrete flexural strength for hybrid fiber reinforced concrete may be attributed to non uniform fiber distribution in the specimens.

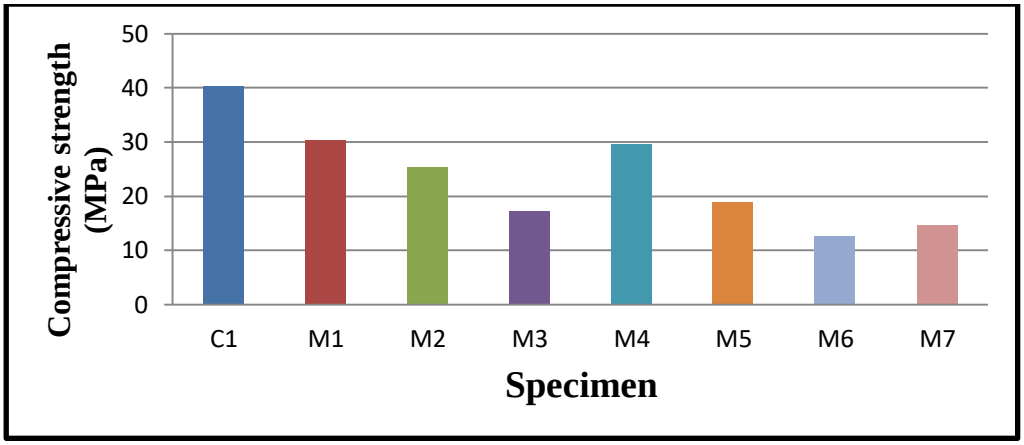

Figure 4.2 Compressive Strengths of Concrete Specimens

Table 4.3 % Difference in Flexural Strengths

Specimen	Flexural Strength (N/mm^2)	Difference Relative to C1 %
C1	4.5	-
M1	4.1	-8.9
M2	4.8	6.7
M3	4.6	2.2
M4	6.5	44.4
M5	3.5	-22.2
M6	4.1	-8.9
M7	2.8	-37.8

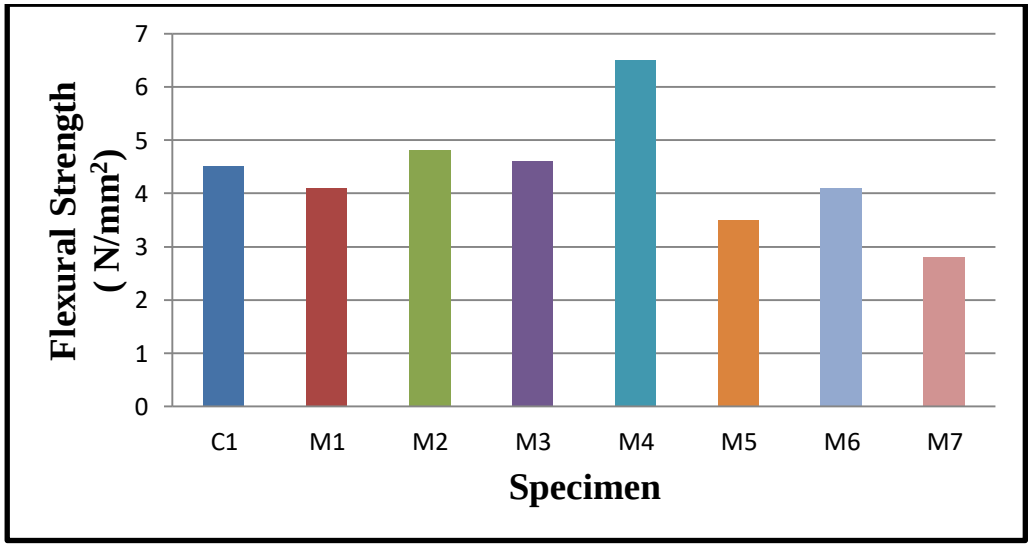

Figure 4.3 Flexural Strengths of Concrete Specimens

Figure 4.4 shows flexural strength versus 3D stel fiber reinforcement the relation defining the best fit of flexural strength using C1, M2 and M3 for 65/35 3D steel fiber, When x= fiber reinforcement ratio, y= expected flexural strength value and R^2=the proportion of the variation in the independent variable.

$$y= 0.2x+4.5 \quad (4.1)$$

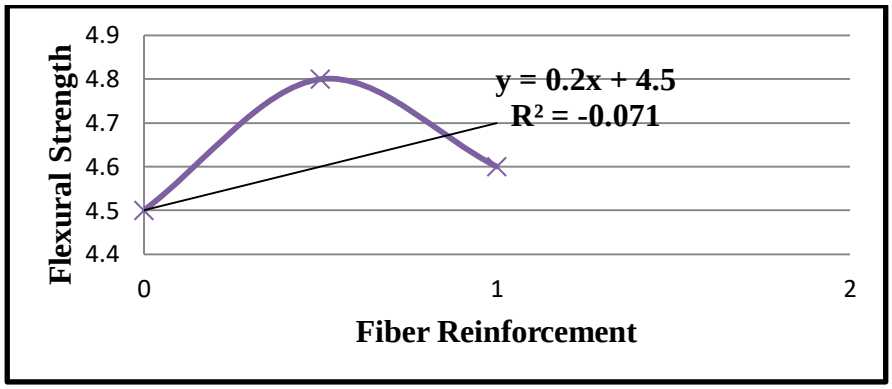

Figure4.4 Flexural Strength versus 3D Steel Fiber Reinforcement

Figure 4.5 shows the relation defining the best fit of flexural strength using C1, M5 and M6 for 65/60 5D steel fiber.

$$y= -0.72x+4.5 \quad (4.2)$$

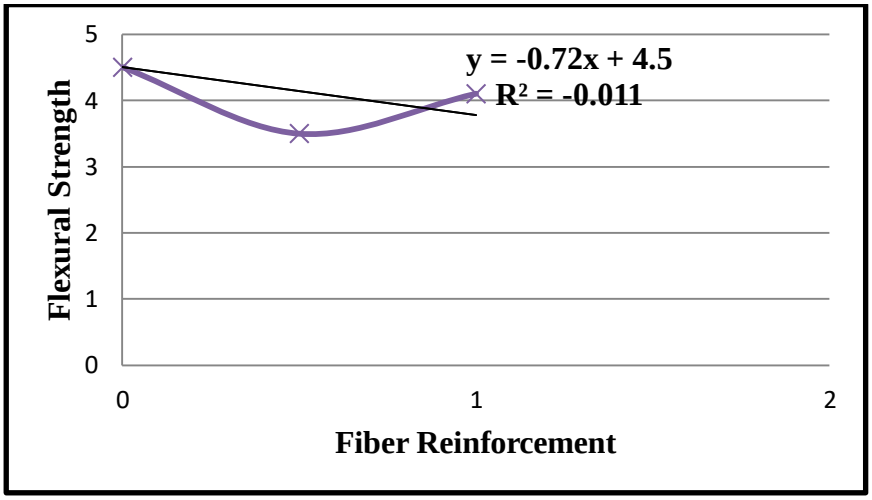

Figure4.5 Flexural Strength versus 5D Fiber Reinforcement

As shown from Figures 4.4 and 4.5, the negative R^2 values mean that prediction tends to be less accurate that average values of the data set over time.

4.3 Impact Load Test

In this test, the specimens were subjected to impact drop to assess the validity of the adopted Hybrid Fiber (PPF and SF) strengthening approach to resist loads with high loading rates such as impact loads. The assessment was made in this study by comparing the results between the strengthened and the non-strengthened slab specimens in terms of the load, the deflection, the failure mode, the crack patterns, and the dissipated energy. The detailed experiments focused on structural behavior of concrete slabs with different hybrid fiber mixes under the impact load

The slab specimens that involved 1 m drop height were C1, M1, M2 and M3 only. Those slabs except C1 had shown no effects at all including no spotted crack. So, the condition before and after the 1 m drop height for slab specimens M1, M2 and M3 were same. Slab specimens M4, M5, M6 and M7 were tested with 2 m drop height only as there were no effects on slabs at 1 m drop height. As mentioned in Chapter 3, data from the sensors were collected with a digital data acquisition system at a 100 Hz sampling rate. Data were read and recorded on computer at a rate of 100 times per second (100000 cycles/second). The obtained results can be summarized as follows:

4.3.1 Deflection Data

The displacement–time histories measured (at a distance of 300mm from the specimen mid span) were found to respond typically as shown in Figures 4.6 to 4.16. from the Figures, it can be seen that, after the initial contact between impactor and specimen, the deflection of the specimens increases to a maximum value and following a number of fluctuations for a short period, obtained its residual value, the latter essentially being dependant on the level of damage suffered by the specimens. Under each impact test, the slab specimen starts to vibrate in same direction of drop weight motion. After the slab specimen reaches the maximum displacement, the slab specimen vibrates in a high frequency at the equilibrium position. When there is no plastic deformation or damage in the slab specimen during impact, the slab specimen except C1 is in a free vibration at zero equilibrium position and there is no offset. However, if the plastic deformation occurred, the slab specimen will vibrate at new equilibrium position. This is similar to what had been concluded by Saatci, 2007. In Figures 4.6 to 4.16, show a lot of variations in the deflection and time relationship, this requires

further studies.All deflection values are positive (upwards) because there are at support.

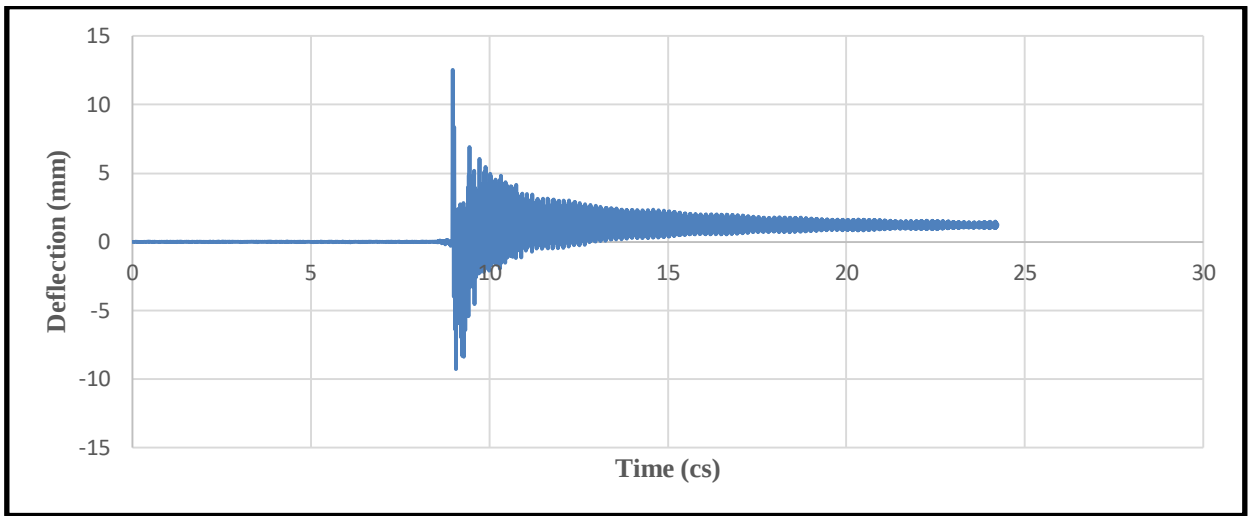

Figure 4.6 Deflections versus Time for C1 at 1 m Drop

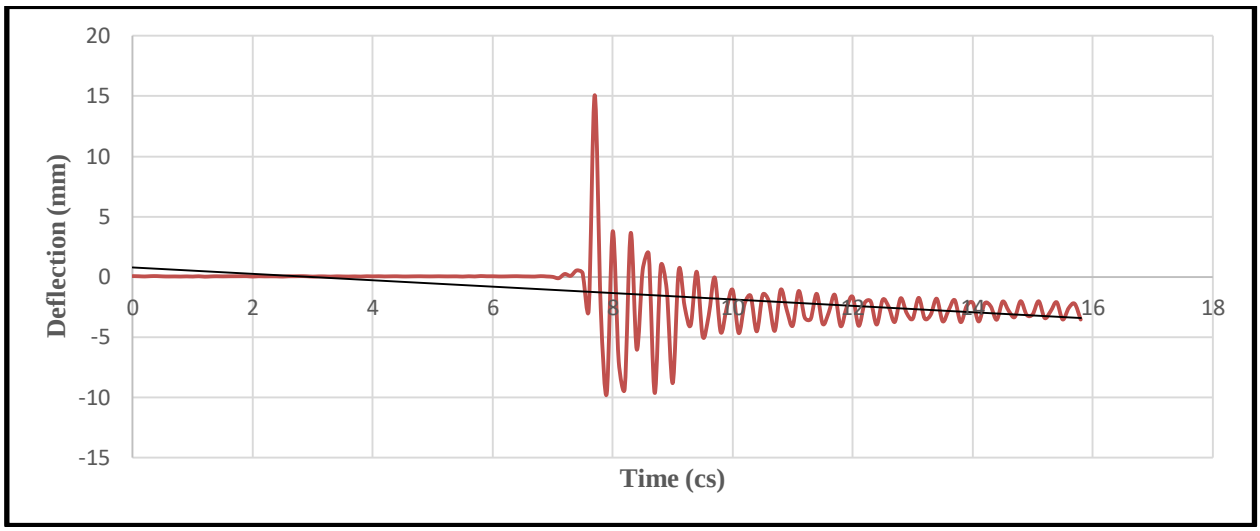

Figure 4.7 Deflections versus Time for M1 at 1 m Drop

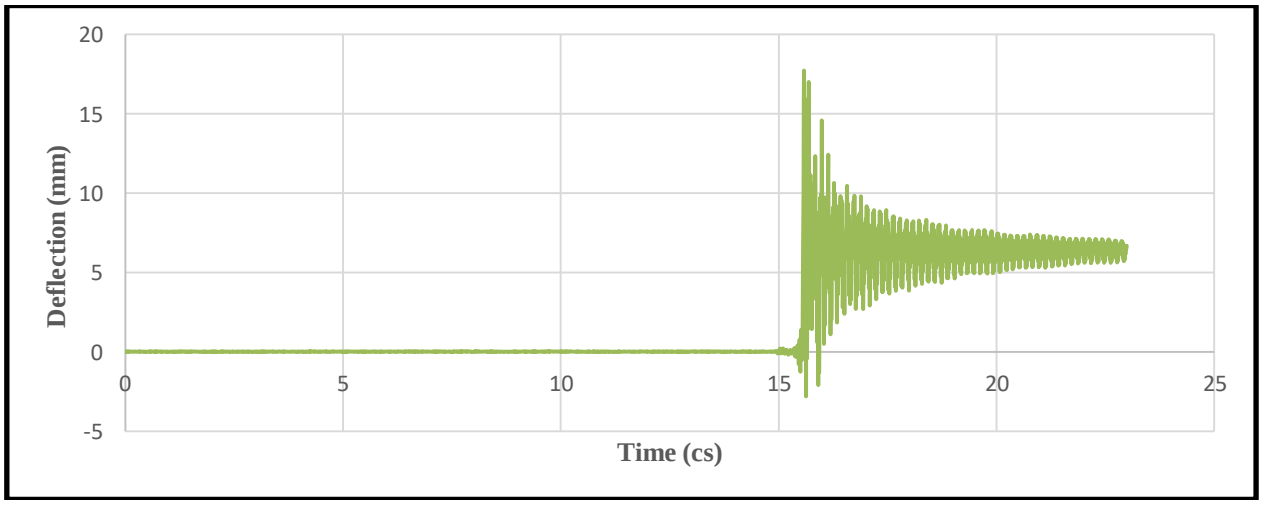

Figure 4.8 Deflections versus Time for M1 at 2m Drop

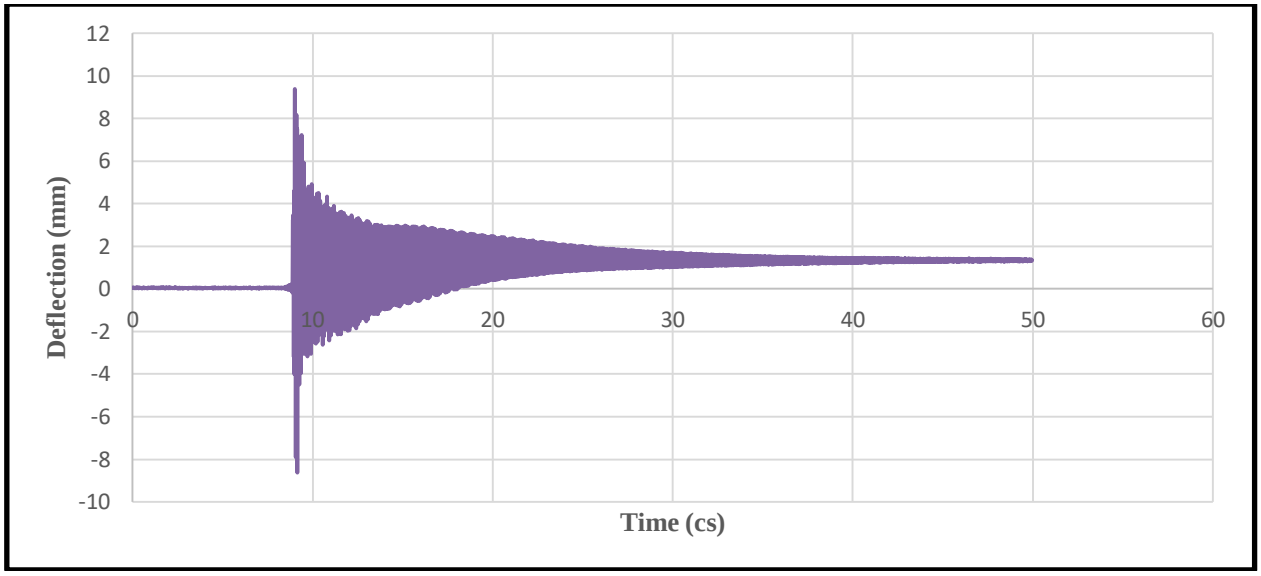

Figure 4.9 Deflections versus Time for M2 at 1m Drop

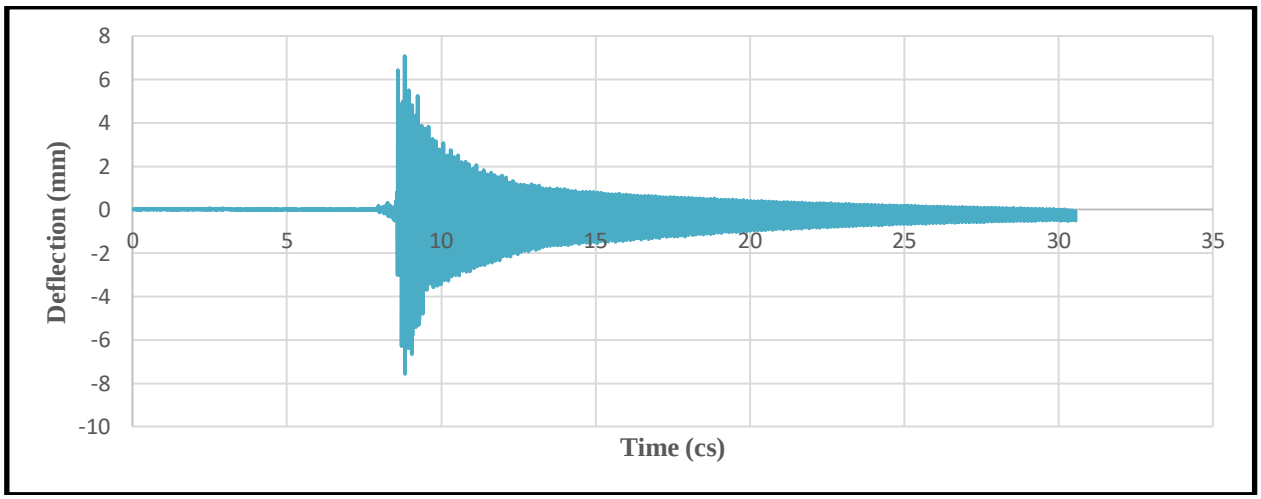

Figure 4.10 Deflections versus Time for M2 at 2m Drop

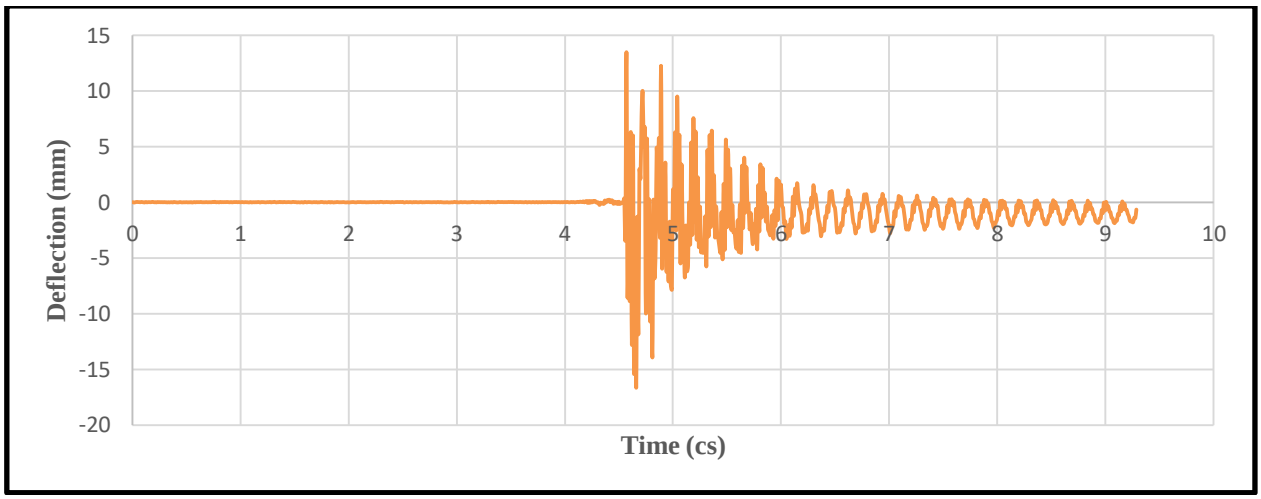

Figure 4.11 Deflections versus Time for M3 at 1m Drop

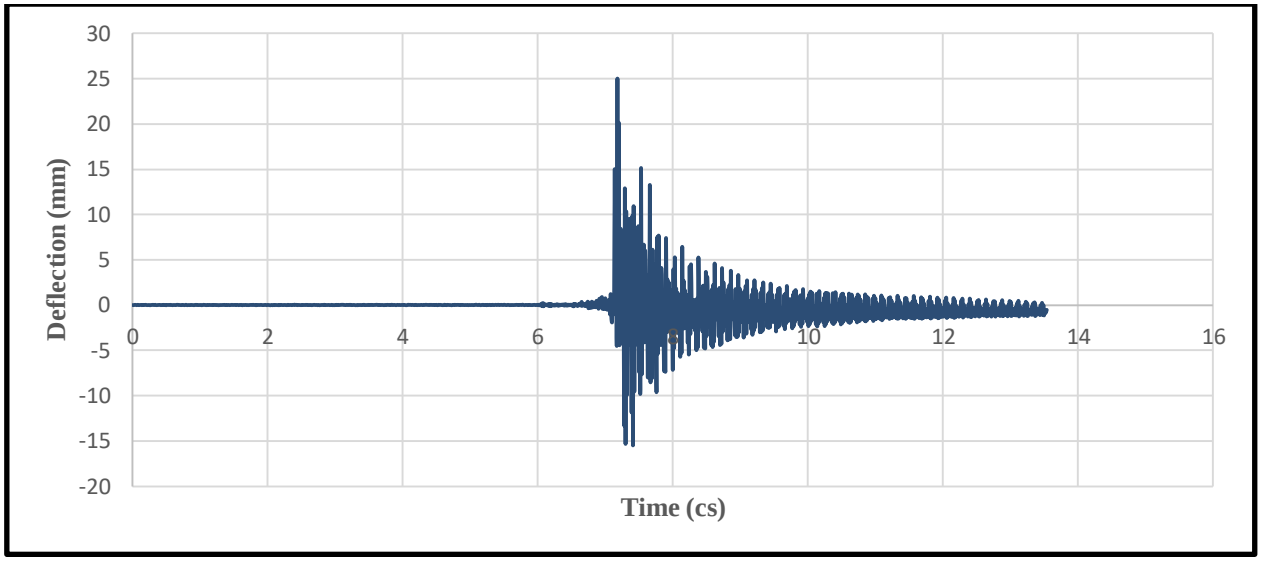

Figure 4.12 Deflections versus Time for M3 at 2m Drop

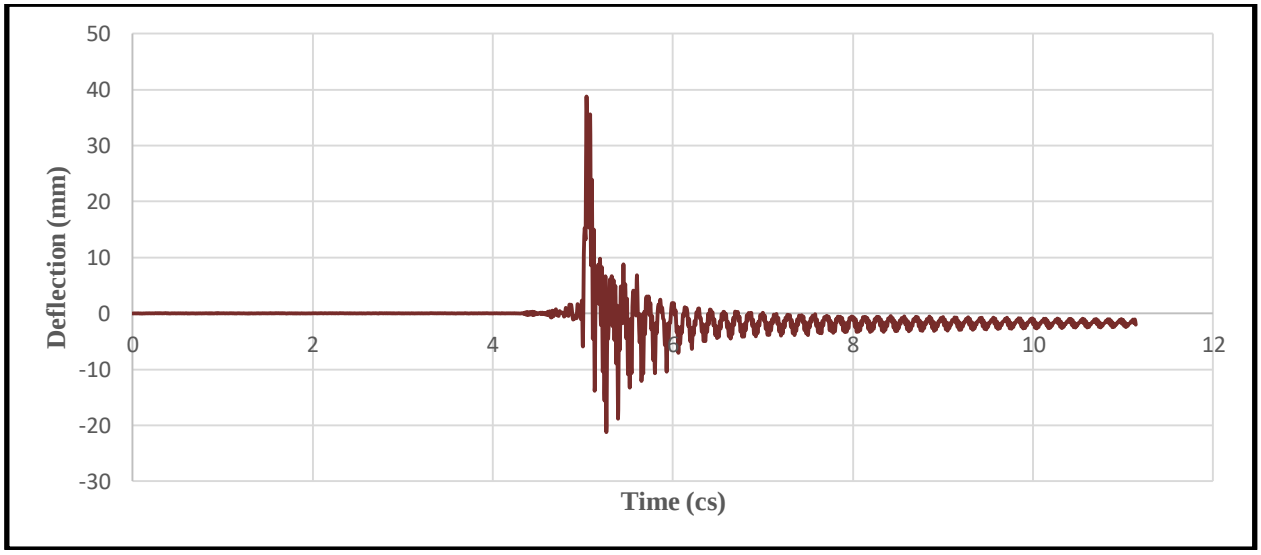

Figure 4.13 Deflections versus Time for M4 at 2m Drop

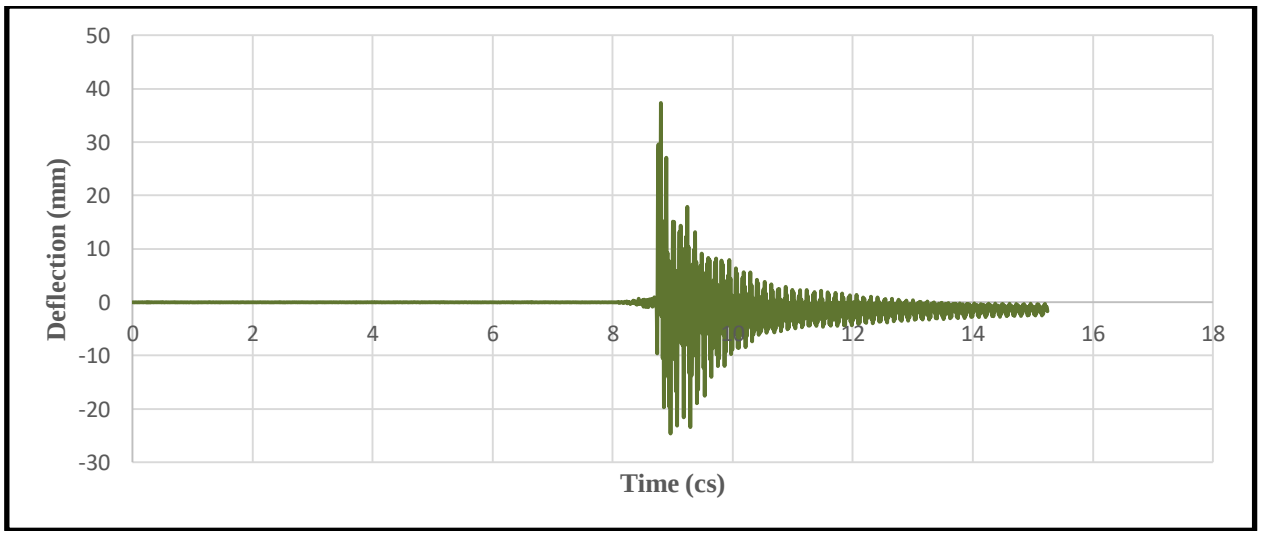

Figure 4.14 Deflections versus Time for M5 at 2m Drop

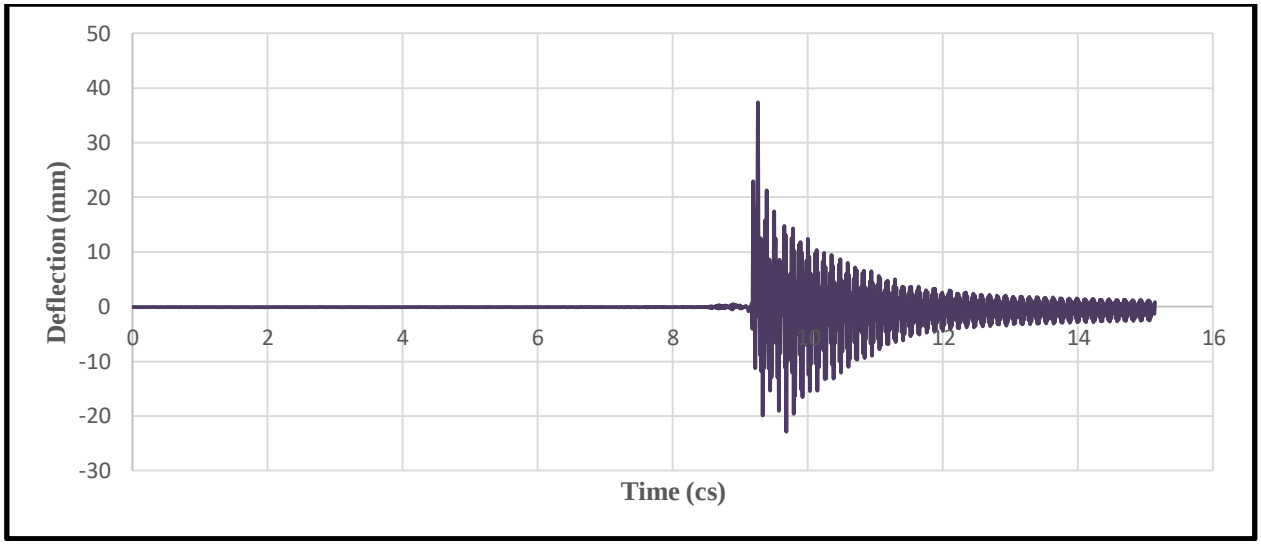

Figure 4.15 Deflections versus Time for M6 at 2m Drop

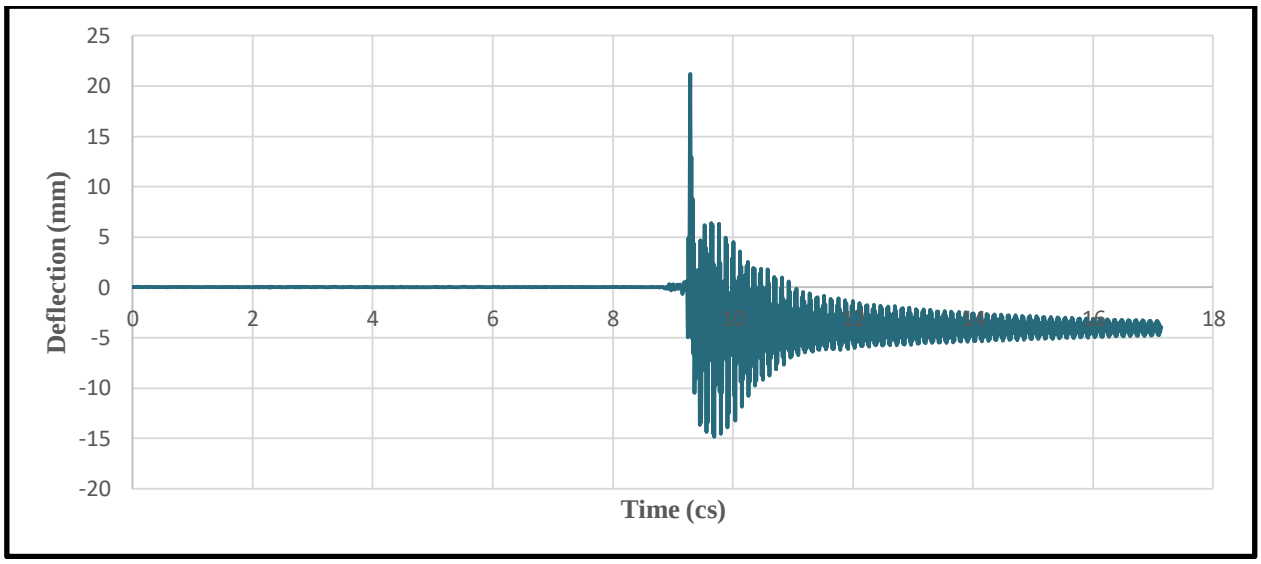

Figure 4.16 Deflections versus Time for M7 at 2 m Drop

4.3.2 Strain Data

Similar analysis had been performed for the other sensors as well. Figures 4.17 to 4.27 present strain versus time for all slab specimens.

As seen in Figure 4.17, significant yielding and deformation occurred in control specimen C1. There were low frequencies due to the irregular nature of the vibrations after the impact. Other specimens were very similar to C1, except M1 at 1m drop and M6 at 2 drop, the exception of a distinctive peak frequency and relatively regular vibrations after impact. With C1, the specimen suffered much damage at 1 m drop.

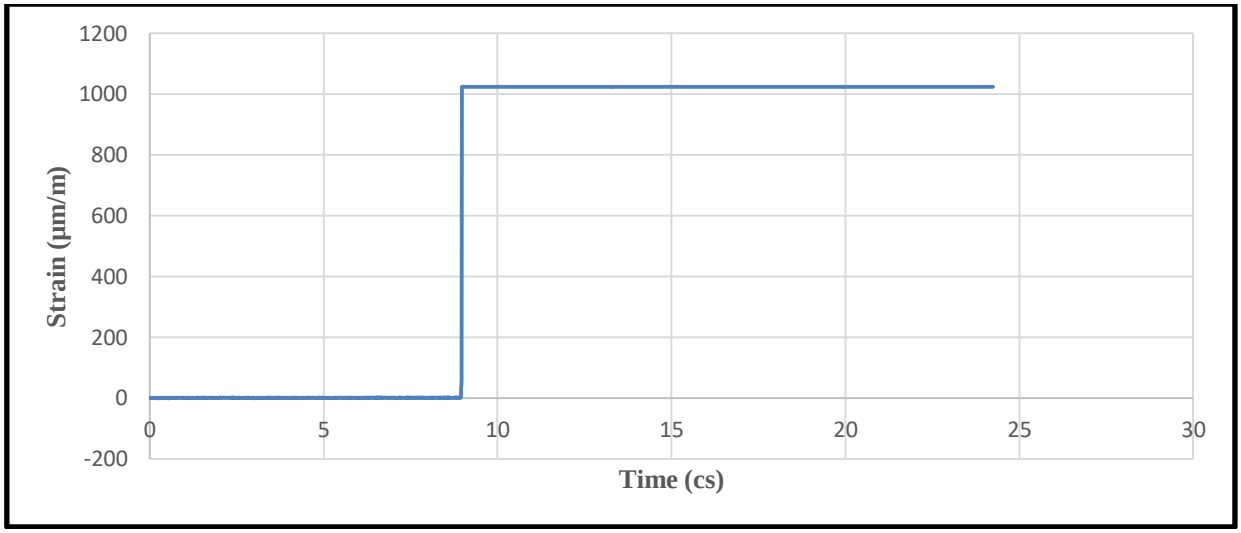

Figure 4.17 Strains versus Time for C1 at 1m Drop

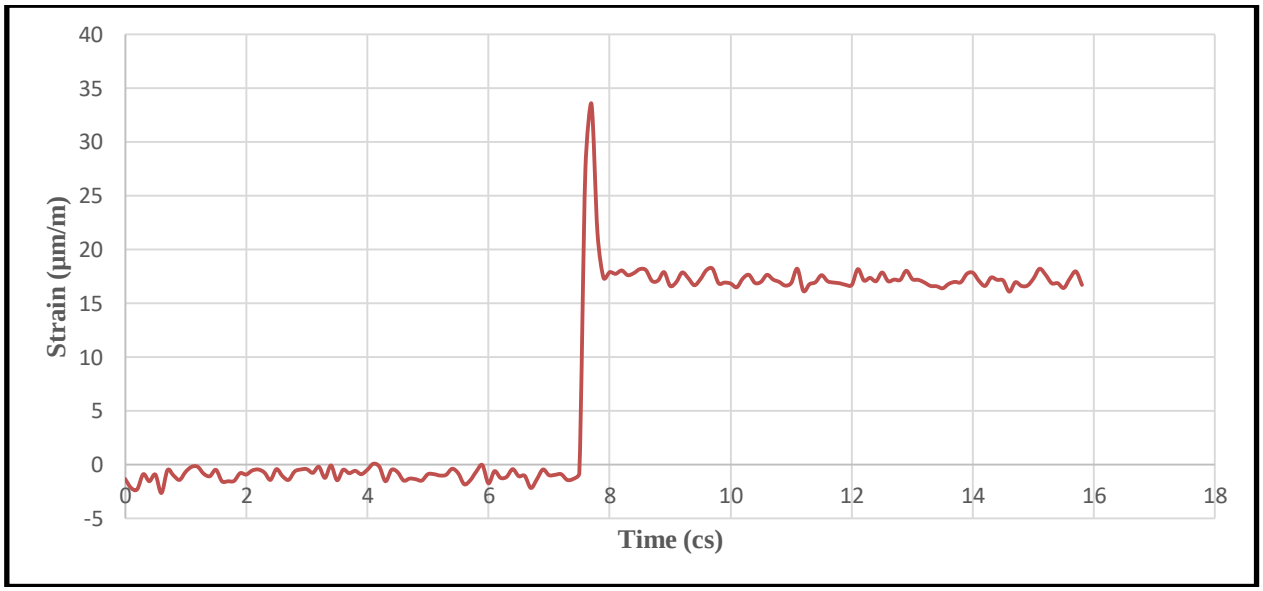

Figure 4.18 Strains versus Time for M1 at 1m Drop

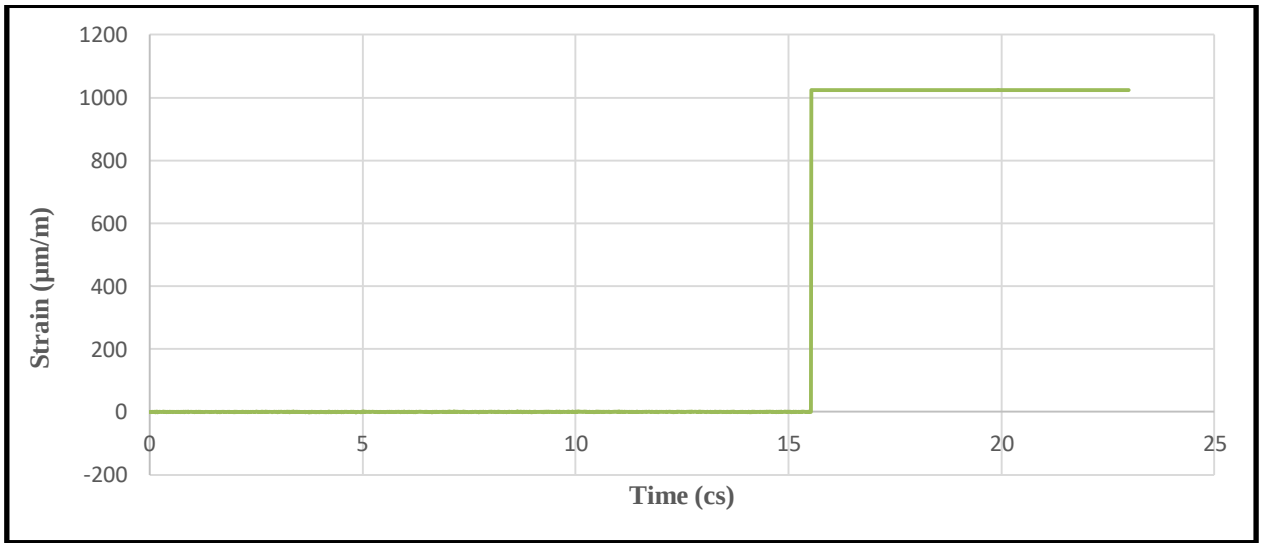

Figure 4.19 Strains versus Time for M1 at 2m Drop

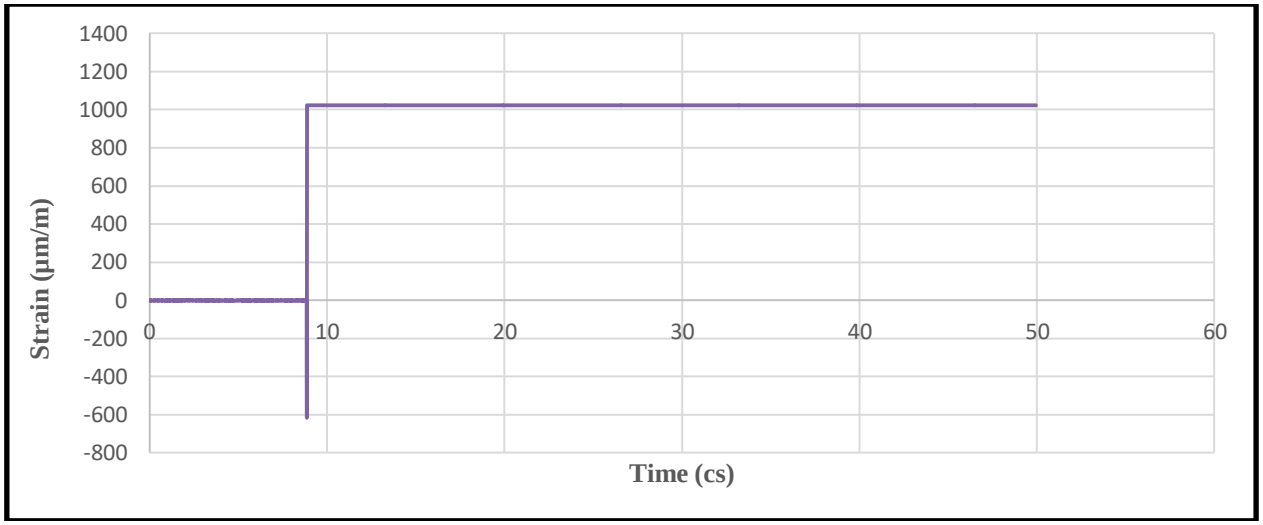

Figure 4.20 Strains versus Time for M2 at 1m Drop

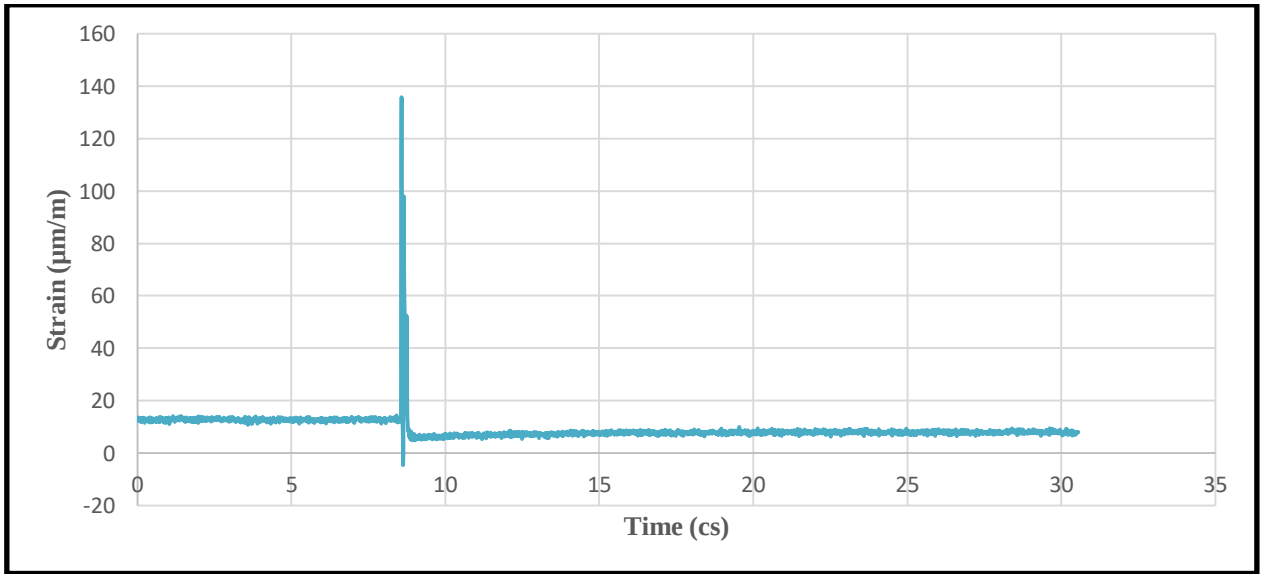

Figure 4.21 Strains versus Time for M2 at 2m Drop

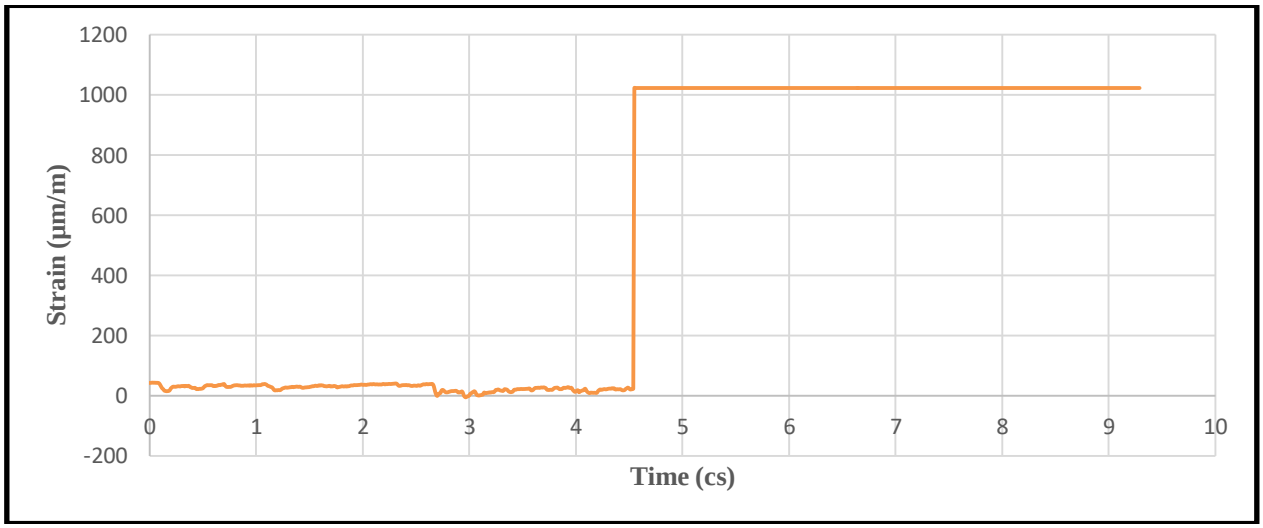

Figure 4.22 Strains versus Time for M3 at 1m Drop

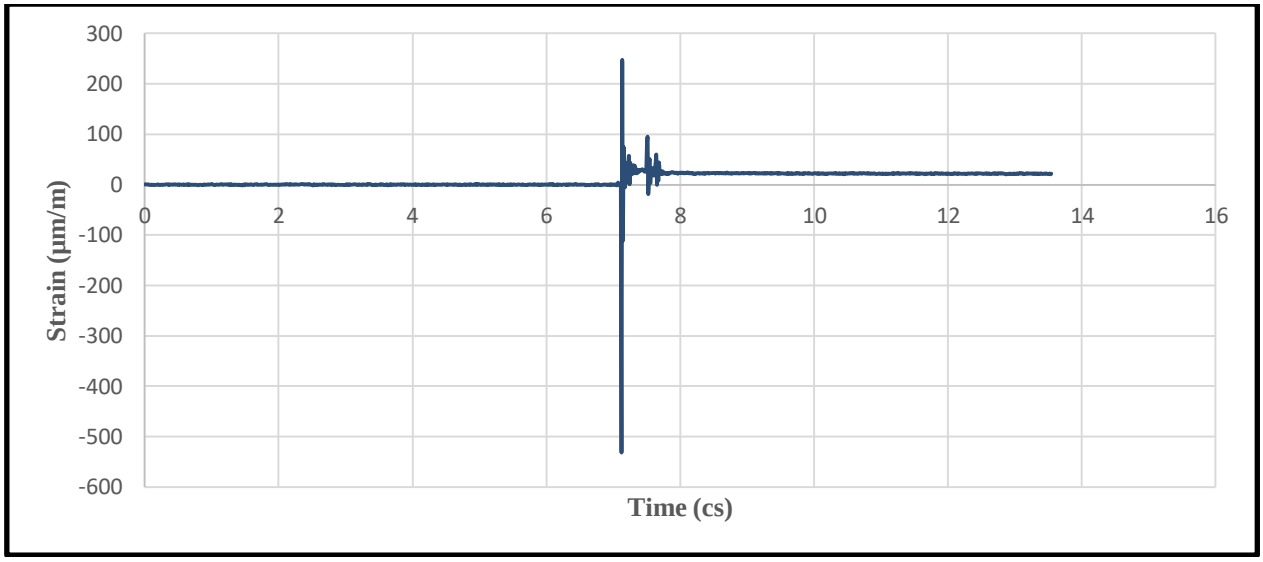

Figure 4.23 Strains versus Time for M3 at 2m Drop

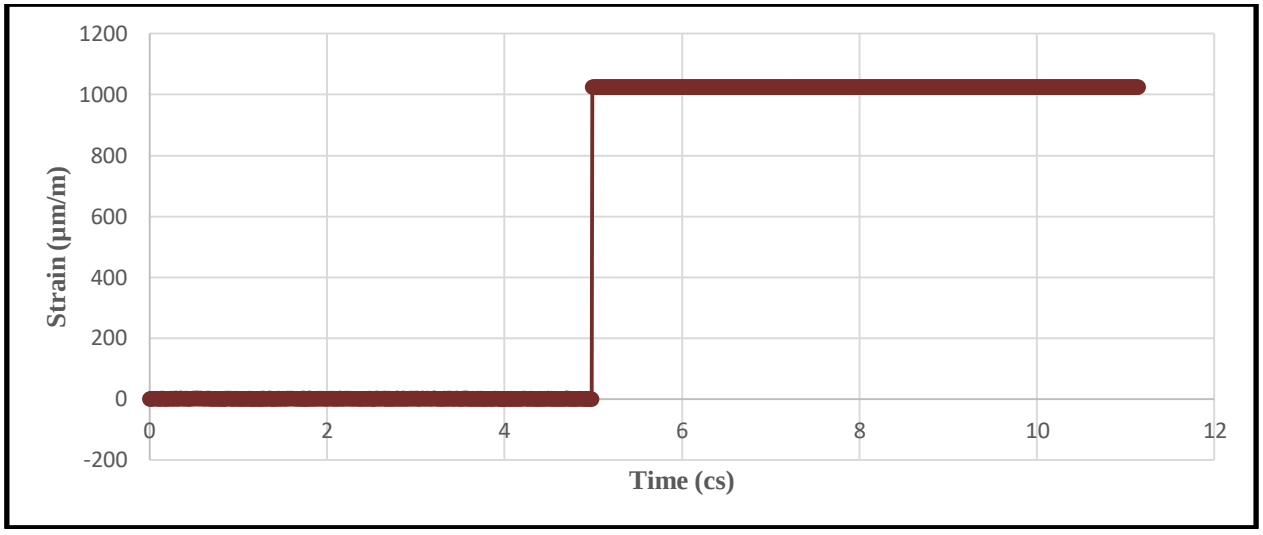

Figure 4.24 Strains versus Time for M4 at 2m Drop

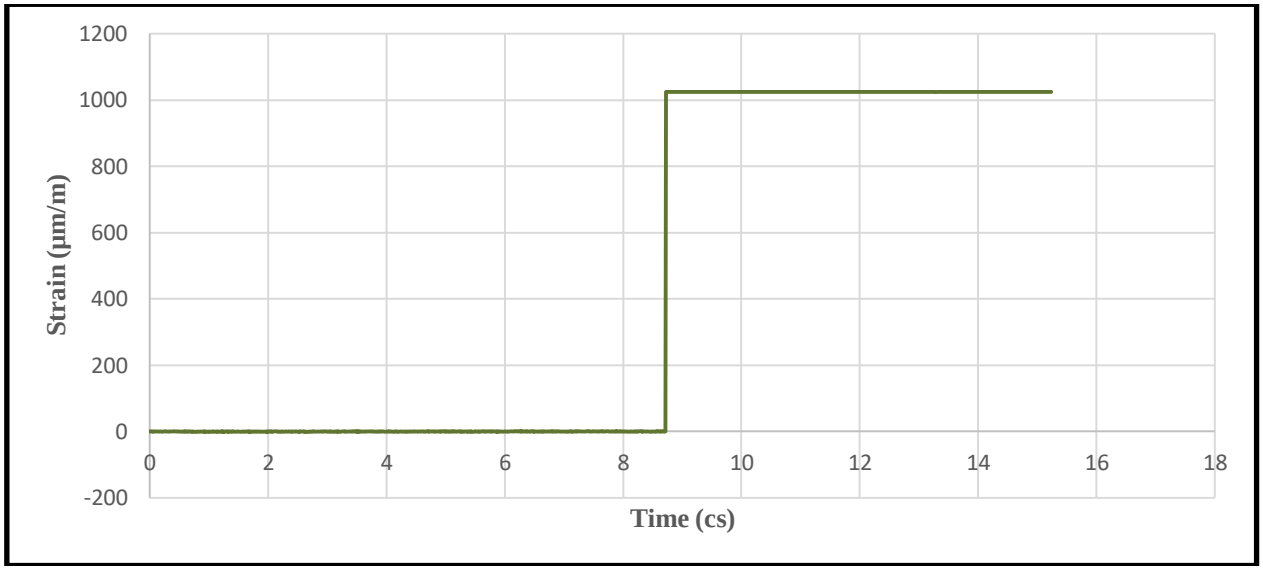

Figure 4.25 Strains versus Time for M5 at 2m Drop

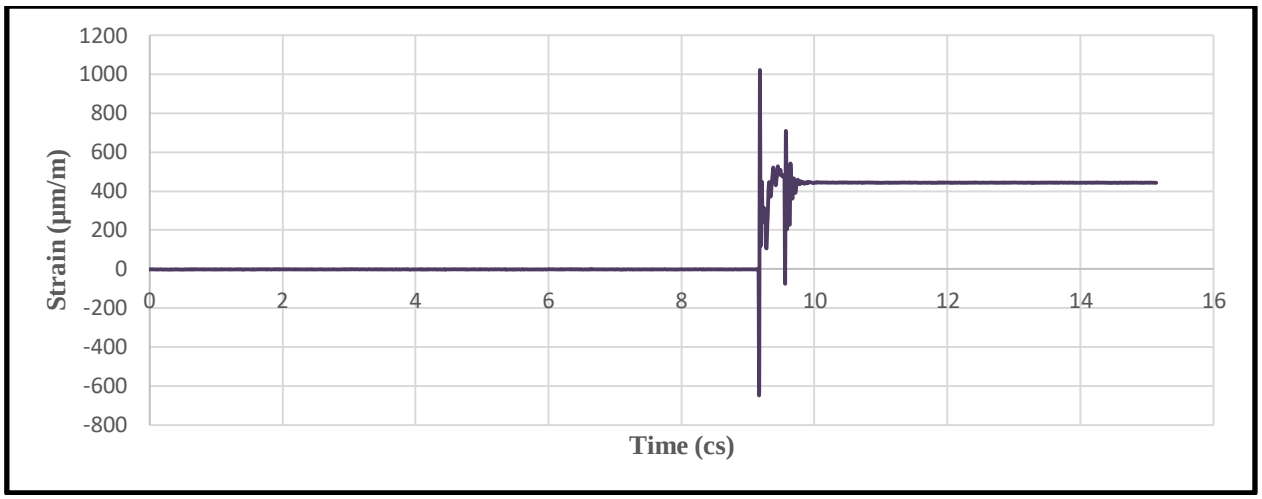

Figure 4.26 Strains versus Time for M6 at 2m Drop

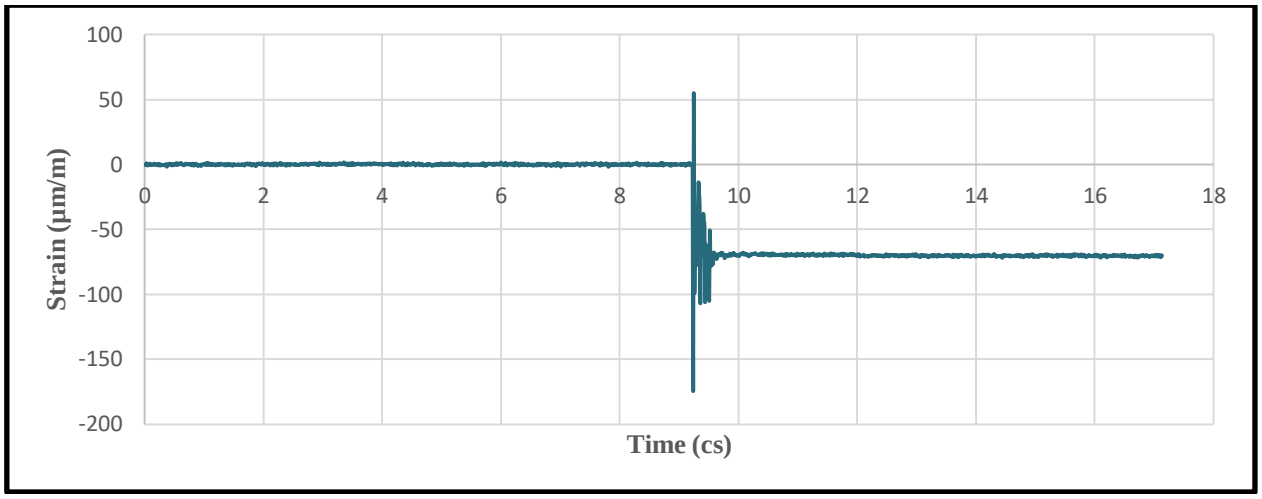

Figure 4.27 Strains versus Time for M7 at 2m Drop

4.3.3 Load Cell Data

To investigate the data obtained from the load cell, load cell readings and impact energies were presented in Table 4.4. As can be seen from Figures 4.28 to 4.38, the load cell data have considerably frequency components. However, the amplitudes for the higher frequency components are mostly insignificant. The oscillations in force are mainly irregular in nature; hence, there is no distinctive single dominant frequency component. As mentioned by Al Nussairi, 2018 this behavior can partially be attributed to the change in force transfer mechanisms due to asymmetric damage and cracking of the specimen.

Also, it is possible to observe that the force increases up to a maximum value, Pmax, followed by a drop after the peak load. As seen in C1, the specimen was compressed, the maximum impact load equaled 209.416 kN at 8.96 cent second (cs) and the specimen

was damaged. For other specimens, the impact energy was not high enough to infiltrate full penetration, because the impactor sticked into specimens and rebounded always. Therefore, non-perforating impact occurred for all laminates. However, when the concentration of the solutions increases there are higher displacements and contact time, which means that major damage occurs.

It is interesting to note that the deflection reaches its maximum value well after the peak impact load is attained.

Finally, it is noted that the residual values of the impact force are approximately equal to the weight of the drop-hammer (200 kg) used to conduct the drop test as shown in Figure 4.28.

Table 4.4 Impact Strength of Impact Load Test on HFRC Slab Specimens

Specimen	Positive values kN	Impact strength kJ	Negative values kN	Impact strength kJ
C1	1.5965	1.5965	209.4162	209.4162
M1 at 1m	0.3259	0.3259	7.2218	7.2218
M1 at 2m	6.9961	13.992	63.9098	127.8196
M2 at 1m	0.37614	0.37614	64.0853	64.0853
M2 at 2m	4.7811	9.5622	116.1845	232.3690
M3 at 1m	6.4445	6.4445	13.7666	13.7666
M3 at 2m	6.3525	12.7050	273.8944	547.7888
M4 at 2m	1.2287	2.4574	57.8331	115.6662
M5 at 2m	4.0038	8.0076	194.1283	389.5766
M6 at 2m	5.3579	10.7158	273.8944	547.7888
M7 at 2m	4.1124	8.2248	194.7469	389.4938

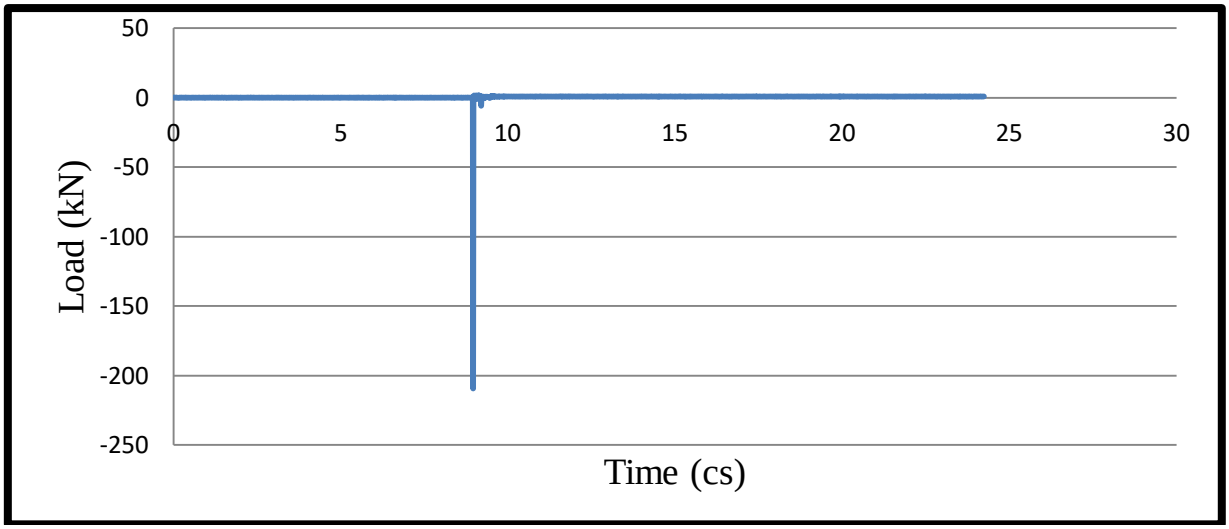

Figure 4.28 Loads versus Time for C1 at 1m Drop

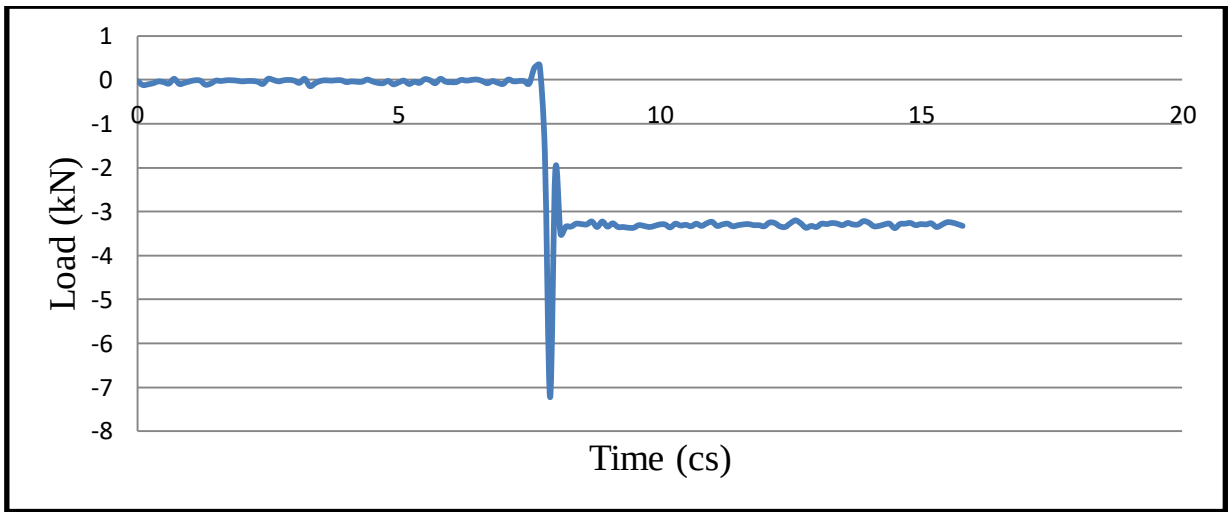

Figure 4.29 Loads versus Time for M1 at 1m Drop

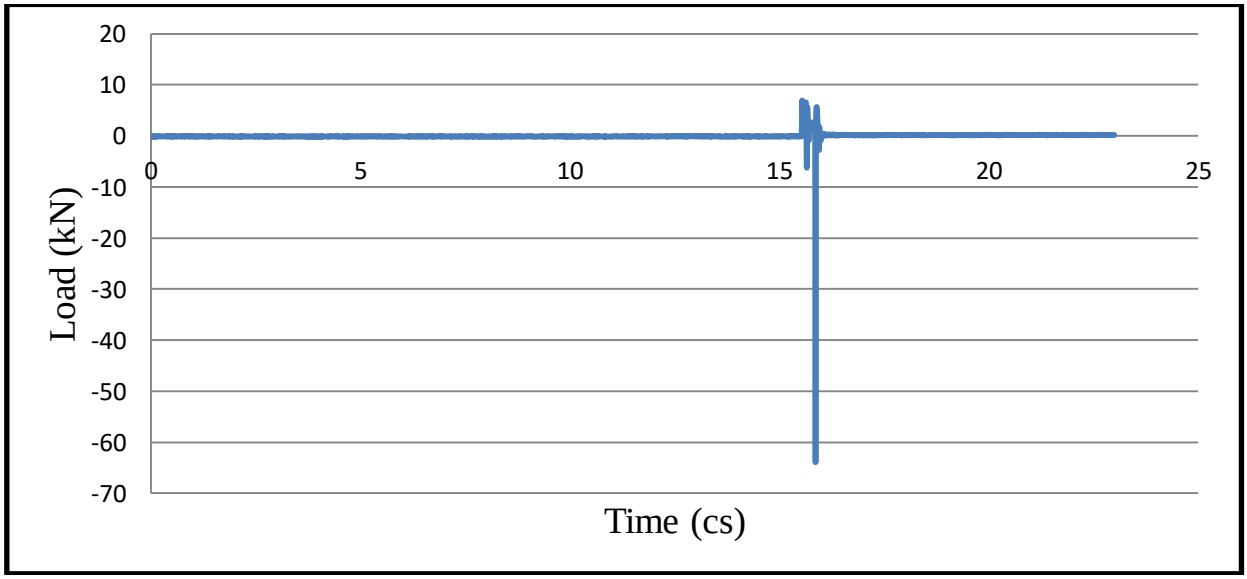

Figure 4.30 Loads versus Time for M1 at 2m Drop

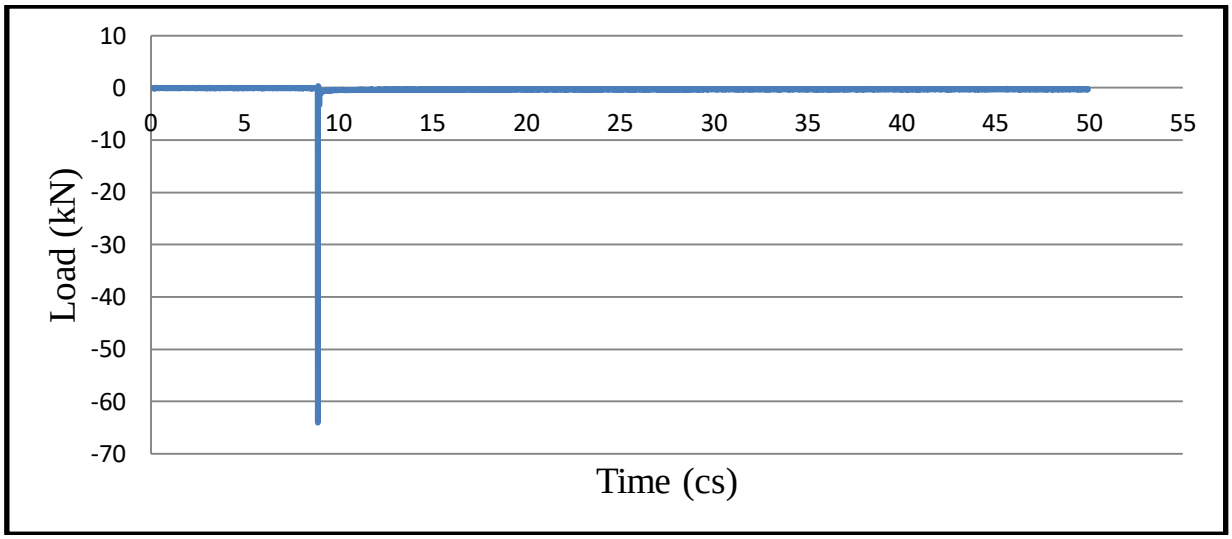

Figure 4.31 Loads versus Time for M2 at 1m Drop

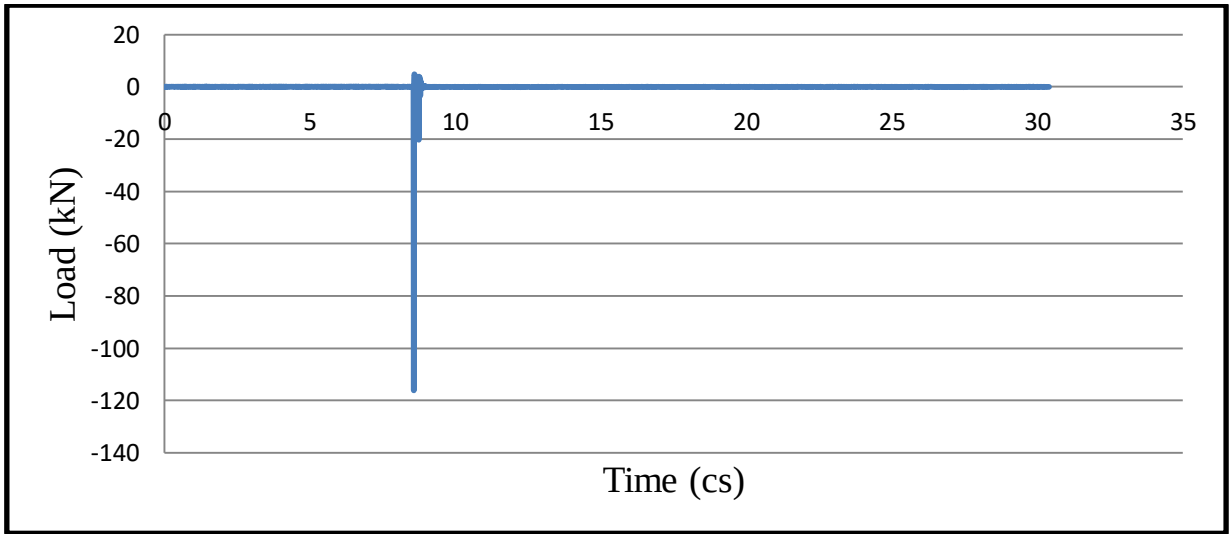

Figure 4.32 Loads versus Time for M2 at 2m Drop

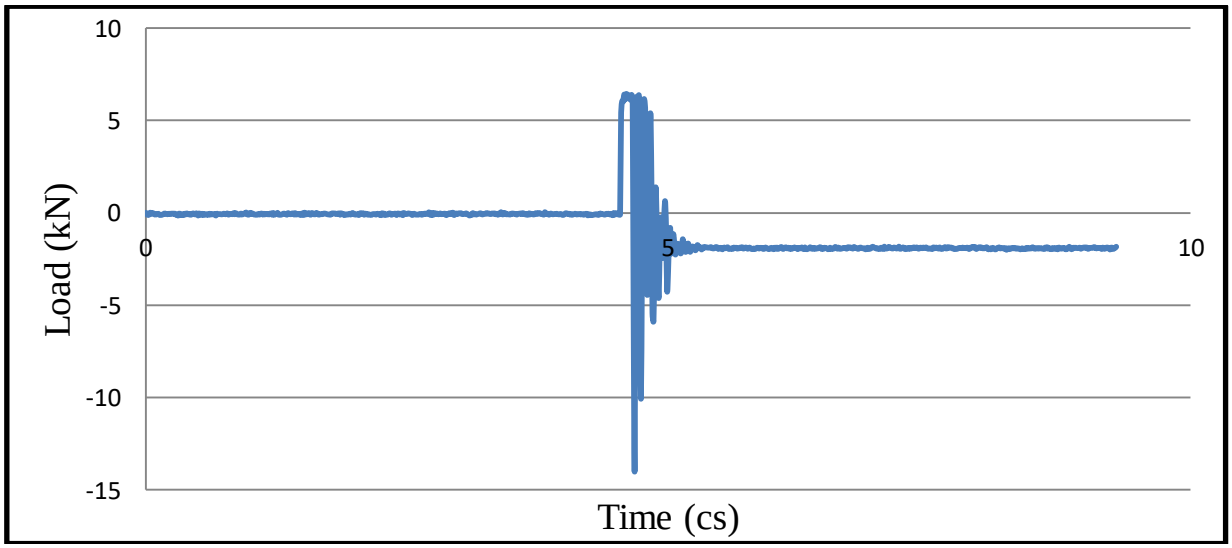

Figure 4.33 Loads versus Time for M3 at 1m Drop

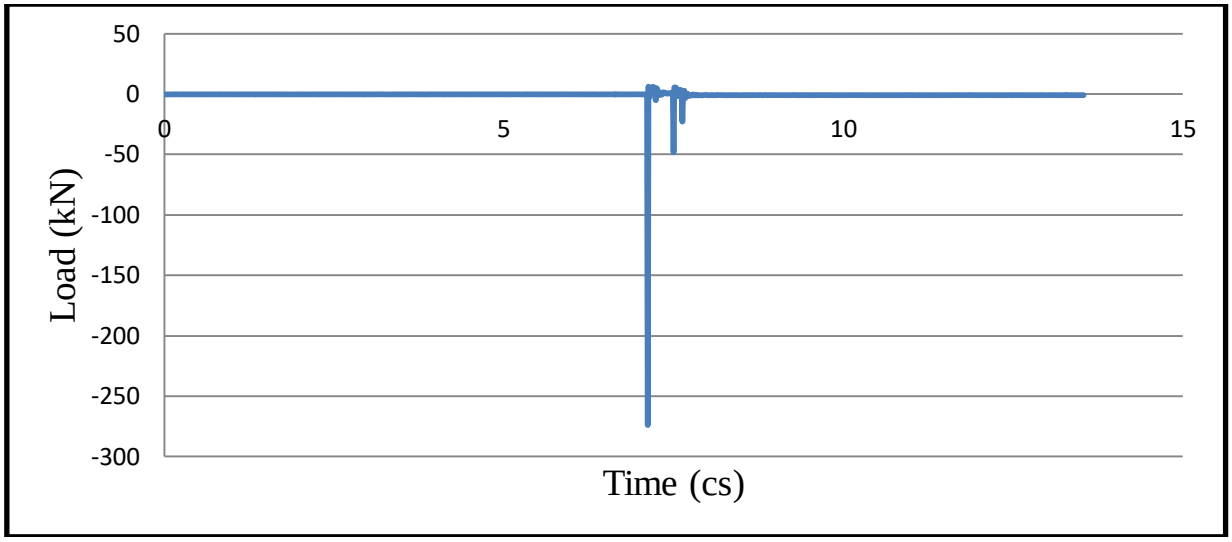

Figure 4.34 Loads versus Time for M3 at 2m Drop

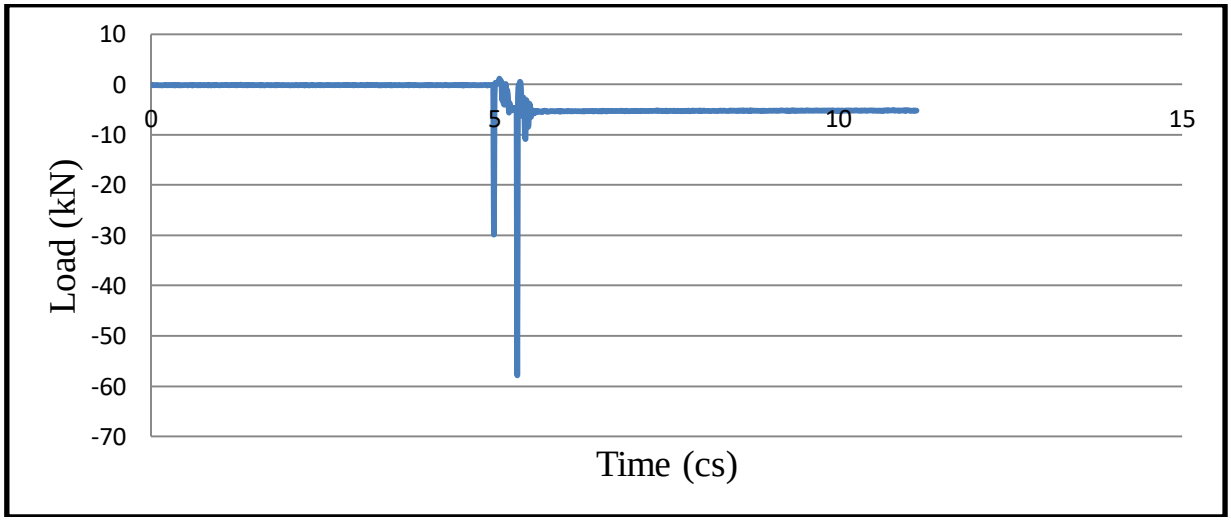

Figure 4.35 Loads versus Time for M4 at 2m Drop

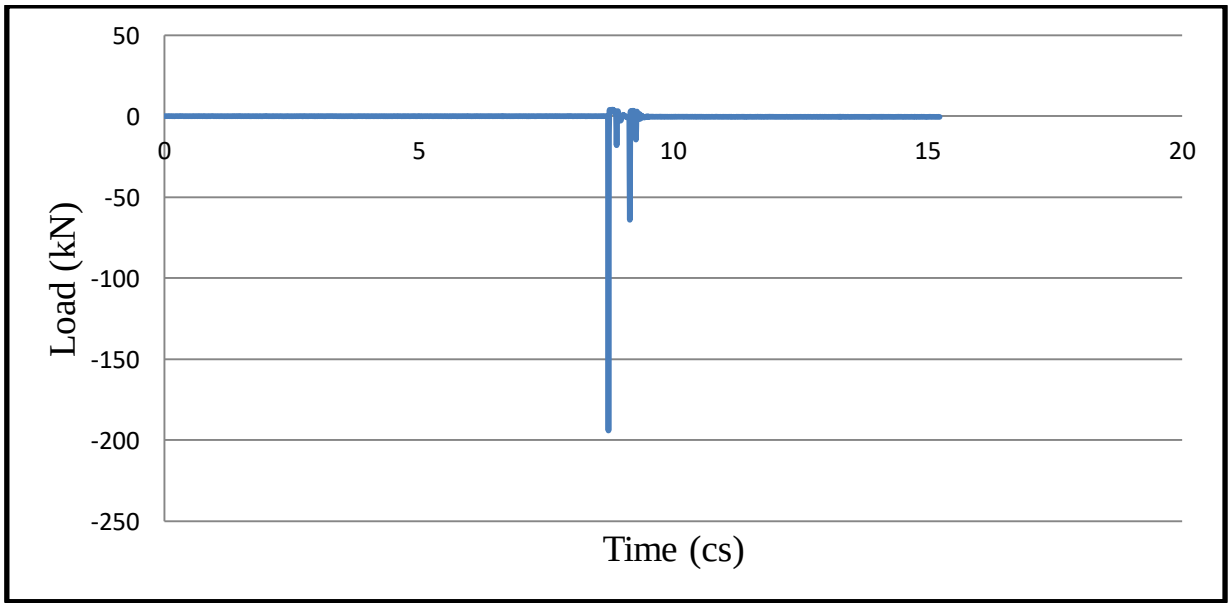

Figure 4.36 Loads versus Time for M5 at 2m Drop

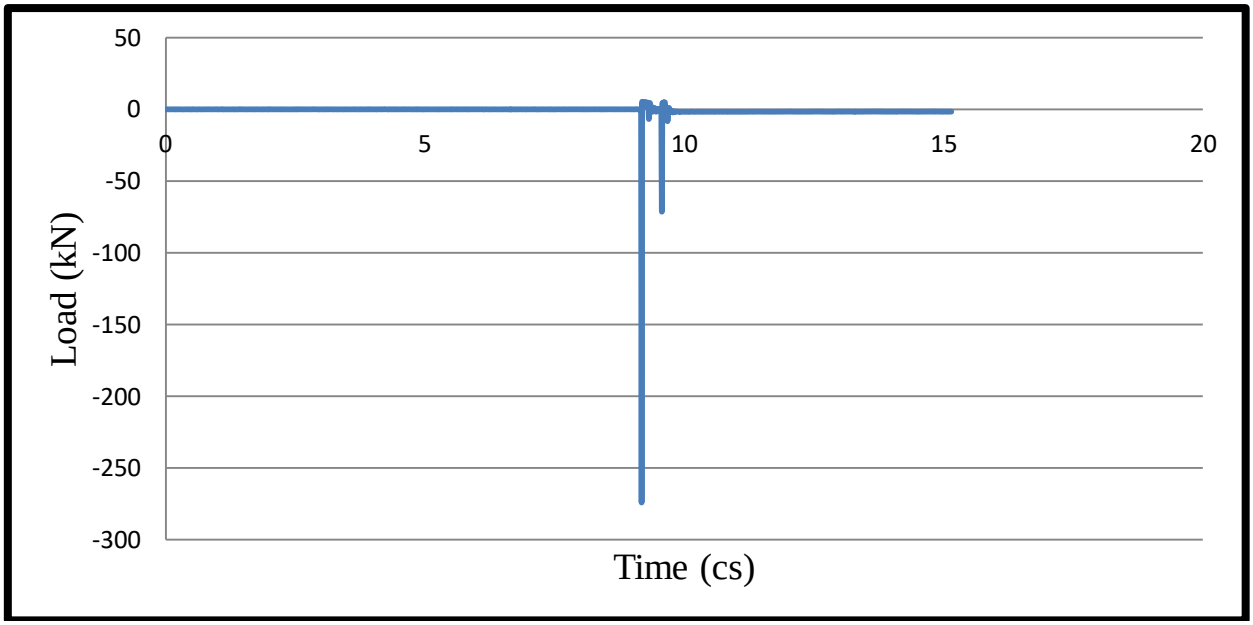

Figure 4.37 Loads versus Time for M6 at 2m Drop

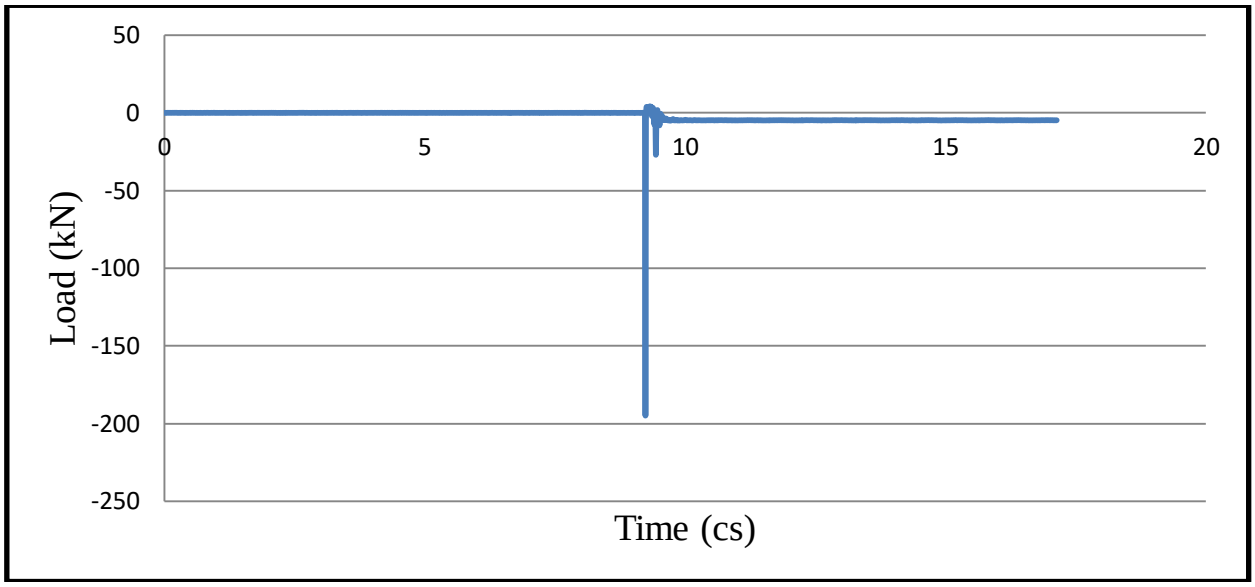

Figure 4.38 Loads versus Time for M7 at 2m Drop

4.3.4 Energy Absorption of HFRC Slabs

The impact load and impact energy test results of the HFRC slab specimens are presented in Table 4.4 and Figure 4.39. It was observed that, the greatest positive impact load was by slab specimen M1 at 2m with an increase of 338.21% from C1, While, M3 and M6 at 2m gave negative values with an increase of 30.79% from C1.

The impact energy absorbed by hybrid fiber reinforced concrete is more than plain concrete slabs. Slab specimens M3 and M6 showed the maximum strength when compared to other slab specimens.

It has to be noted that, in an impact test, a part of the energy imparted to the specimen is dissipated through the damage, cracking and permanent deformations of the specimen, whereas the remainder is absorbed and released by other means, such as kinetic energy during the vibrations. In other words, total energy dissipated by the specimen at each impact is always somewhat less than the input energy.

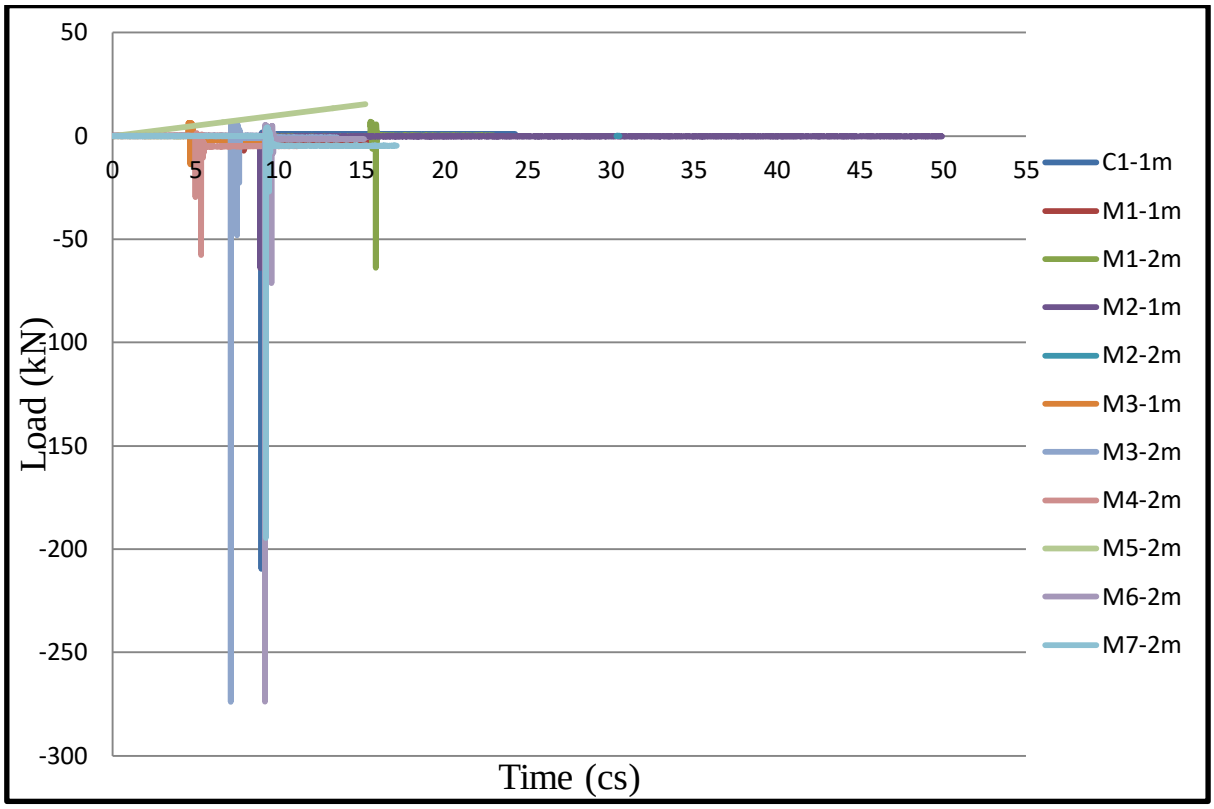

Figure 4.39 Impact Load Distributions for 1m and 2m Drop Heights for All Specimens

4.3.3 The Strain Rate of HFRC Slabs

In dynamic tests, the strain rate is a critical parameter. A structural specimen's strain rate, on the other hand, cannot be defined because all points of the specimen have different strain rates at the same time (Lee et al., 2020). As a result, only the maximum strain rates at the slab specimens' tensile and compressive zones are supplied as reference values, which can explain the properties of specimens during impact testing. Even after a 1m or 2m drop, almost all Slab specimens had the same strain value of 1023.969μm/m. When the slab specimen attained maximum strain in compression and load

0.0502 kN, it was discovered. While, slab specimen M2 reached 1024μm/m with an increase of 74.18% from C1 but M1 recorded the lowest value 60.90625μm/m.

Stain gauges were connected to slab specimens as illustrated in Figure 3.19 to get the strain rate, and measured strains were discriminated with regard to time. Figures 4.40 to 4.50 depict the strain rate behavior for all eight M2 strain rates. These strain rates represent the strains' instantaneous slopes.

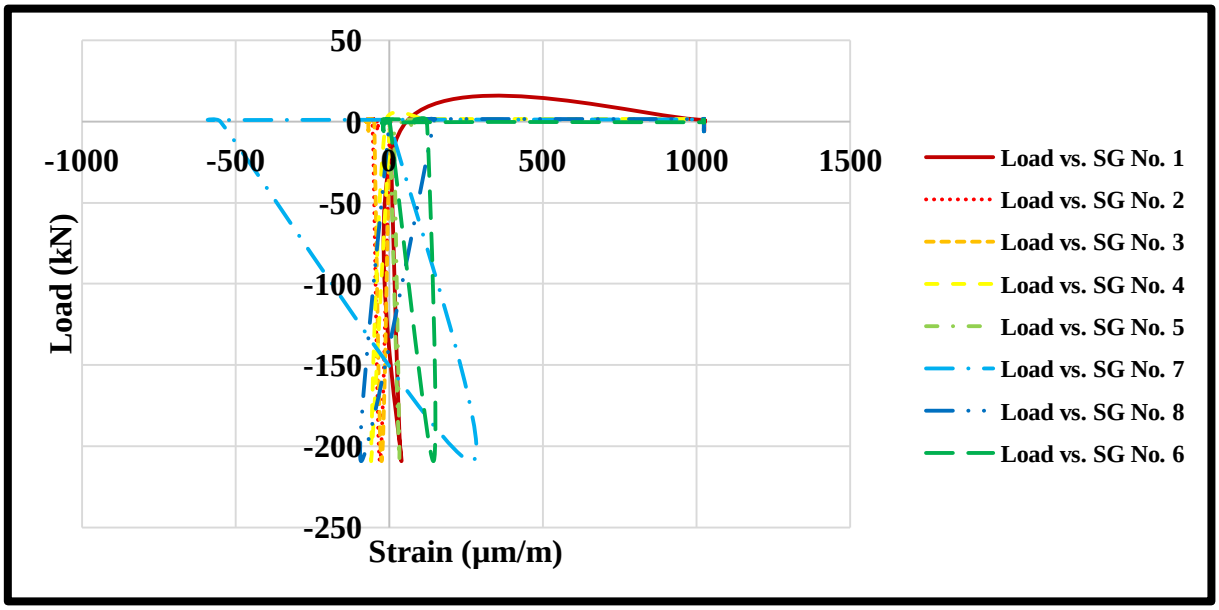

Figure 4.40 Load versus Strain: Slab Specimen C1 for All Strain Gauges

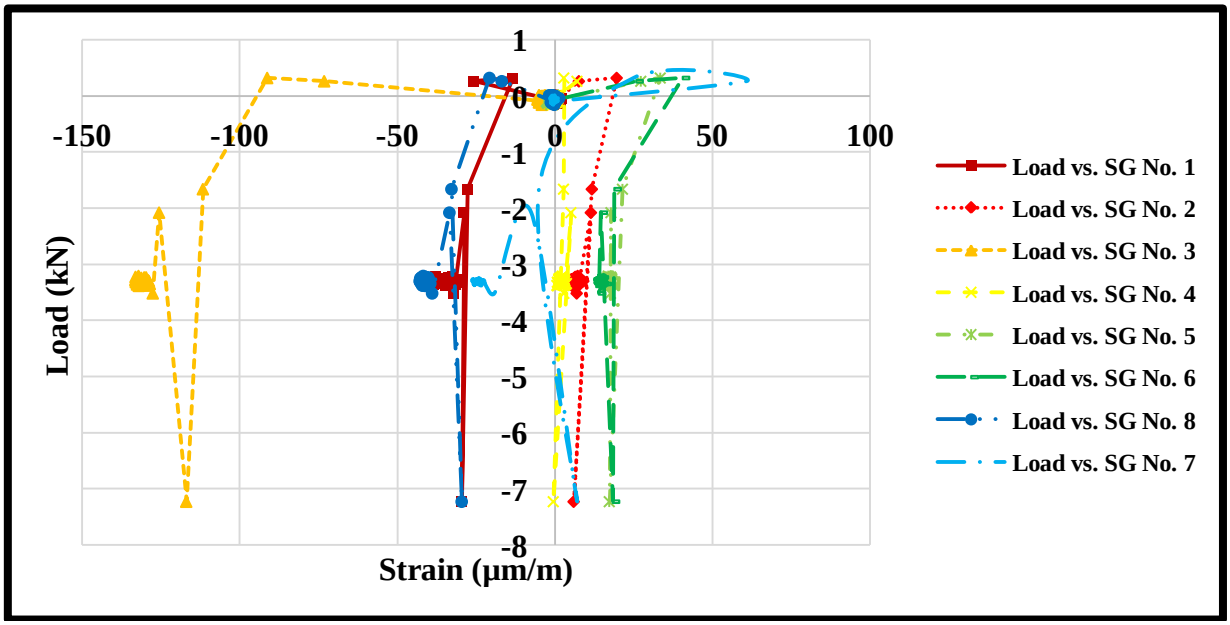

Figure 4.41 Load versus Strain: Slab Specimen M1 at 1m for All Strain Gauges

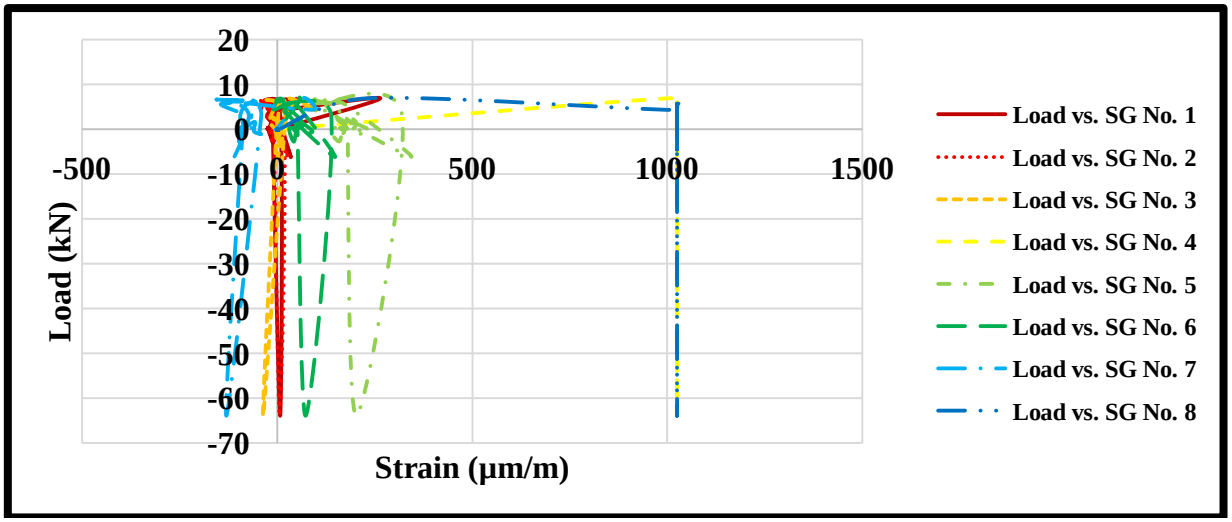

Figure 4.42 Load versus Strain: Slab Specimen M1 at 2m for All Strain Gauges

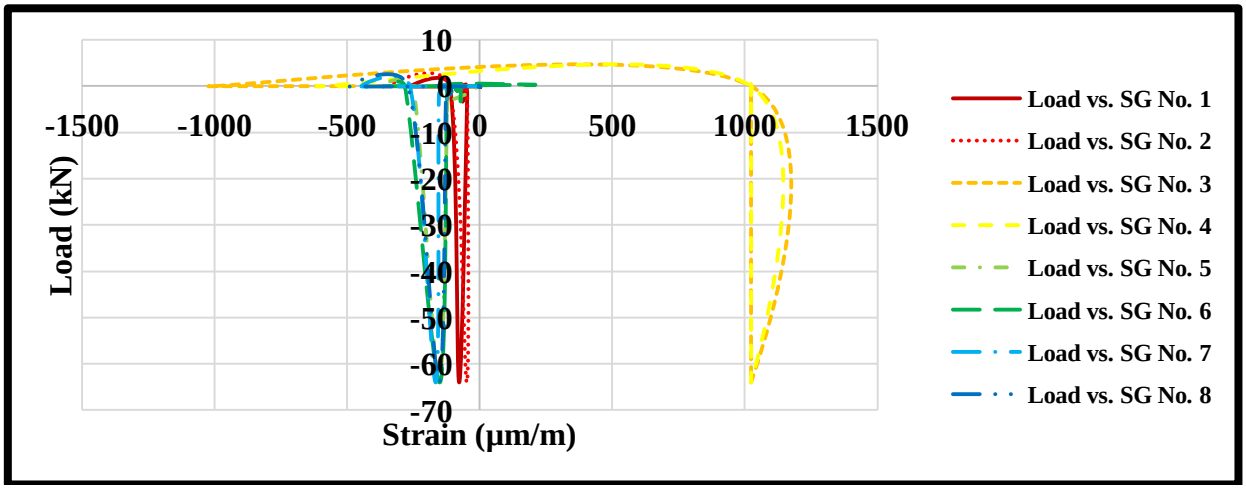

Figure 4.43 Load versus Strain: Slab Specimen M2 at 1m for All Strain Gauges

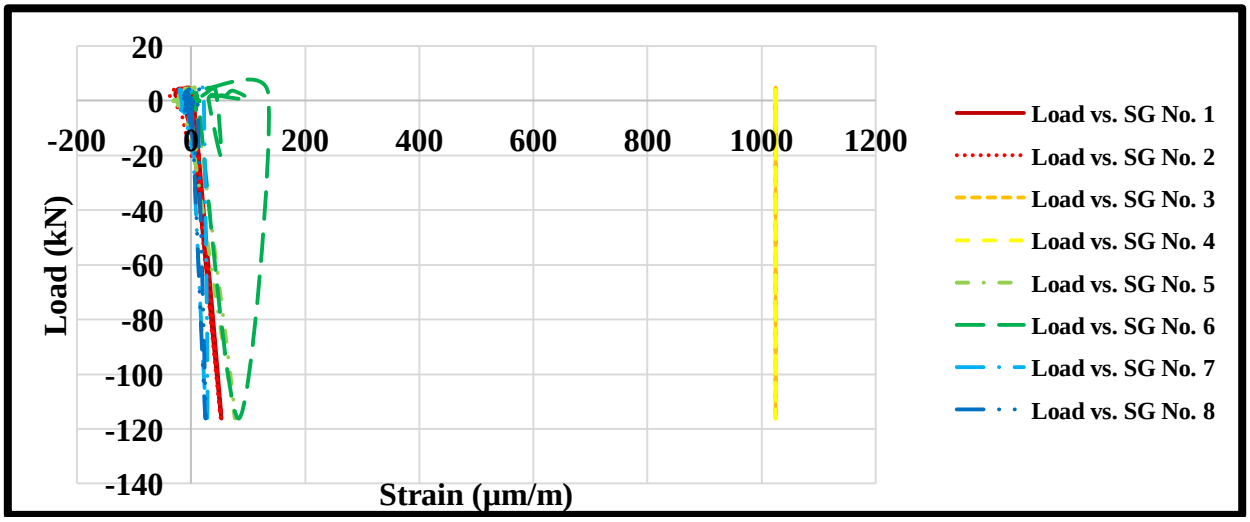

Figure 4.44 Load versus Strain: Slab Specimen M2 at 2m for All Strain Gauges

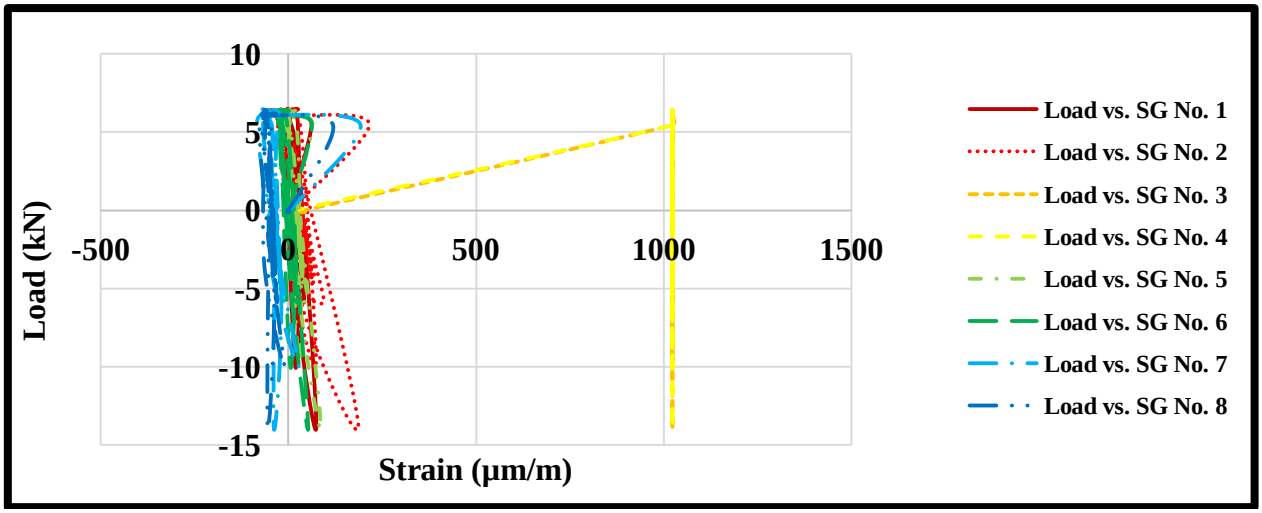

Figure 4.45 Load versus Strain: Slab Specimen M3 at 1m for All Strain Gauges

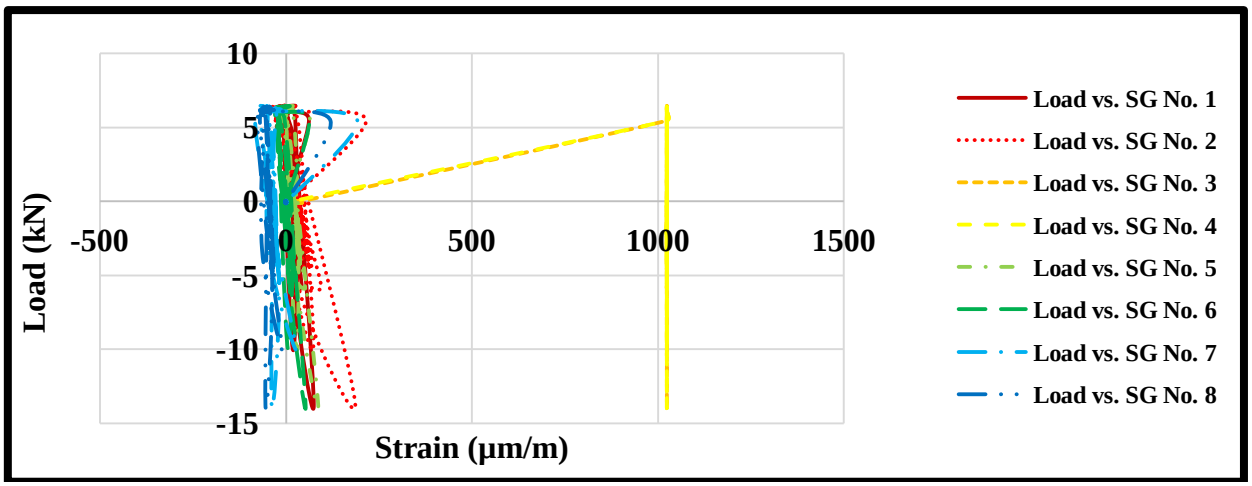

Figure 4.46 Load versus Strain: Slab Specimen M3 at 2m for All Strain Gauges

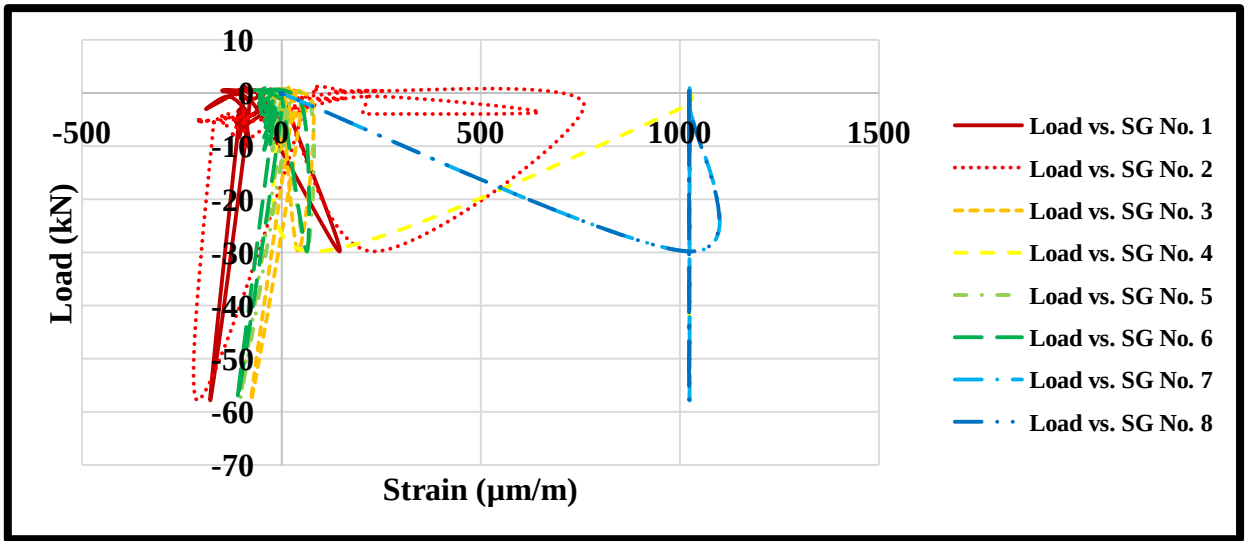

Figure 4.47 Load versus Strain: Slab Specimen M4 at 2m for All Strain Gauges

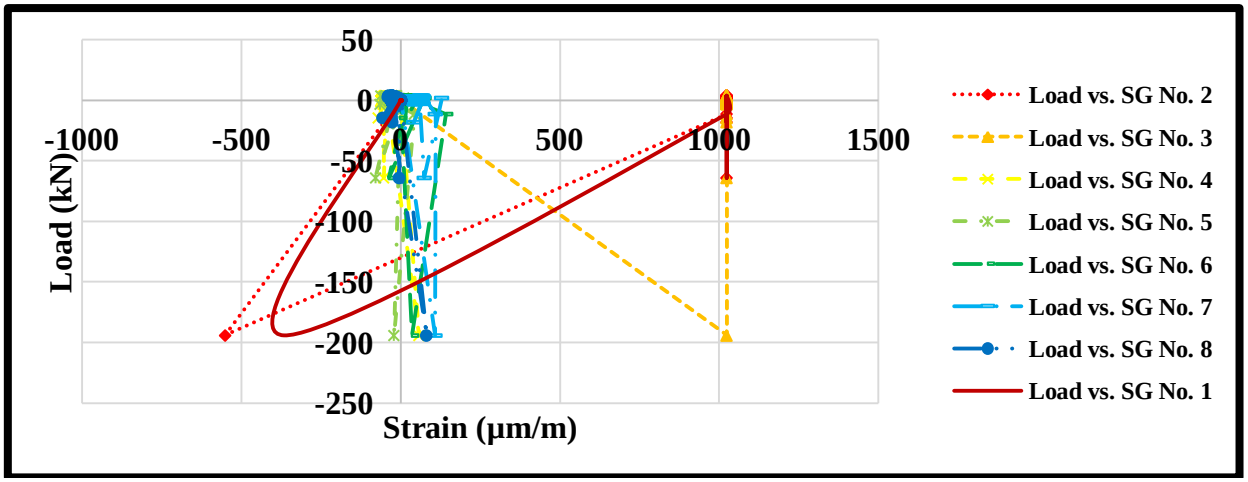

Figure 4.48 Load versus Strain: Slab Specimen M5 at 2m for All Strain Gauges

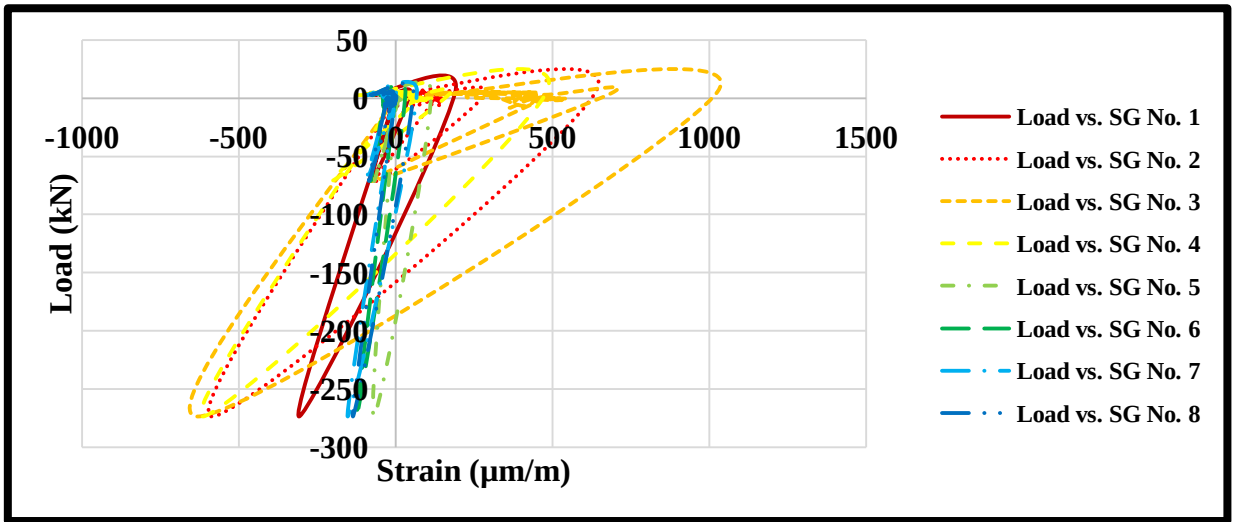

Figure 4.49 Load versus Strain: Slab Specimen M6 at 2m for All Strain Gauges

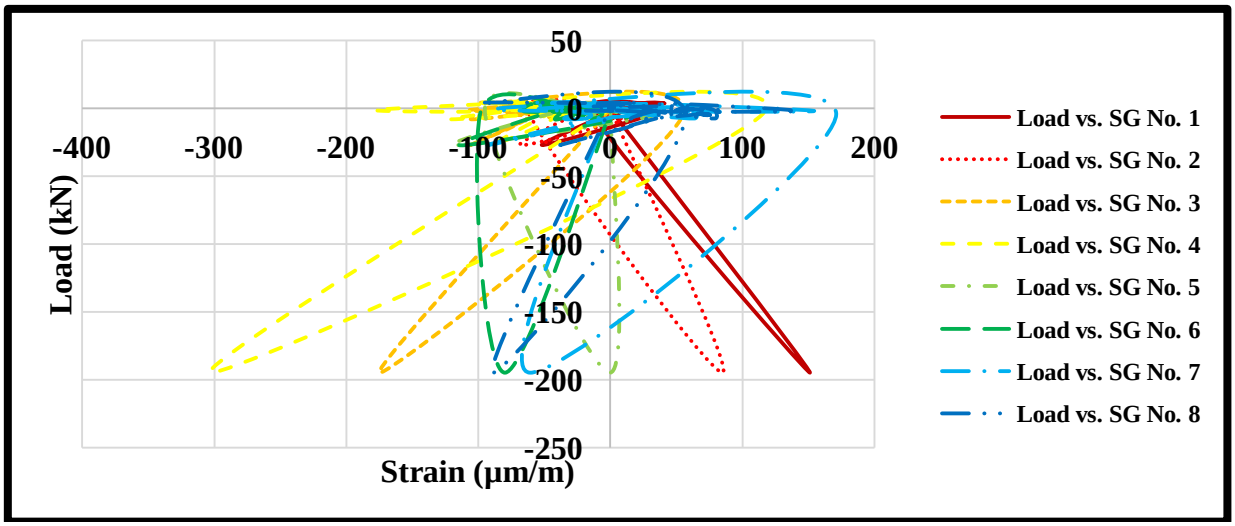

Figure 4.50 Load versus Strain: Slab Specimen M7 at 2m for All Strain Gauges

4.3.4 Load Deflection of Impact Load Test of HFRC Slabs

As shown from Table 3.24, Slab specimen M1 at 2m reached maximum deflection 47 mm with increasing 138.64% from C1, when the slab upward. While, M2 at 2m reached the minimum deflection 8 mm with decreasing 58.97% from C1, when the slab upward also. Figures 4.51 to 4.61 present impact load versus deflection.

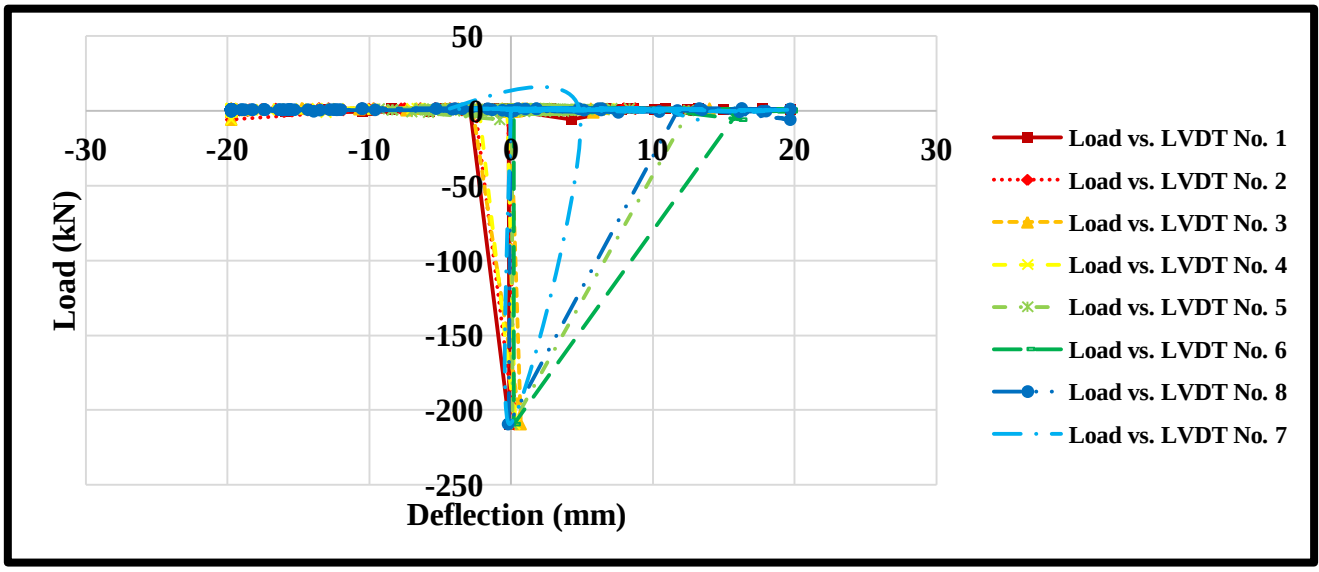

Figure 4.51 Load versus Deflection: Slab Specimen C1 for All LVDTs

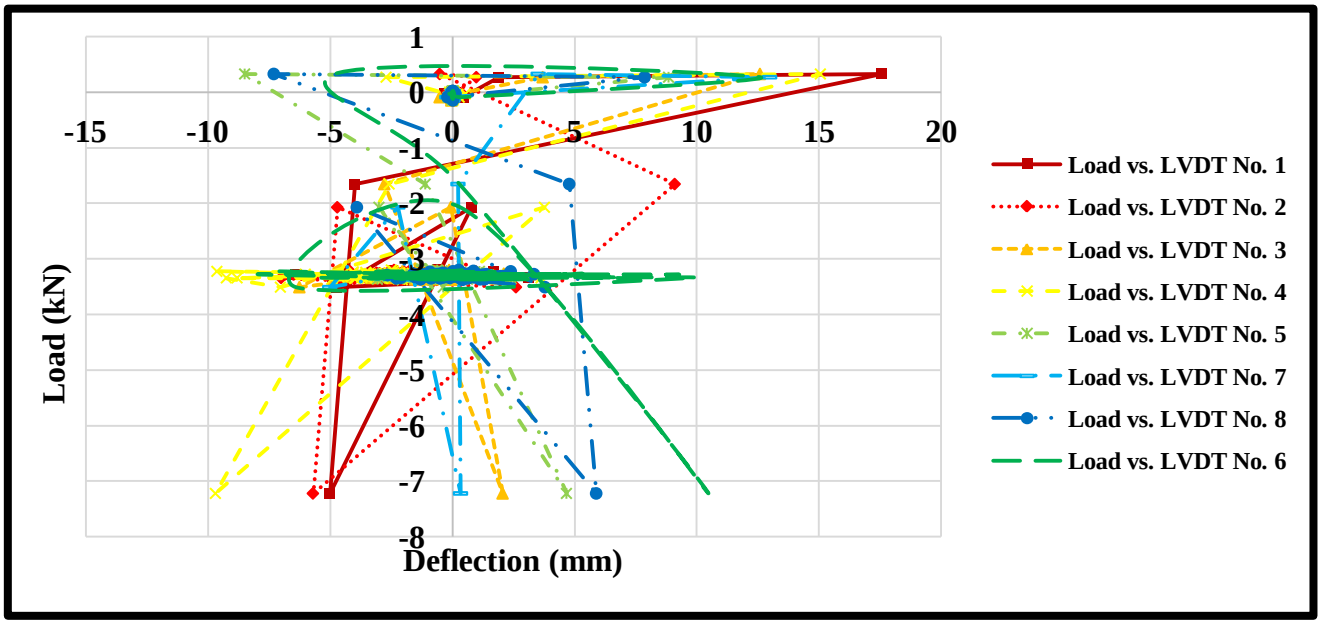

Figure 4.52 Load versus Deflection: Slab Specimen M1 at 1m for All LVDTs

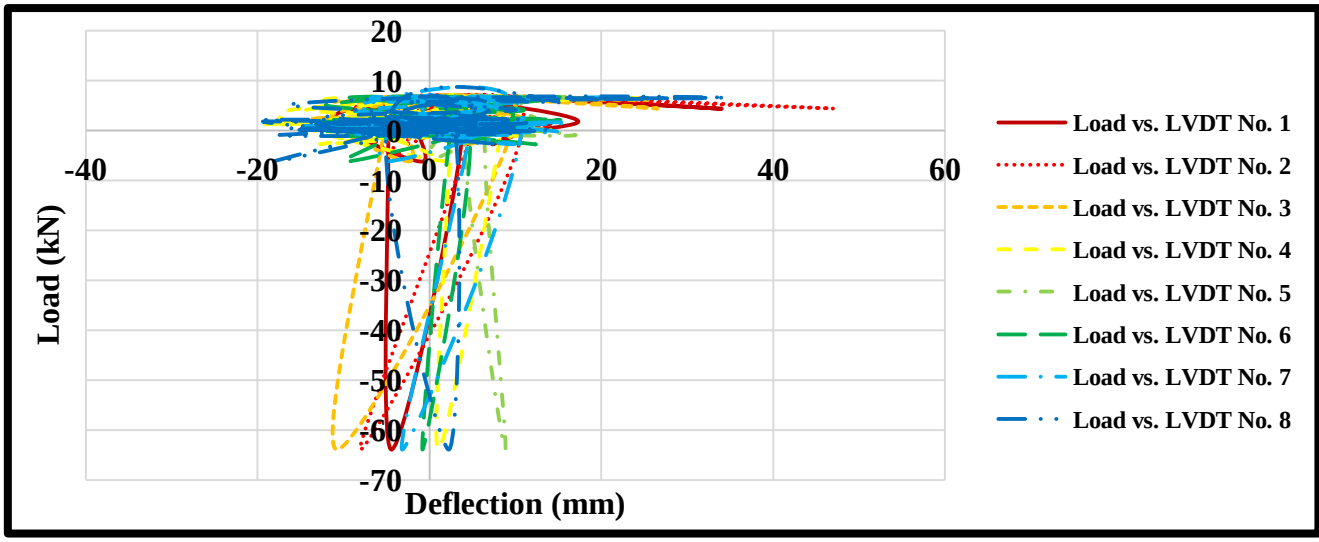

Figure 4.53 Load versus Deflection: Slab Specimen M1 at 2m for All LVDTs

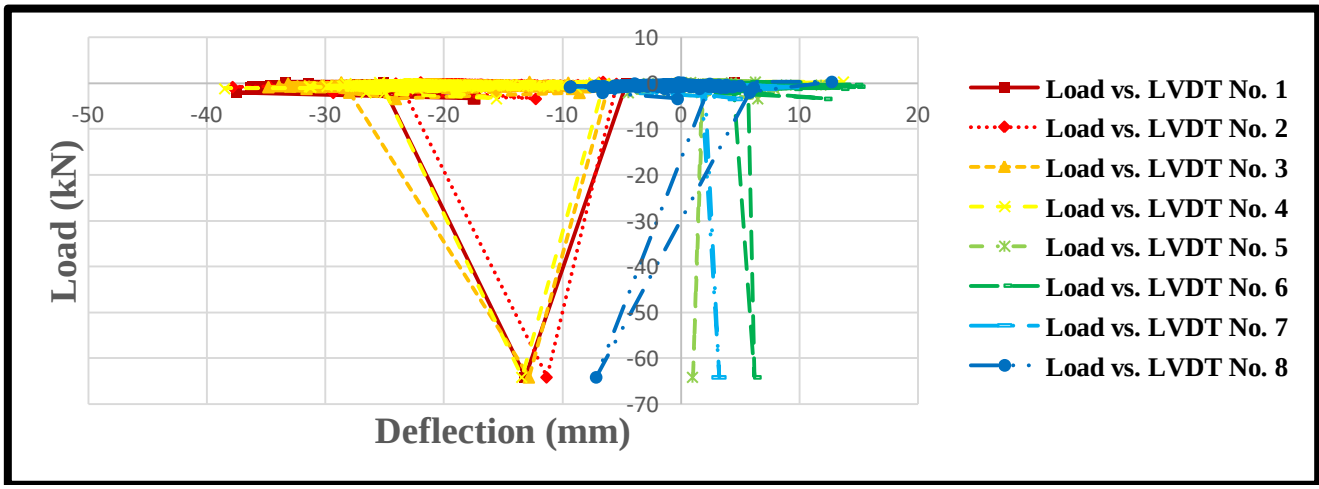

Figure 4.54 Load versus Deflection: Slab Specimen M2 at 1m for All LVDTs

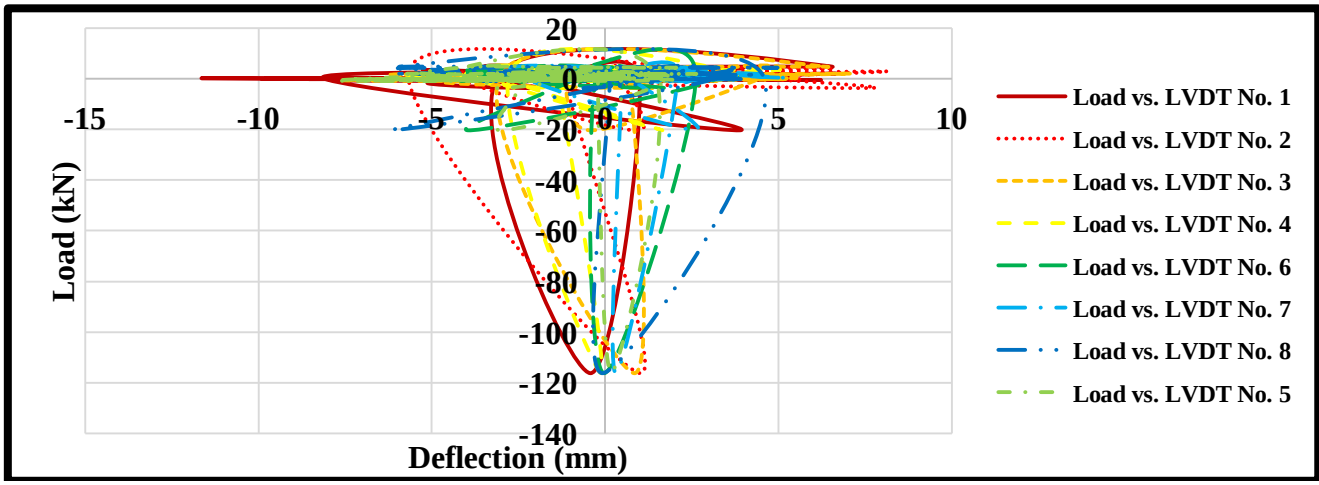

Figure 4.55 Load versus Deflection: Slab Specimen M2 at 2m for All LVDTs

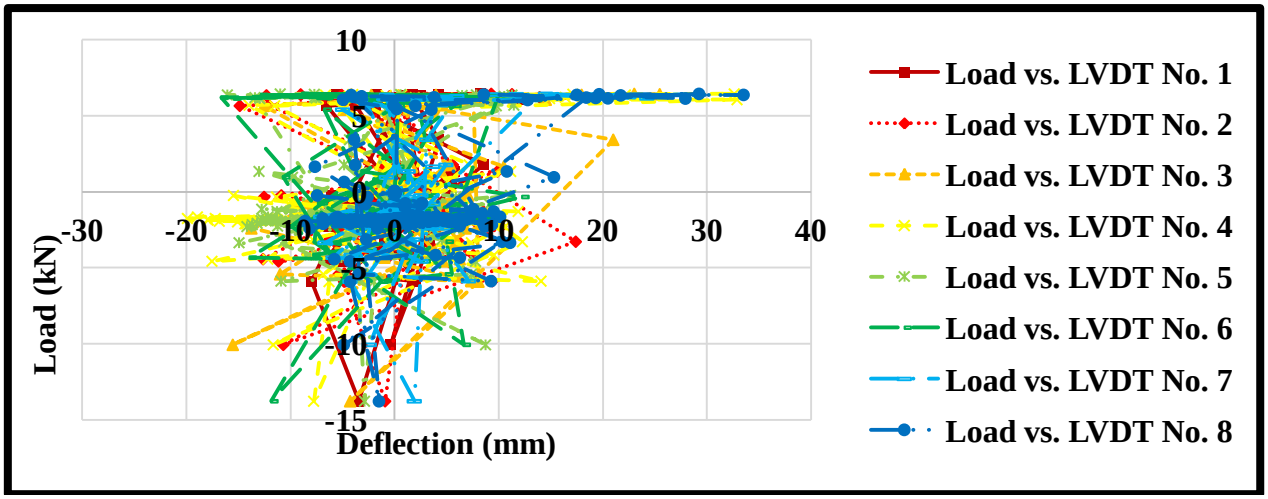

Figure 4.56 Load versus Deflection: Slab Specimen M3 at 1m for All LVDTs

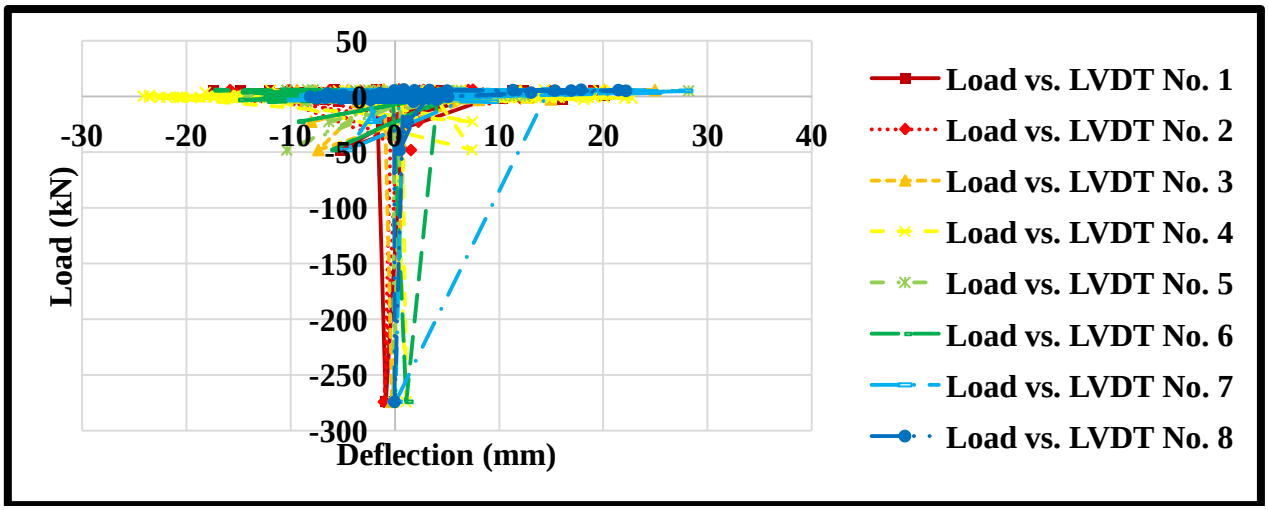

Figure 4.57 Load versus Deflection: Slab Specimen M3 at 2m for All LVDTs

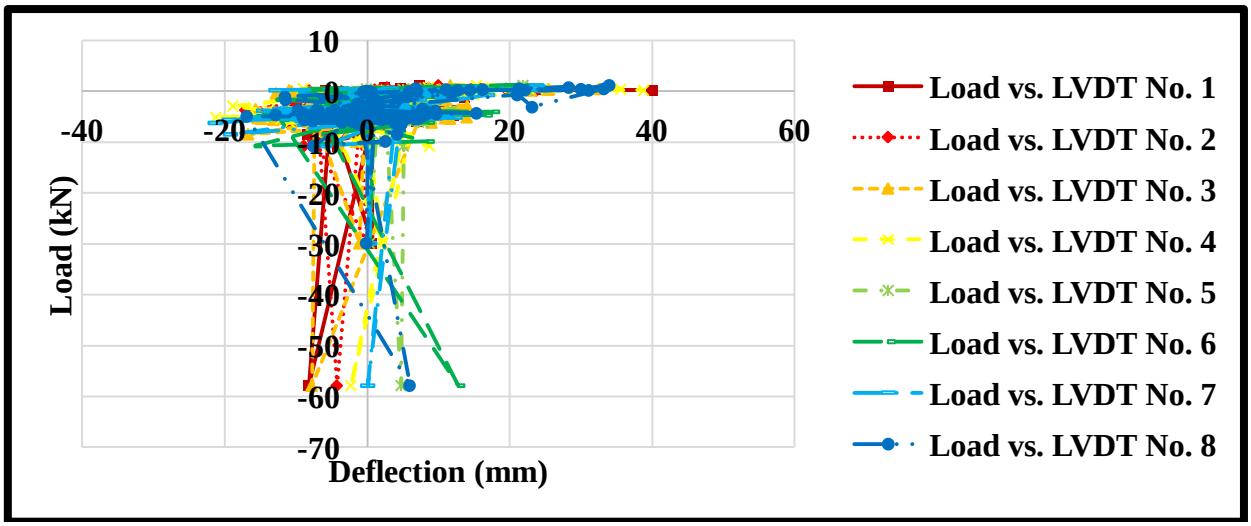

Figure 4.58 Load versus Deflection: Slab Specimen M4 at 2m for All LVDTs

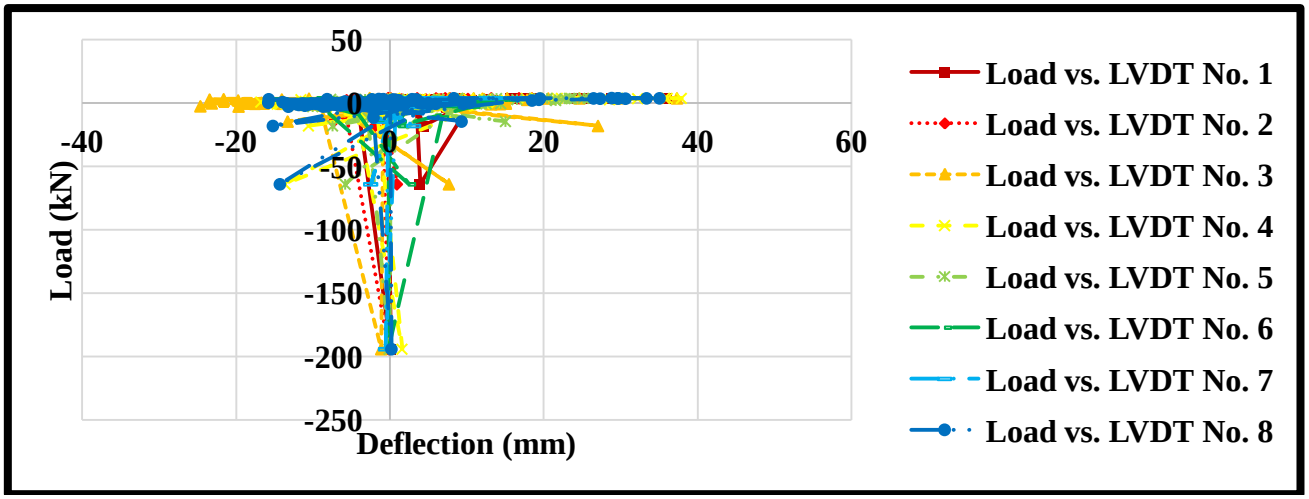

Figure 4.59 Load versus Deflection: Slab Specimen M5 at 2m for All LVDTs

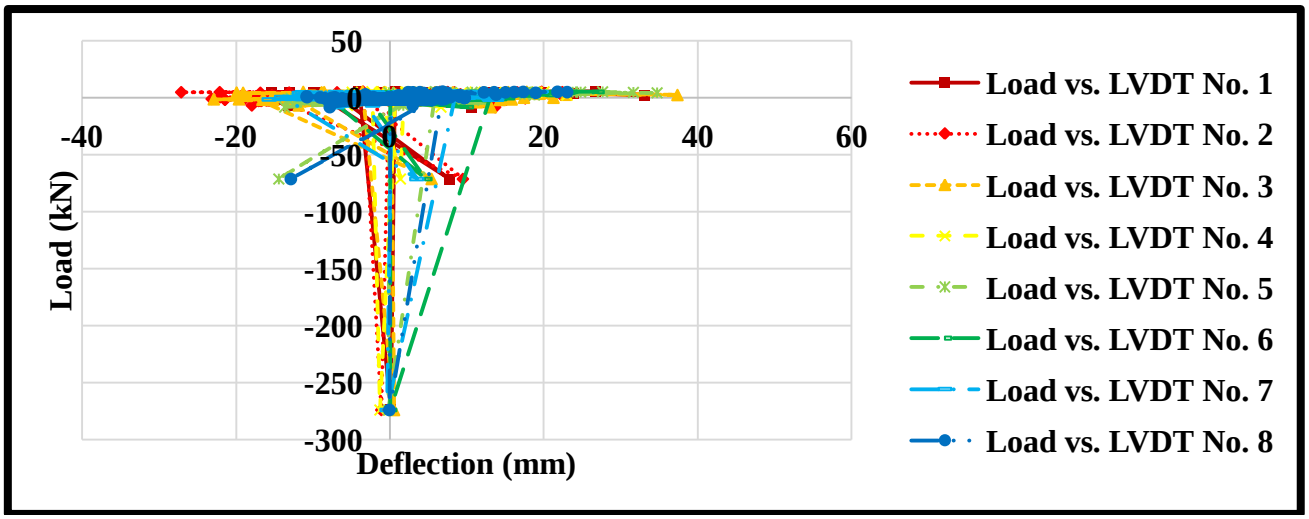

Figure 4.60 Load versus Deflection: Slab Specimen M6 at 2m for All LVDTs

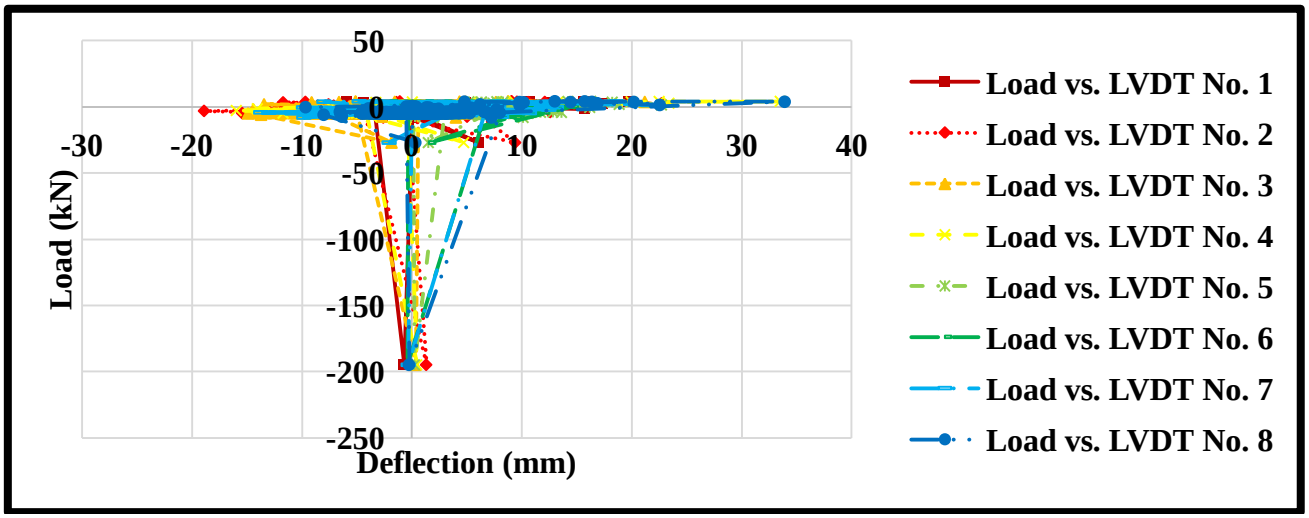

Figure 4.61 Load versus Deflection: Slab Specimen M7 at 2m for All LVDTs

4.3.5 Crack and Failure Patterns

The final crack patterns of the impact test specimens are shown in Figures 4.62 to 4.69. The failure modes of the identical specimens were similar. Except for slab specimen C1 (control plain concrete specimen), the fracture pattern of all evaluated slab specimens under impact loading conditions displayed several flexural cracks that steeply progressed into the compression zone (top face). The impact event was catastrophic in the case of plain concrete slab specimen C1. As shown in Figure 4.60, the projectile pierced the slab and caused a shear cone-shaped fracture and completely perforated and the slab shattered into pieces. As a result of radial crack formation, the slab lost its integrity and gained velocity. Crack widths of all tested slab specimens are presented in Table 4.4. In contrast, the other HFRC slab specimens showed different behavior where the slabs were subjected to same impact energy for 1 m drop with no sign of any damage in the compression face. The impact height was increased to 2m. So, then, the slabs developed diagonal cracks, originating at the impact point and propagating downwards with an angle of approximately 45 degrees, forming a shear-plug after second impact; similar to what had been represented by Sangi, 2011.

As seen in Table 4.5 and Figure 4.62 which show the different crack widths in specimens, the hooked steel fiber used has a higher bonding strength, improved impact values and reduce deflection.

In the case of HFR concrete slabs, the projectile perforated the slab containing M4-1% (65/60 5D SF only). As the volume fraction is increased from M6-1% (65/60 5D SF) + 0.5% PPF, as shown in Table 4.5, an improvement in the resistance against projectile perforation was observed. Undoubtedly, there is an improvement in the case of HFRC slabs in terms of integrity after failure. The addition of steel and PP fibers to concrete slabs resulted in considerable improvement in the impact resistance when compared to slab without fibers. Appendix B shows other failure plan views.

Table 4.5 Crack Widths of Slab Specimens after Impact Load

Specimen	Crack width (mm)
C1- no fiber	-
M1- 1% (65/35 3D SF)	0.1- 0.2
M2- 0.5%(65/35 3D SF + PPF)	1.0 - 2.5
M3-1%(65/35 3D SF)+ 0.5% (PPF)	0.1 - 0.2 - 1.0
M4-1%(65/60 5D SF)	0.1
M5-0.5%(65/60 5D SF + PPF)	0.1 - 0.2 - 0.3
M6-1%(65/60 5D SF) + 0.5% PPF	0.1
M7- 1% PPF	0.1- 0.2- 1.4- 1.6

Figure 4.62 Final Crack Patterns for Impact Test Specimen C1

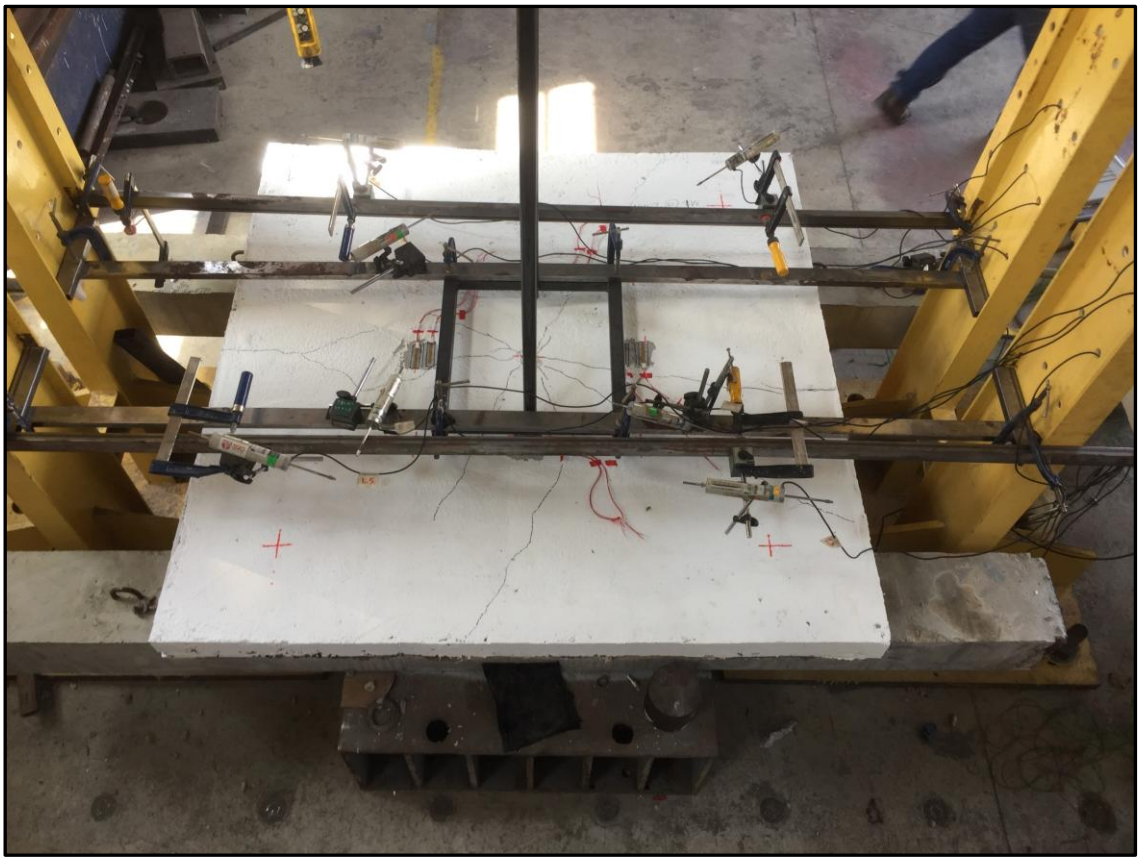

Figure 4.63 Final Crack Patterns for Impact Test Specimen M1

Figure 4.64 Final Crack Patterns for Impact Test Specimen M2

Figure 4.65 Final Crack Patterns for Impact Test Specimen M3

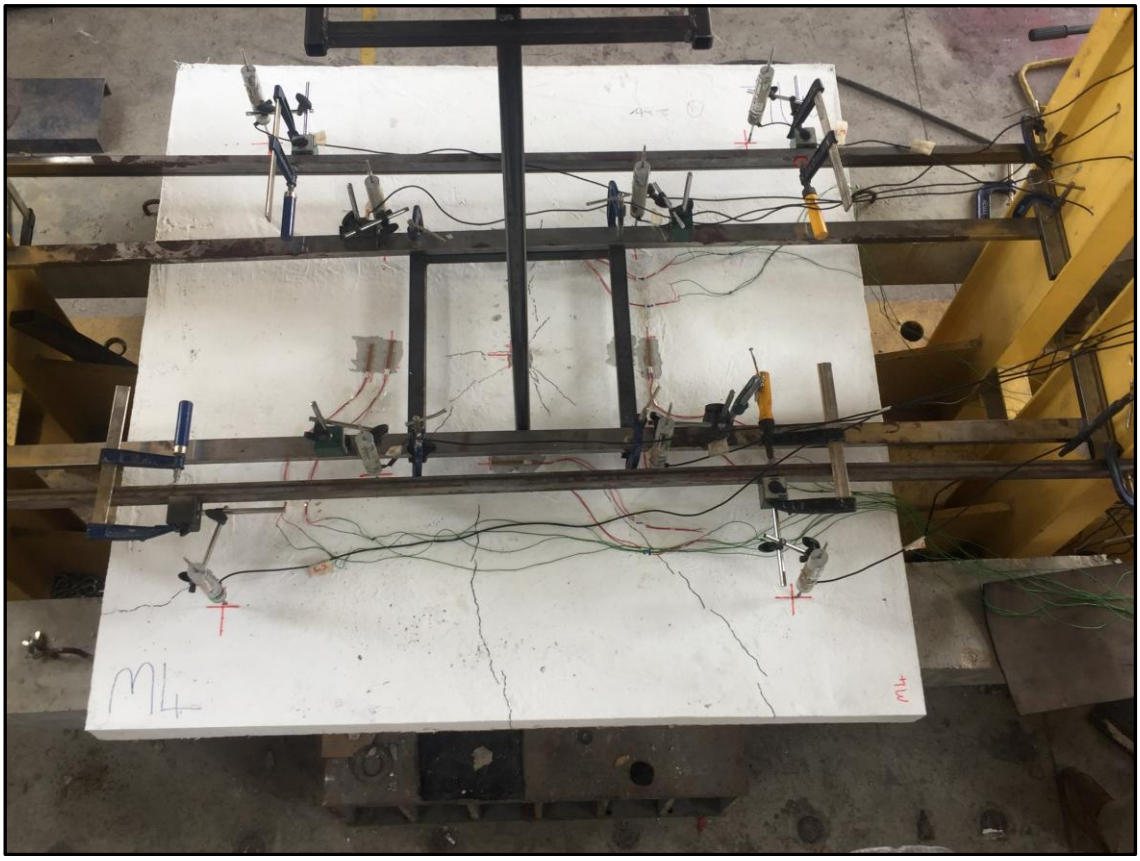

Figure 4.66 Final Crack Patterns for Impact Test Specimen M4

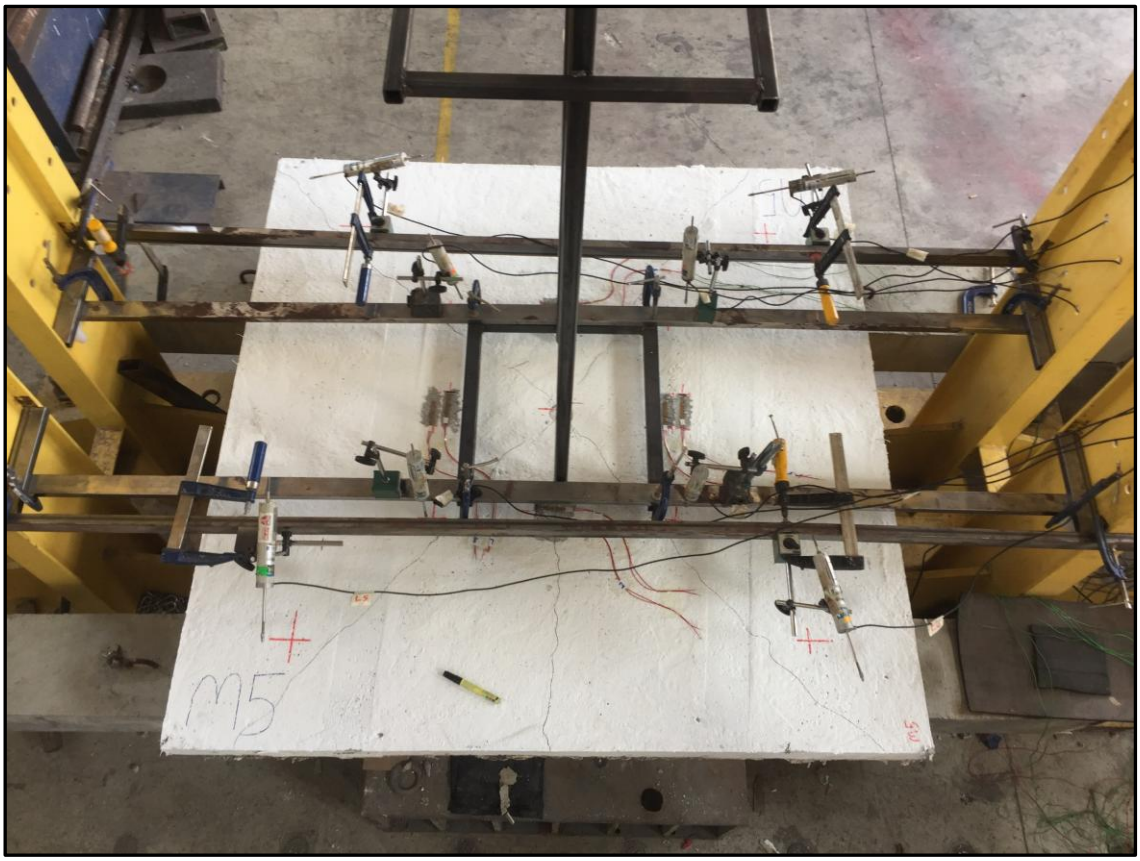

Figure 4.67 Final Crack Patterns for Impact Test Specimen M5

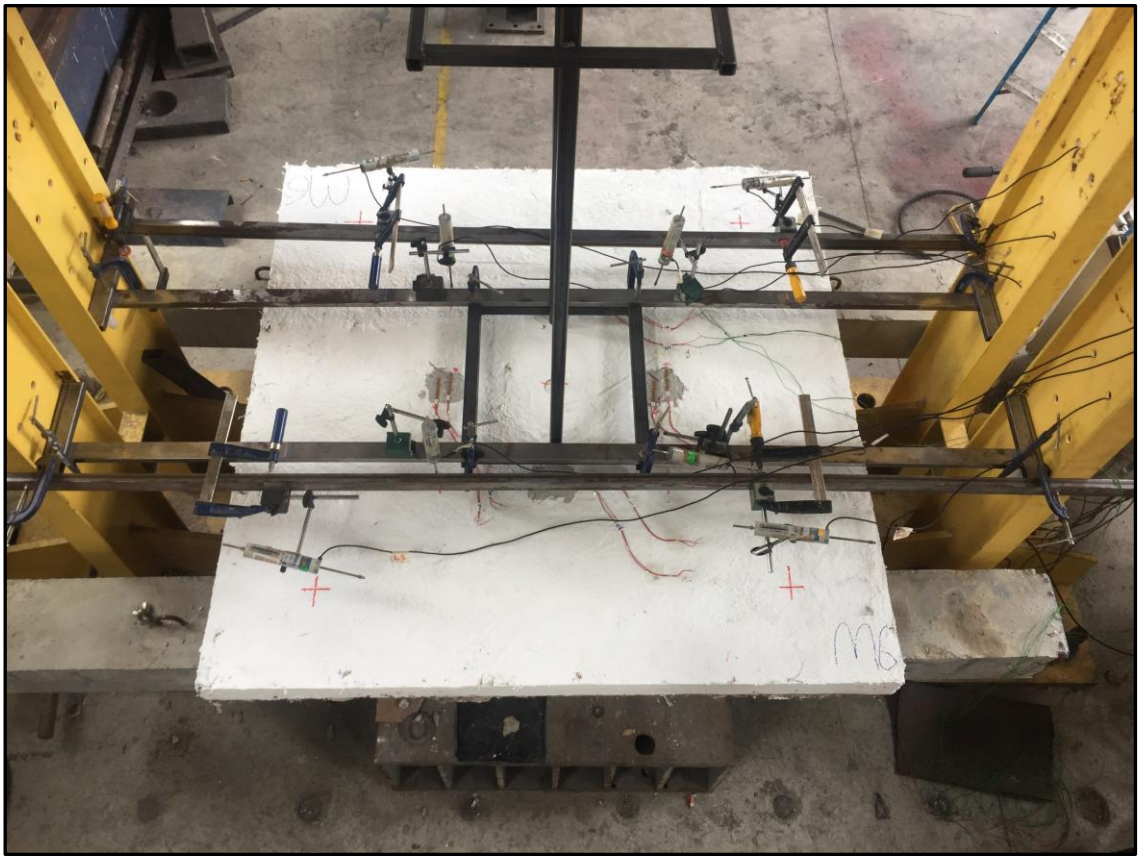

Figure 4.68 Final Crack Patterns for Impact Test Specimen M6

Figure 4.69 Final Crack Patterns for Impact Test Specimen M7

4.4 Discussion of Concrete Mechanical Properties

The mechanical properties of Hybrid fiber reinforced concrete were investigated using experimental test results on varying percentage proportions of SF and PPF in plain concrete. Based on these findings, the following conclusions can be drawn:

(i) When the content of hybrid fiber and diameter of fresh concrete were increased, the workability of the concrete reduced. When PPF fiber is mixed with steel fiber, it has a higher workability than other specimens. Due to congestion, too much fiber in concrete will result in limited workability, but the values are within the designed ranges.

(ii) The addition of hybrid fibers has a considerable impact on the compressive and flexural strength of concrete. The results demonstrate that increasing the volume of steel fibers rather than PPF fibers boosted flexural strength significantly. On the other hand, it was demonstrated that the usage of fibers may become a

more essential option for steel and PPF fiber reinforced combinations as well as environmental needs.

(iii) Concrete hybrid fibers aid in the formation of association cracks, hence reducing crack growth. With a 44.44 percent increase in flexural strengths above the control specimen, the percentage of 1% steel fiber (M4) delivers the greatest value in flexural strengths (C1). SF and PPF, on the other hand, add to flexural strength. This demonstrates that, despite improving flexural strengths, HFRC are less significant in compression. According to the results of the experiments, the control prism specimens suddenly split into two parts at failure, whereas the HFRC slab specimens do not split into two halves at failure and may still transmit extra weight at ultimate load capacity. On the other hand, it was demonstrated that the usage of fibers might become a more appealing solution for steel fiber reinforced combinations and environmental requirements.

4.5 Discussion of the Impact Test

In the impact test, the slab specimens were subjected to two impact drops to assess the validity of the adopted HFR approach to resist loads with high loading rates such as impact and blast loads. The assessment was made in this study by comparing the results between the HFRC and the plain concrete slabs in terms of the load, the deflection, the failure mode, the crack patterns, and the dissipated energy. The obtained results can be summarized as follows:

(1) Upon impact, the slab experienced a rapid increase in the load giving rise to the maximum load. This sudden increase in load to the maximum value occurs within 1cs for all the slabs tested. The peak loads may be influenced by various parameters, such as, contact velocity, mass of the projectile, nose shape of projectile, target thickness, target stiffness, concrete strength, roughness of the slab surface, boundary conditions of the slab, etc. However, in the present study, the above parameters did not vary significantly between specimens and hence did not affect the peak load measured.

(2) In comparison to plain concrete that has been exposed to an impact load, hybrid fiber reinforcing minimizes the extent of damage and maintains damaged concrete more compact. Even with mono-fiber reinforcement, slabs showed enhanced spall and cratering resistance.

(3) The HFRC system also significantly reduced residual displacements of slab specimens, for example C1=19.712mm are reduced by 97.8% for M1,2 and 99.3% for M6,2.

(3) In terms of mass lost, steel-PP hybrid fiber reinforcement was found to give a significant improvement in performance under impact load when compared to mono-fiber (steel only or PP only) reinforced concrete specimens. The steel-PP combination provides outstanding impact resistance due to the extraordinary fiber-matrix bond strength, high tensile strength, and modulus of elasticity of PP fibers.

(4) The impact resistance of HFRC is influenced by the fiber concentration in hybrid fiber mixtures as well as the length ratio. In hybrid systems, specimens with fibers fared better on average than specimens with simply one fiber. Specimens M3 and M6, which included 1% SF and 0.5% PPF, provide the best impact resistance because they provide enough bonding (anchoring) area while remaining short enough to uniformly fill the matrix spaces between the SF and PPF.

(5) In comparison to PPF alone, the overall impact resistance of all PPF-steel hybrid systems was shown to be higher. The incorporation of polymer fibers in concrete can thereby increase the structure's longevity while also reducing its weight.
(6) Based on the findings, it can be concluded that the impact test was effective in determining the HFRC system's resistance to high loading rates such as impact loads.

CHAPTER FIVE

CONCLUSIONS AND RECOMMENDATIONS

5.1 SUMMARY

This research is intended to investigate the behavior of hybrid fiber reinforced concrete slabs exposed to impact loading. Experimental program is discussed in details in chapter 3. Penetration, scabbing, and perforation are the local damage modes that can form in a HFRC slabs due to impact load. Different ratios of steel and PP fibers were used.

This research concluded that hybrid fiber reinforcement must be considered in the development of concrete slabs strength to resist impact load.

5.2 CONCLUSIONS

From the results of the laboratory tests conducted to investigate of using the various ratios of steel and PP fiber as reinforcing materials to improve the impact resistance of concrete slabs, the following conclusions are valid within the study domain of scale specimens of 100 mm thickness, simply supported conditions, concrete strength 40 MPa:

5.2.1 General Conclusions

The general conclusions that can be drawn, based on the experimental work results presented, are that hybrid fiber reinforced (by adding SF and PP fibers) improves the fracture toughness and ductility behavior of concrete. It was also demonstrated that hybrid fiber reinforcement improves crack pattern. And there is an improvement in the case of HFRC slabs in terms of integrity after failure. The addition of steel and PP fibers to concrete slabs resulted in considerable improvement in the impact resistance when compared to slab without fibers.

Although the present results gives better understanding of hybrid fiber reinforced system in the case of impact load.

5.2.2 Conclusions Based on Concrete Properties

-Aspect ratio of fibers exerts an important influence on the mechanical properties of SFRC. It is found that an optimal aspect ratio of fibers exists for the HFRC strengths. Beyond the value, the addition of steel and PP fibers into concrete may cause an increase in the toughness rather than the strengths. It is found that the fibers act as a barrier to coarse aggregates movement reducing the materials mobility. So, increasing the aggregate size or the fiber aspect ratio the flowability of the material will be reduced.

-The results of tests carried out on fresh concrete show that HFRC mixes produce lower slump values (with 38.3% decrease) than plain concrete mixes due to the high mortar need. The addition of fibers negatively affects the slump values of ordinary concrete. With the increase in SF and PP fibers content, the slump values of fresh concrete decrease because of the high mortar need.

-Compressive strengths for hybrid fiber concrete specimens are decreased by 58% compared with plain concrete. M1 and M4 (65/35 3D and 65/60 5D steel fiber) have the highest value, while M6 (65/60 5D steel fiber with PP fiber) has the lowest. This indicates that when two fibers are combined, their compressive strength decreases. M7 (PP fiber alone) has a greater value 16.7% than M6.

-The flexural strength of hybrid concrete increased by 6.7% for M2 (0.5% (65/35 3D steel and PP) fibers from plain concrete. While decreased by 22.2% for M5 (0.5% (65/60 5D steel and PP) fibers. However, with increasing 44.4% for M4 (1% 65//60 5D steel fiber) and decreased 37.8% for PPF only.

-The fracture energy was increased by reducing crack growth at hybrid fiber reinforced concrete (only cracks appeared) compared to plain concrete when splitted in two sections.

From this, it is clear that the hybridization is not always conducive, and the synergy of fibers is proposed and divided into positive and negative effects.

5.2.3 Conclusions Based on Impact Load Test

-Although the higher fiber aspect ratio may induce lower compressive strength and elastic modulus, the toughness and peak strain of HFRC increased with 74.18% from C1, which lead to more energy absorption and better crack control. A lower residual deflections and strains of projectile and (0.1 mm) smaller penetration craters in HFRC with higher aspect ratio of fibers are observed.

-In comparison to ordinary concrete that has been exposed to an impact load, fiber reinforcing minimizes the extent of damage and maintains damaged concrete more compact. Even with mono-fiber reinforcement, slabs showed enhanced spall and cratering resistance.

-In terms of mass loss, steel-PP hybrid fiber reinforcement was found to give a significant improvement in performance under impact load when compared to PPF only reinforced concrete specimens. The steel-PP combination provides outstanding impact resistance due to the extraordinary fiber-matrix bond strength, high tensile strength, and modulus of elasticity of PP fibers.

-The impact resistance of HFRC is influenced by the fiber concentration in hybrid fiber mixtures as well as the length ratio. In hybrid systems, specimens with fibers fared better on average than specimens with simply one fiber. Specimens M3 and M6, with an increase of 30.79% from C1, which include 1 percent SF and 0.5 percent PPF, provide the best impact resistance because they provide enough bonding (anchoring) area while remaining short enough to uniformly fill the matrix spaces between the SF and PPF.

-In comparison to PPF alone, the overall impact resistance of all PPF-steel hybrid systems was shown to be higher; crack width 1.6 mm for M7(1% PPF) and 0.1 mm for M6(1% 65/60 5D SF+0.5PPF). The incorporation of polypropylene fibers in concrete can thereby increase the structure's longevity while also reducing its weight.

-Based on the findings, it can be concluded that the impact test was effective in determining the HFRC system's resistance to high loading rates such as impact loads.

Finally, it can be concluded that, hybrid fibers subsequently enhanced the tensile and flexural strengths, thereby increasing the ductility as well as the higher impact resistance of concrete. Moreover, the hybridisation of steel and PP can improve the load bearing capacity.

5.3 RECOMMENDATIONS:

5.3.1 Recommendations based on study results:

From the study results it is recommended:

1. To use hybrid fiber reinforcement in plain concrete slabs to enhance their flexural and tensile resistance under impact loading.

2. Not to use hybrid reinforcement of concrete elements under compression.

3. To use equations 4.1 and 4.2 to predict flexural strength for hybrid fiber reinforced concrete.

4. To use 1% of 65/60 5D steel fiber and 0.5% polypropylene fiber to improve crack pattern, displacements and strains.

5. To use 1% of 65/35 3D steel fiber and 0.5% polypropylene fiber to prevent perforation, scabbing and slab failure or damaged.

5.3.2 Recommendations for Further Research

The following are recommendations for future research work:

1- To study tensile strength of hybrid fiber reinforced of concrete.

2- To study the possibility of using impact test results obtained to predict blast load resistance of hybrid reinforced concrete slabs.

3- To develop a numerical model to predict the change in the crack patterns and their contribution to the energy dissipation under different loading rates.

4- To conduct more experimental tests with measuring width, number and positions of the cracks instrumentally then using them to improve the developed crack model.

5- To carry out more studies of shear resistance and the quantity of dissipated energy by adding S and PP fibers of the slab.

6- To improve the SDOF method by including the hardening behavior of the load-deflection curve for better estimating the maximum response of the slab under impact loads.

7- To study the effect of addition of a super plasticizer to increase the workability of hybrid fiber reinforced concrete mix.

8- To study the effect of using different ratios of fibers, other shapes of impact mass, different drop heights and different thicknesses of slab specimens on the behavior of hybrid fiber reinforced concrete.

9- To study in deep the variation of relationships between deflections and strains time due to impact loads.

REFERENCES

ACE. (1946). Fundamentals of protective structures. Army Corps of Engineers, Office of the Chief of Engineers Washington, DC.

ACIFC, (1999) An Introduction Guide: Steel fiber reinforced concrete industrial ground floors, ACIFC, Warwickshire.

Adhikary, S. D. (2013). Dynamic behavior of reinforced concrete beams under varying rates of concentrated and impact loadings (Doctoral dissertation, PhD thesis, School of Civil and Environmental Engineering, Nanyang Technological University, Singapore).

Al Nussairi, A. (2018). Characterizing the static and impact load resistance of one-way RC slabs strengthened by NSM CFRP rods (Doctoral dissertation, University of Bristol).

Alhadid, M. M. A., Soliman, A. M., Nehdi, M. L., & Youssef, M. A. (2014). Critical overview of blast resistance of different concrete types. Magazine of Concrete Research, 66(2), 72–81.

Almusallam, T. H., Siddiqui, N. A., Iqbal, R. A., & Abbas, H. (2013). Response of hybrid-fiber reinforced concrete slabs to hard projectile impact. International Journal of Impact Engineering, 58, 17-30. https://doi.org/10.1016/j.ijimpeng.2013.02.005.

Al-Rousan, R. Z. (2018). Failure analysis of polypropylene fiber reinforced concrete two-way slabs subjected to static and impact load induced by free falling mass. Latin American Journal of Solids and Structures, 15(1).

Amirikian, A. (1950). Design of protective structures (A new concept of structural behavior). Bureau of Yards and Docks.

Angelucci, F., Sayed, A. A., Williams, D. L., Boumis, G., Brunori, M., Dimastrogiovanni, D., & Bellelli,A. (2009). Inhibition of Schistosoma mansoni thioredoxin-glutathione reductase by auranofin: structural and kinetic aspects. Journal of Biological Chemistry, 284(42), 28977-28985.

Antoniou, A. (2018). Discrete element modeling of concrete structures under impact (Doctoral dissertation, Université Grenoble Alpes).

ASTM-E208-17e1. (2018). American Standard Test Method for Conducting Drop-Weight Test to Determine Nil-Ductility Transition Temperature of Ferritic Steels.

Banthia, N., Majdzadeh, F., Wu, J., & Bindiganavile, V. (2014). Fiber synergy in Hybrid Fiber Reinforced Concrete (HyFRC) in flexure and direct shear. Cement and Concrete Composites, 48, 91-97.

Batarlar, B., Hering, M., Bracklow, F., Kühn, T., Beckmann, B., & Curbach, M. (2021). Experimental investigation on reinforced concrete slabs strengthened with carbon textiles under repeated impact loads. Structural Concrete, 22(1), 120–131.

Bazgir, A. (2016). The behaviour of steel fibre reinforced concrete material and its effect on impact resistance of slabs (Doctoral dissertation, City University London).

Bhaduri, A. (2018). Mechanical properties and working of metals and alloys (Vol. 264). Springer. https://doi.org/10.1007/978-981-10-7209-3.

Brandt, A. M. (2008). Fiber reinforced cement-based (FRC) composites after over 40 years of development in building and civil engineering. Composite structures, 86(1-3), 3-9.

Buchan, P. A., & Chen, J. F. (2007). Blast resistance of FRP composites and polymer strengthened concrete and masonry structures–A state-of-the-art review. Composites Part B: Engineering, 38(5-6), 509-522.

Chen, Y. and May, I. (2009). Reinforced concrete members under drop weight impacts. Proceedings of the ICE-Structures and Buildings, 162(1), pp. 45–56.

Choudhary, S., Jain, A., Bhavsar, H., Chaudhary, S., & Choudhary, R. (2021). Analysis of steel fiber reinforced concrete wall panels under compression, flexural and impact loading. Materials Today: Proceedings, 38, 2471-2475.

Dahlberg, E. C. (2012). Applied hydrodynamics in petroleum exploration. Springer Science & Business Media.

Dancygier, A. N. (2017). High-performance concrete engineered for protective barriers. Philosophical Transactions of the Royal Society A: Mathematical, Physical and Engineering Sciences, 375(2085), 20160180.

Daudeville, L., & Malécot, Y. (2011). Concrete structures under impact. European journal of environmental and civil engineering, 15(sup1), 101-140.

Eibl, J. (1987). Design of concrete structures to resist accidental impact. Struct. Eng.;(United Kingdom), 65(1).

Elavenil, S., & Knight, G. S. (2012). Impact response of plates under drop weight impact testing. Daffodil International University Journal of Science and Technology, 7(1), 1-11.

El-Dakhakhny, M., Hassan, M. A., & Abd El-Aziz, G. (2009). Effect of thymoquinone and polythymoqunione on chemically-induced oral epithelial dysplasia (experimental study). Int Acad Res J, 1(2), 107-117.

Elnagar, A. B., Afefy, H. M., Baraghith, A. T., & Mahmoud, M. H. (2019). Experimental and numerical investigations on the impact resistance of SHCC-strengthened RC slabs subjected to drop weight loading. Construction and Building Materials, 229, 116866. https://doi.org/10.1016/j.conbuildmat.2019.116866

Figueiredo, A. D. D., & Ceccato, M. R. (2015). Workability analysis of steel fiber reinforced concrete using slump and Ve-Be test. Materials Research, 18, 1284-1290.

Fujikake, K., Li, B., & Soeun, S. (2009). Impact response of reinforced concrete beam and its analytical evaluation. Journal of structural engineering, 135(8), 938-950.

Groover, M. P. (2020). Fundamentals of modern manufacturing: materials, processes, and systems. John Wiley & Sons.

Guo, G., Alam, S., & Peel, L. D. (2020). Numerical analysis of ballistic impact performance of two ceramic-based armor structures. Composites Part C: Open Access, 3, 100061.

Hering, M., Bracklow, F., Scheerer, S., & Curbach, M. (2020). Reinforced Concrete Plates under Impact Load—Damage Quantification. Materials, 13(20), 4554.

Hrynyk, T. D. (2013). Behaviour and modelling of reinforced concrete slabs and shells under static and dynamic loads (Doctoral dissertation, University of Toronto).

Hrynyk, T. D., & Vecchio, F. J. (2014). Behavior of steel fiber-reinforced concrete slabs under impact load. Structural Journal, 111(5), 1213-1224. https://doi.org/10.14359/51686923.

Hummeltenberg, A., Beckmann, B., Weber, T., & Curbach, M. (2011). Investigation of concrete slabs under impact load. In Applied Mechanics and Materials (Vol. 82, pp. 398-403). Trans Tech Publications Ltd.

Hu, X., Guo, Y., Lv, J., & Mao, J. (2019). The mechanical properties and chloride resistance of concrete reinforced with hybrid polypropylene and basalt fibres. Materials, 12(15), 2371.

Iqbal, M. A., Rajput, A., & Bhargava, P. (2017). Plain and reinforced concrete targets subjected to projectile impact. Procedia engineering, 173, 138-144. https://doi.org/10.1016/j.proeng.2016.12.050.

Jonas, W., Rüdiger, E., Gries, M., Riech, H., & Rützel, H. (1982). Kinetic limit-bearing capacity of reinforced concrete slabs. Technical report RS, 162.

Kantar, E., Erdem, R. T., & Anıl, Ö. (2011). Nonlinear finite element analysis of impact behavior of concrete beam. Mathematical and Computational Applications, 16(1), 183-193. https://doi.org/10.3390/mca16010183.

Kassahun, A. (2012). Blast loading and blast effects on RC frame buildings. Lap Lambert Academic Publ.

Kataoka, S., Beppu, M., Ichino, H., & Mase, T. (2017). Failure behavior of reinforced concrete slabs subjected to moderate-velocity impact by a steel projectile. https://doi.org/10.1177/2041419617721550.

Kennedy, R. P. (1976). A review of procedures for the analysis and design of concrete structures to resist missile impact effects. Nuclear Engineering and Design, 37(2), 183–203.

Kiran, T., Murali, A., & Zai, S. A. K. (2017). Impact Analysis on Slabs–A Review. Int. Res. J. Eng. Technol., 4(5), 423-426.

Kishi, N, Matsuoka, K. G., Mikami, H., & Goto, Y. (1997). Impact resistance of large scale RC slabs. Proceedings of the Second Asia-Pacific Conference on Shock & Impact loads in Structures, Melbourne, Australia (pp. 213–220).

Kishi, N., Kurihashi, Y., Ghadimi Khasraghy, S., & Mikami, H. (2011). Numerical simulation of impact response behavior of rectangular reinforced concrete slabs under falling-weight impact loading. Applied Mechanics and Materials (Vol. 82, pp. 266-271). Trans Tech Publications Ltd. https://doi.org/10.4028/www.scientific.net/AMM.82.266.

Kishi, N., Mikami, H., Matsuoka, K. G., & Ando, T. (2002). Impact behavior of shear-failure-type RC beams without shear rebar. International Journal of Impact Engineering, 27(9), 955-968.

Knapton, J. (2003). Ground bearing concrete slabs: specification, design, construction and behaviour. Thomas Telford.

Kœchlin, P., & Potapov, S. (2009). Classification of soft and hard impacts—Application to aircraft crash. Nuclear Engineering and Design, 239(4), 613-618. https://doi.org/10.1016/j.nucengdes.2008.10.016.

Krauthammer, T. (2008). Modern protective structures. CRC Press.

Kumar, A. A., Sharma, O., Bansal, S., & Singhai, V. (2018). Strength and durability of high performance engineered cementitious composites. Indian Concr. J, 1-5.

Langdon, G. S., Cantwell, W. J., Guan, Z. W., & Nurick, G. N. (2014). The response of polymeric composite structures to air-blast loading: a state-of-the-art. International Materials Reviews, 59(3), 159-177, https://doi.org/10.1179/1743280413y.0000000028.

Lee, J. Y., Yuan, T., Shin, H. O., & Yoon, Y. S. (2020). Strategic use of steel fibers and stirrups on enhancing impact resistance of ultra-high-performance fiber-reinforced concrete beams. Cement and Concrete Composites, 107, 103499.

Li, Q. M., Reid, S. R., Wen, H. M., & Telford, A. R. (2005). Local impact effects of hard missiles on concrete targets. International Journal of impact engineering, 32(1-4), 224-284. https://doi.org/10.1016/j.ijimpeng.2005.04.005.

Liu, Y., Zhang, Z., Shi, C., Zhu, D., Li, N., & Deng, Y. (2020). Development of ultra-high performance geopolymer concrete (UHPGC): Influence of steel fiber on mechanical properties. Cement and Concrete Composites, 112, 103670.

Mallick, P. K. (2007). Fiber-reinforced composites: materials, manufacturing, and design. CRC press.

Manibalan, P., & Baskar, R. (2019). An influence of basalt fiber on mechanical properties of concrete. International Journal of Recent Technology and Engineering, 8(3), 2909–2912. https://doi.org/10.35940/ijrte.C4789.098319.

McMorrow, B. (2009). Tomahawk Missile Impact on Al-Shifa Factory in Sudan [Photograph]. PBase. Al Shifa Pharmaceutical Factory ruins, Khartoum North photo - Brian McMorrow photos at pbase.com.

Memon, D., Maazoun, A., Matthys, S., & Lecompte, D. (2019). Low-velocity impact behaviour of plain concrete beams. In 12th European LS-DYNA Conference 2019. DYNAmore.

Mohajerani, A., Hui, S. Q., Mirzababaei, M., Arulrajah, A., Horpibulsuk, S., Abdul Kadir, A., ... & Maghool, F. (2019). Amazing types, properties, and applications of fibers in construction materials. Materials, 12(16), 2513.

Mohammadhosseini, H., Tahir, M. M., Alyousef, R., & Alabduljabbar, H. (2020). Production of sustainable concrete composites comprising waste metalized plastic fibers and palm oil fuel ash. In New Materials in Civil Engineering (pp. 435-457). Butterworth-Heinemann.

Mortas, N., Er, O., Reis, P. N. B., & Ferreira, J. A. M. (2014). Effect of corrosive solutions on composites laminates subjected to low velocity impact loading. Composite Structures, 108, 205-211.

Ngo, T., Mendis, P., Gupta, A., & Ramsay, J. (2007). Blast loading and blast effects on structures–an overview. Electronic Journal of Structural Engineering, 7(S1), 76-91.

Nia, A. A., Hedayatian, M., Nili, M., & Sabet, V. A. (2012). An experimental and numerical study on how steel and polypropylene fibers affect the impact resistance in fiber-reinforced concrete. International Journal of Impact Engineering, 46, 62-73. https://doi.org/10.1016/j.ijimpeng.2012.01.009.

Ong, K. C. G., Basheerkhan, M., & Paramasivam, P. (1999). Resistance of fibre concrete slabs to low velocity projectile impact. Cement and Concrete Composites, 21(5-6), 391-401.

Othman, H., & Marzouk, H. (2016). An experimental investigation on the effect of steel reinforcement on impact response of reinforced concrete plates. International Journal of Impact Engineering, 88, 12-21. https://doi.org/10.1016/j.ijimpeng.2015.08.015

Özkan, Ş., & Demir, F. (2020). The hybrid effects of PVA fiber and basalt fiber on mechanical performance of cost effective hybrid cementitious composites. Construction and Building Materials, 263, 120564.

Parmar, R. M., Singh, T., Sharma, S., Reddy, G. R., & Singh, R. K. (2014). Experimental investigation on behaviour of reinforced concrete structures under fire and impact loads. Report. Bhabha Atomic Research Centre, Mumbai.

Pashah, S., Massenzio, M., & Jacquelin, E. (2008). Prediction of structural response for low velocity impact. International Journal of Impact Engineering, 35(2), 119–132.

Pellini, W. S. (1971). Integration of Analytical Procedures for Fracture-Safe Design of Metal Structures. Naval Research Lab Washington DC.

Pellini, W. S., & Puzak, P. P. (1964). Practical considerations in applying laboratory fracture test criteria to the fracture-safe design of pressure vessels.

Pétry. (1910). Monographs of artillery systems. Brussel.

Pichandi, S., Rana, S., Oliveira, D., & Fangueiro, R. (2013). Fibrous and composite materials for blast protection of structural elements— a state-of-the-art reviews. Journal of Reinforced plastics and composites, 32(19), 1477-1500.

Prakash, A. (2017). Steel Fiber Reinforced Concrete (Doctoral dissertation, KIIT University).

Qadir Bux alias Imran Latif. (2012). Critical Impact Energy for Local Impact Damage of Hard Projectile on Concrete Slab (Doctoral dissertation, Universiti Tun Hussein Onn Malaysia).

Qian, C., & Stroeven, P. (2000). Fracture properties of concrete reinforced with steel–polypropylene hybrid fibres. Cement and Concrete Composites, 22(5), 343-351.

Riera, J. D. (1980). A critical reappraisal of nuclear power plant safety against accidental aircraft impact. Nuclear Engineering and Design, 57(1), 193–206.

Robinson, P., & Davies, G. A. O. (1992). Impactor mass and specimen geometry effects in low velocity impact of laminated composites. International journal of impact engineering, 12(2), 189-207.

Ruta, D. (2017). Numerical and experimental study of concrete structures under extreme conditions: impact and fire (Doctoral dissertation, Institut für Werkstoffe im Bauwesen, Universität Stuttgart).

Saatcı, S. (2007). Behavior and modelling of reinforced concrete structures subjected to impact loads (Doctoral dissertation, University of Toronto).

Sadraie, H., Khaloo, A., & Soltani, H. (2019). Dynamic performance of concrete slabs reinforced with steel and GFRP bars

under impact loading. Engineering Structures, 191(April), 62–81. https://doi.org/10.1016/j.engstruct.2019.04.038

Saleh, Z., Sheikh, M. N., Remennikov, A., & Basu, A. (2020). Overload damage mechanisms of GFRP-RC beams subjected to high-intensity low-velocity impact loads. Composite Structures, 233, 111578.

Sangi, A. J. (2011). Reinforced concrete structures under impact loads (Doctoral dissertation, Heriot-Watt University).

Silva, P. F., & Lu, B. (2007). Improving the blast resistance capacity of RC slabs with innovative composite materials. Composites Part B: Engineering, 38(5-6), 523 534, https://doi.org/10.1016/j.compositesb.2006.015.

Sivakumar, V., Karthik, K., Jachin, S. B., & Xavier, C. A. (2021). Experimental investigation on strength properties of hybrid fibre reinforced high strength concrete. Materials Today: Proceedings.

Song, P. S., Wu, J. C., Hwang, S., & Sheu, B. C. (2005). Statistical analysis of impact strength and strength reliability of steel–polypropylene hybrid fiber-reinforced concrete. Construction and building materials, 19(1), 1-9.

Sugano, T., Tsubota, H., Kasai, Y., Koshika, N., Orui, S., Von Riesemann, W. A., ... & Parks, M. B. (1993). Full-scale aircraft impact test for evaluation of impact force. Nuclear Engineering and Design, 140(3), 373-385.

Tahmasebinia, F. and Remennikov, A., (2008). “Simulation of the Reinforced Concrete Slabs under Impact Loading”. Australasian Structural Engineering Conference, 88 pp.

Tamayo, L. M. Z. (2017). Discrete Element Modelling of Concrete subjected to Edge-on Impact tests (Master Dissertation, Université Grenoble Alpes)

Tuğrul Erdem, R. (2021). Dynamic responses of reinforced concrete slabs under sudden impact loading. Revista de la construcción, 20(2), 346-358.

Tuğrul Erdem, R. (2021). Dynamic responses of reinforced concrete slabs under sudden impact loading. Revista de la construcción, 20(2), 346-358.

Tung, S. C. and Totten, G. E. (2012). Automotive lubricants and testing. SAE International and ASTM.

UFC 3 340 02 (2008); Unified Facilities Criteria, Structures to Resist the Effects of Accidental Explosions, DoD, U.S.A

Vivas, J. C., Zerbino, R. L., Torrijos, M. C., & Giaccio, G. M. (2020, September). Impact Response of Different Classes of Fibre Reinforced Concrete. RILEM-fib International Symposium on Fibre Reinforced Concrete (pp. 189-198). Springer, Cham.

Walter, T. A., & Wolde-Tinsae, A. M. (1984). Turbine missile perforation of reinforced concrete. Journal of Structural Engineering, 110(10), 2439–2455.

Wang, J. (2017). Polyvinyl alcohol (PVA) fiber-reinforced rubber concrete and rubberized self-compacting concrete (Master Dissertation, Michigan Technological University)

Xiao, Y. (2016). Dynamic behavior of reinforced concrete slabs under rapid loading and low velocity impact (Doctoral thesis, Nanyang Technological University, Singapore).

Yao, W., Sun, W., Shi, Z., Chen, B., Chen, L., & Feng, J. (2020). Blast-resistant performance of hybrid fiber-reinforced concrete (hfrc) panels subjected to contact detonation. Applied Sciences, 10(1), 241.

Yoo, D. Y., Min, K. H., Lee, J. Y., & Yoon, Y. S. (2012). Enhancing impact resistance of concrete slabs strengthened with FRPS and steel fibers. In 6th International Conference on FRP Composites in Civil Engineering, CICE 2012. International Institute for FRP in Construction (IIFC).

Yoshida, H., Nomura, T., Wyllie, D. C., & Morris, A. J. (2007). Rock fall sheds—application of Japanese designs in North

America. In Proceedings of the 1st North American Landslide Conference (pp. 179–196). Landslides/slope Instability AEG Special Publication: Conference Presentations.

Yuan, P., & Harik, I. E. (2010). Equivalent barge and flotilla impact forces on bridge piers. Journal of Bridge Engineering, 15(5), 523-532.

Zielinski, A. J. (1984). Concrete structures under impact loading rate effects. Report Stevin Laboratory, Concrete Structures 5-84-14.

Zineddin, M., & Krauthammer, T. (2007). Dynamic response and behavior of reinforced concrete slabs under impact loading. International Journal of Impact Engineering, 34(9), 1517-1534.

Appendix A

Figure A1: Setting for Slab's Support

Figure A2: Adjustment the Frame of Impact Load Test with Height with Max. 2 m Free Fall

Figure A3: Fabrication Works for the Glider

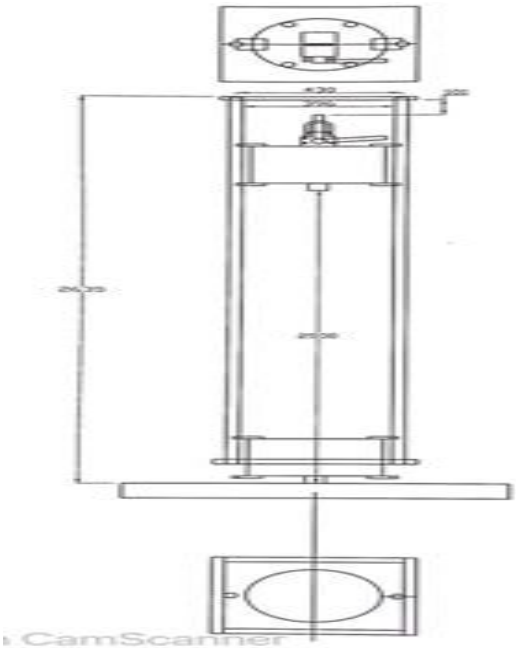

Figure A4: Details of impact load system with max. 2 m free fall

Figure A5: Setting up glider and mass of 200 kg into the frame

Figure A6: Complete Frame Set Up for Impact Load Test

Appendix B

Figure B1: Failure for Slab Specimen C1 (1m drop) – side view

Figure B2: Failure for Slab Specimen C1 (1m drop) – other side view

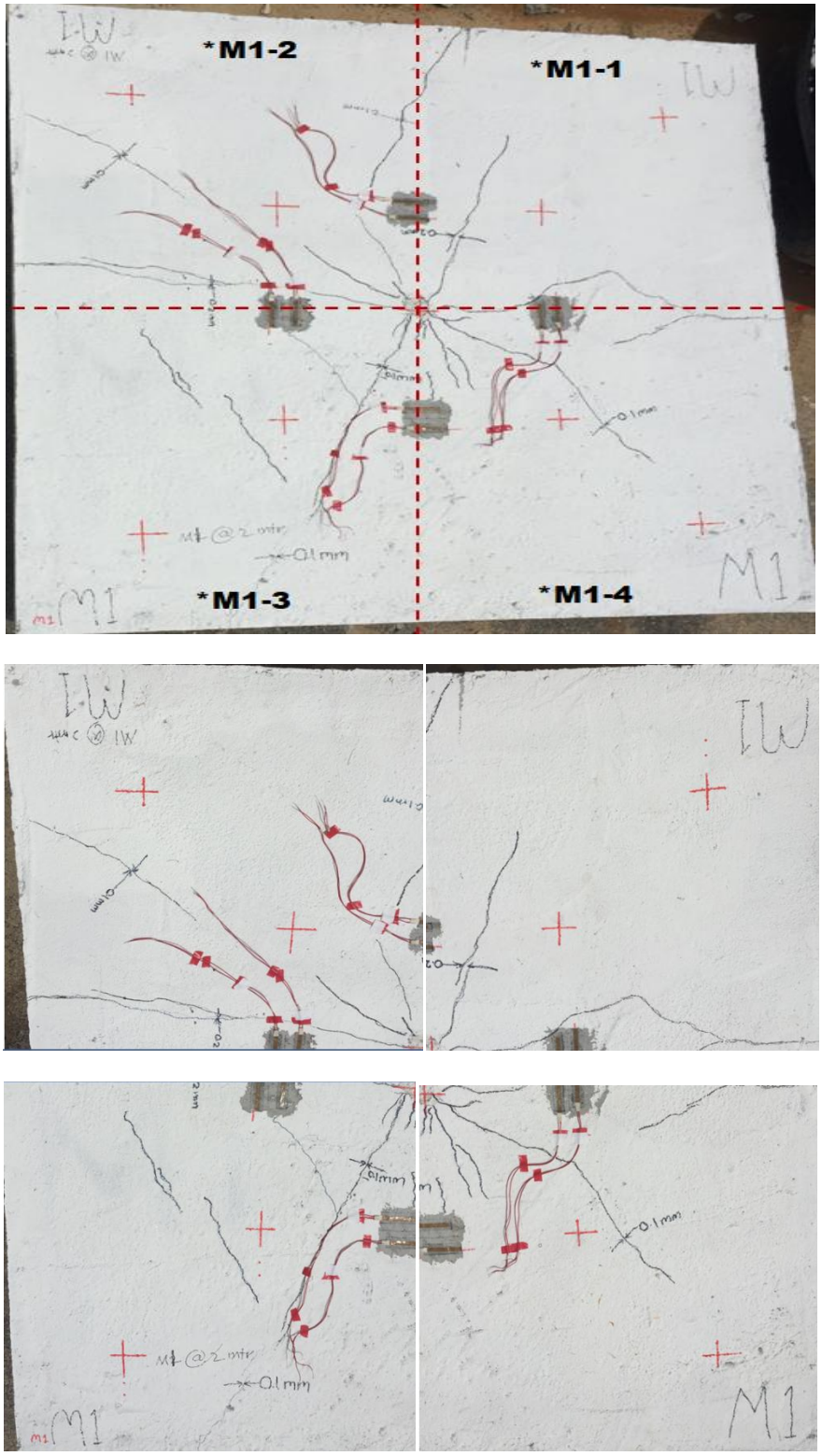

Figure B3: Failure for Slab Specimen M1 (2m drop) – another plan view

(0.1 and 0.2 mm crack width)

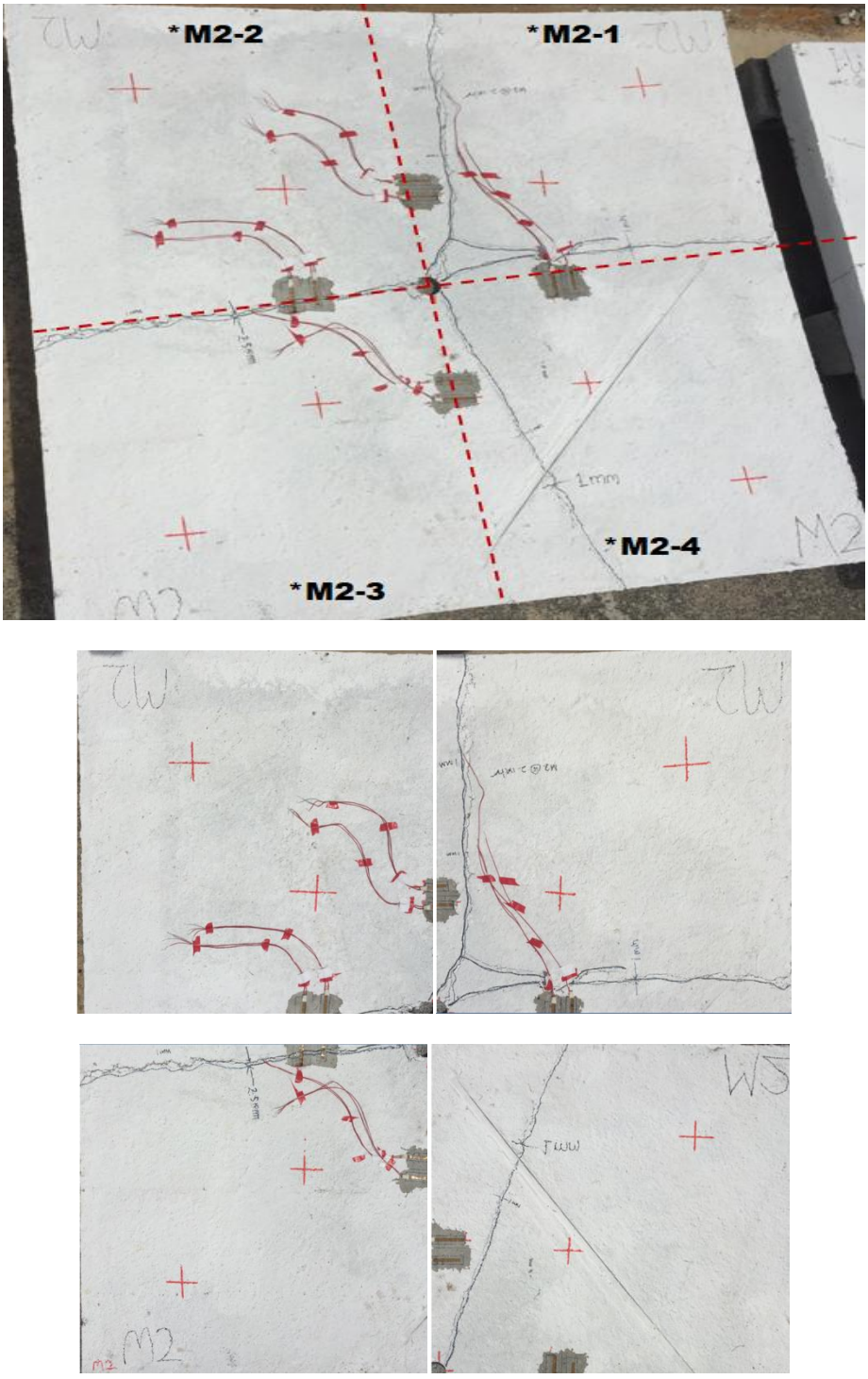

Figure B4: Failure for Slab Specimen M2 (2m drop) – another plan view

(1 and 2.5 mm crack widths)

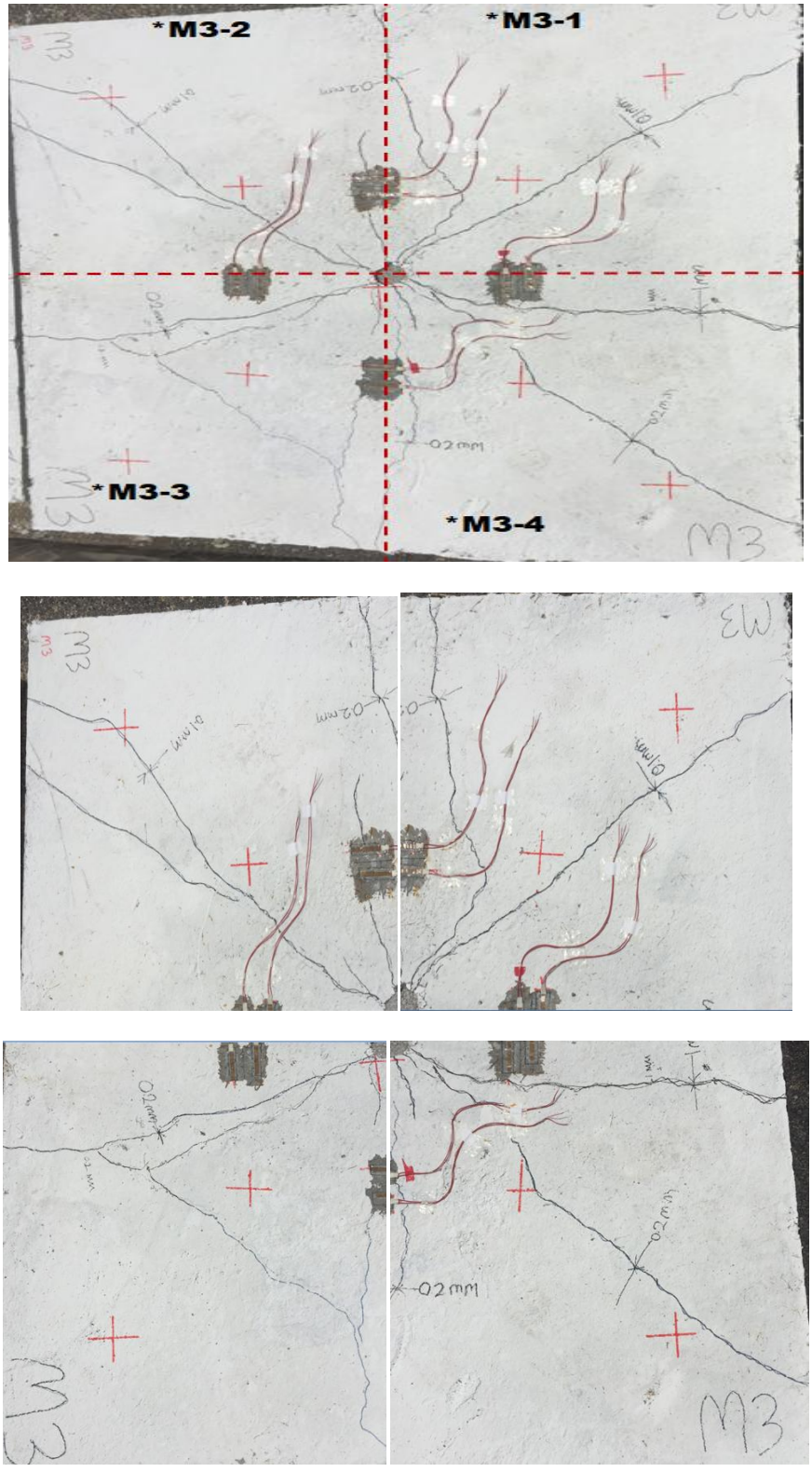

Figure B5: Failure for Slab Specimen M3 (2m drop) – another plan view

(0.1, 0.2 and 1 mm crack widths)

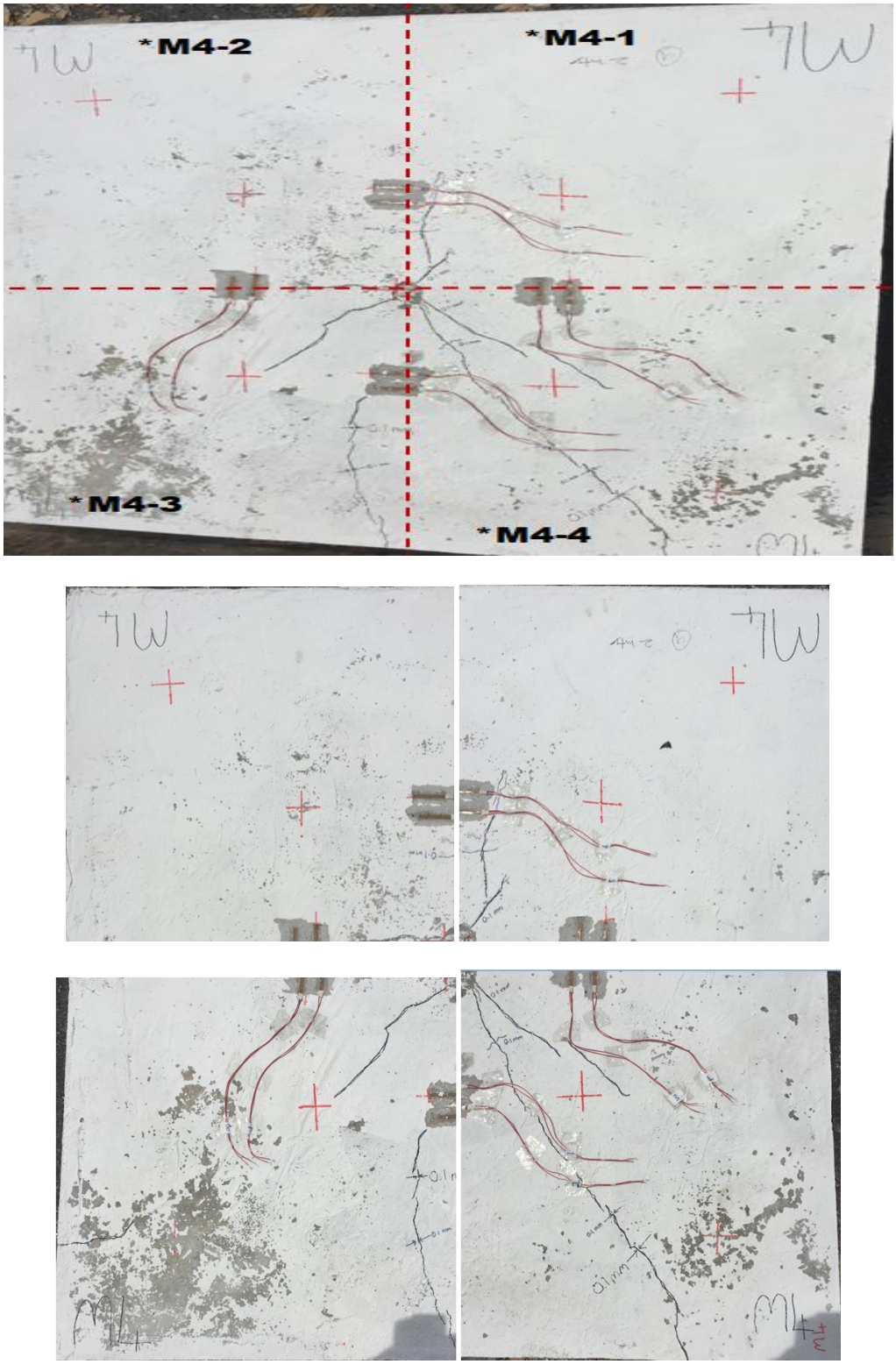

Figure B6: Failure for Slab Specimen M4 (2m drop) – another plan view (0.1mm crack width)

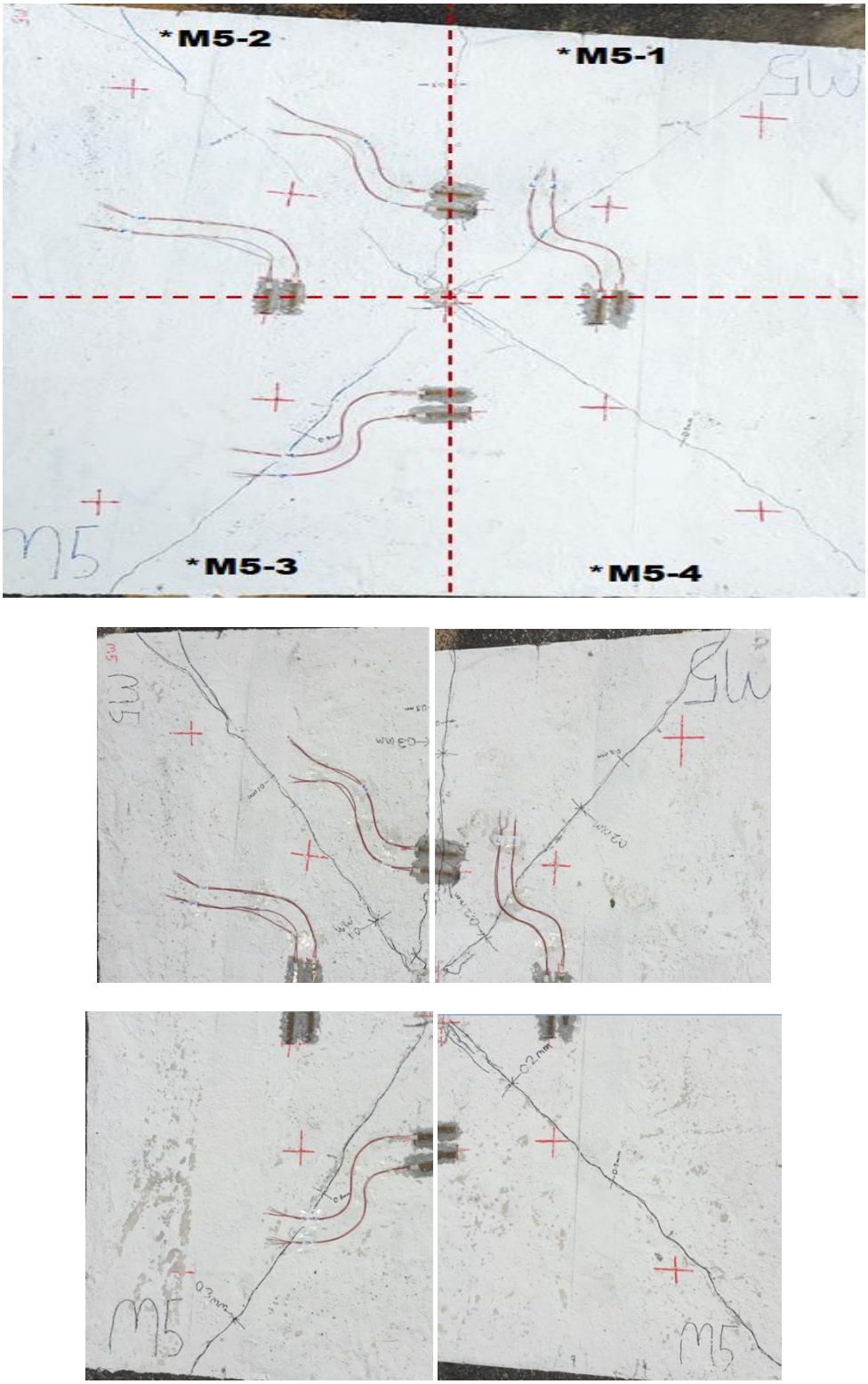

Figure B7: Failure for Slab Specimen M5 (2m drop) – another plan view

(0.1, 0.2 and 0.3mm crack widths)

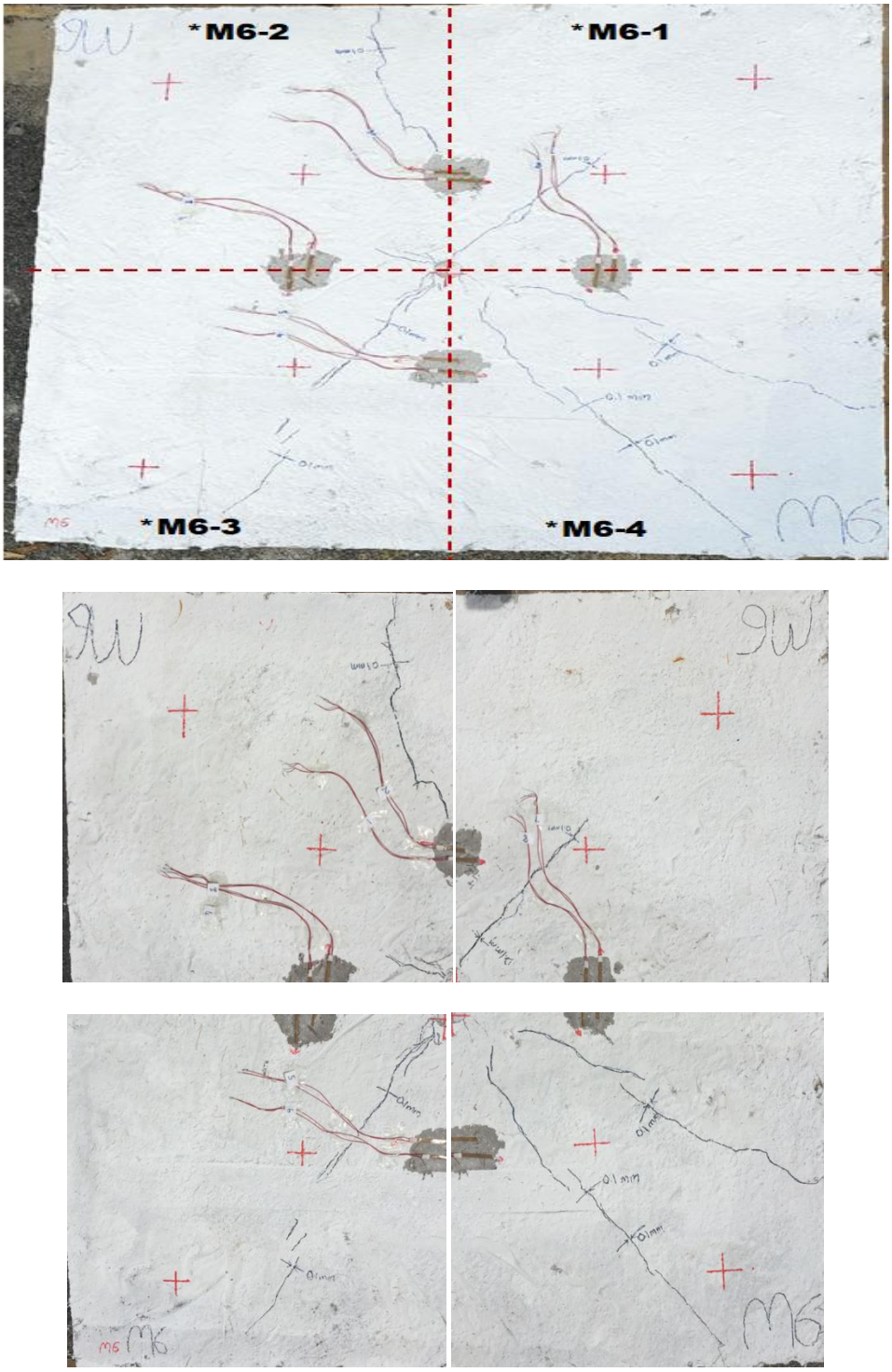

Figure B8: Failure for Slab Specimen M6 (2m drop) – another plan view (0.1mm crack width)

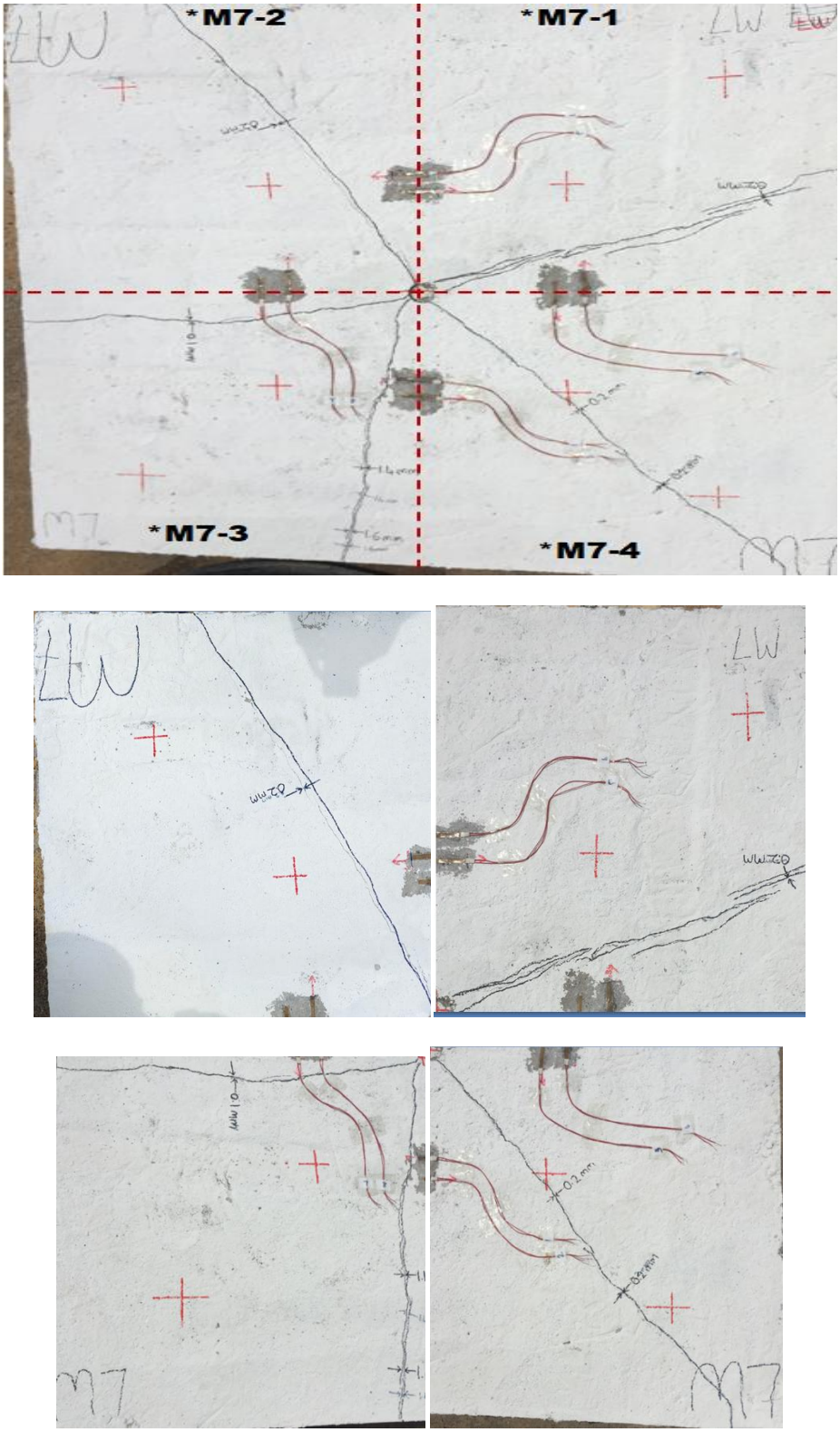

Figure B9: Failure for Slab Specimen M7 (2m drop) – another plan view

(0.1, 0.2, 1.4 and 1.6 mm crack widths)